UNIVERSITÀ DEGLI STUDI DI MILANO

CORSO DI DOTTORATO IN MEDICINA TRASLAZIONALE
XXXV CICLO

DIPARTIMENTO DI SCIENZE BIOMEDICHE PER LA SALUTE

IMPAIRMENT OF TOLL-LIKE RECEPTOR 9 AGONIST ANTI-TUMOR ACTIVITY BY ANTI-PD-1 ANTIBODY: ROLE OF MACROPHAGES

BIO/16

Serena Lucia INDINO

Tutor: Dott. **Michele SOMMARIVA**

Coordinatore di Dottorato: Prof.ssa **Chiarella SFORZA**

A.A. 2021-2022

ABSTRACT

Background: Toll-like receptor 9 (TLR9) agonists are known for their ability to activate innate immune cells and have been extensively tested for the treatment of different types of tumors. However, no satisfied results have been achieved so far. Indeed, to prevent uncontrolled and potentially harmful immune reactions, TLR9 activation induces several immunoregulatory mechanisms that, eventually, restrain the immune response. Among such processes, it has been observed that TLR9 triggering determines PD-1 receptor up-regulation on immune cells. PD-1 is reported to be expressed by adaptive and innate immune cells and to dampen immune system function upon binding to its two ligands (PD-L1 and -L2). By over-expressing such ligands, tumor cells exploit PD-1/PD-Ls axis to evade immune system attack. The blockade of PD-1 using specific monoclonal antibodies, disrupting PD-1/PD-Ls interaction, is able to restore the activity of the immune cells. However, only 30% of patients with advanced cancer benefit of this kind of therapy. Therefore, a combinatorial immunotherapeutic regimen based on the activation of the immune system, by TLR9 agonists administration, and on the abrogation of an immunosuppressive mechanism, utilizing anti-PD-1 antibody, represent a promising immunotherapeutic strategy in the treatment of cancer.

Aim: The efficacy of the co-administration of these two immunotherapeutic drugs have been deeply investigated in several clinical and preclinical studies that mainly focused on the role played by the adaptive immune system. Considering that TLR9 agonists primarily targets innate immune cells and PD-1 can be also expressed by the innate immune system, the aim of the present study was to evaluate the contribution of the innate immune cells to the final outcome of this combinatorial therapy.

Methods: Athymic mice, intraperitoneally xenografted with IGROV-1 human ovarian cancer cell line, received TLR9 agonist (CpG-ODN), anti-PD-1 antibody or their

combination. *In vivo* macrophages depletion was achieved by liposomal-containing clodronate administration. Tumor immune contexture was evaluated by immunofluorescence analysis. *In vitro* studies were carried out by exposing RAW264.7 mouse macrophage cell line to CpG-ODN and/or anti-PD-1 antibody. The effect of the combinatorial treatment on macrophages was assessed by microarray profile and subsequent bioinformatic analysis, Real-time PCR, multiplex ELISA and ^{51}Cr-release assays. To unravel the specific contribution of the antigen-binding site and the fragment crystallizable (Fc) domain of anti-PD-1 antibody, modified anti-PD-1 antibodies were utilized. The involvement of TRIM21 was investigated by pharmacological inhibition and silencing experiments.

Results: Mice receiving CpG-ODN/anti-PD-1 antibody combination experienced an acceleration of tumor growth paralleled by a marked infiltration of CD206$^+$ and IL-10$^+$ macrophages compared to CpG-ODN-treated animals. The increased tumor progression observed in the combination group was completely abrogated by macrophage depletion. *In vitro* experiments showed that RAW264.7 cells stimulated with CpG-ODN and anti-PD-1 antibody exhibited a gene expression profile completely different to those exposed to each drug alone, acquiring a phenotype characterized by the up-regulation of both M1- and M2-related markers. Multiplex ELISA assays confirmed an augmented secretion of M1 and M2 cytokines, validating gene profile data. Functional assay showed that combination-primed macrophages were able to dampen NK cell cytotoxic activity compared to CpG-ODN- or anti-PD-1- antibody-treated cells. The use of engineered anti-PD-1 antibodies revealed that either the Fc domain and the antigen-binding site of anti-PD-1 antibody are necessary for determining the changes in gene expression profile on macrophage when combined with TLR9 agonists. Finally, TRIM21 was found to be involved in shaping macrophage phenotype by interacting with anti-PD-1 antibody Fc domain.

Conclusions: Our results indicate that, when TLR9 signaling is activated, the co-administration of anti-PD-1 antibody induces in macrophages the acquisition of a “mixed” M1/M2 phenotype with enhanced immunosuppressive features, eventually negatively impacting on the immune response and promoting tumor growth. Since TLR9 stimulation and PD-1 blockade combinatorial immunotherapy is under investigation in different clinical trials, the impact of both agents on macrophages should be taken into consideration to avoid potentially harmful adverse effects, especially in tumors where the infiltration of macrophages is particularly abundant.

INTRODUCTION

1. Toll-like receptors (TLRs)

1.1 TLRs and innate immunity

Toll-like receptors (TLRs) are type I transmembrane proteins belonging to the family of pattern-recognition receptors (PRRs), known for their ability to recognize the so-called Pathogen- or Damage-Associated molecular patterns (PAMPs or DAMPs) deriving from bacteria, viruses, fungi and protozoa or from injured or altered host cell and tissues, respectively [1,2].

Ten TLRs have been identified in humans and 13 in mice, with TLR1-TLR9 exhibiting highly degree of similarity between the two species [3].

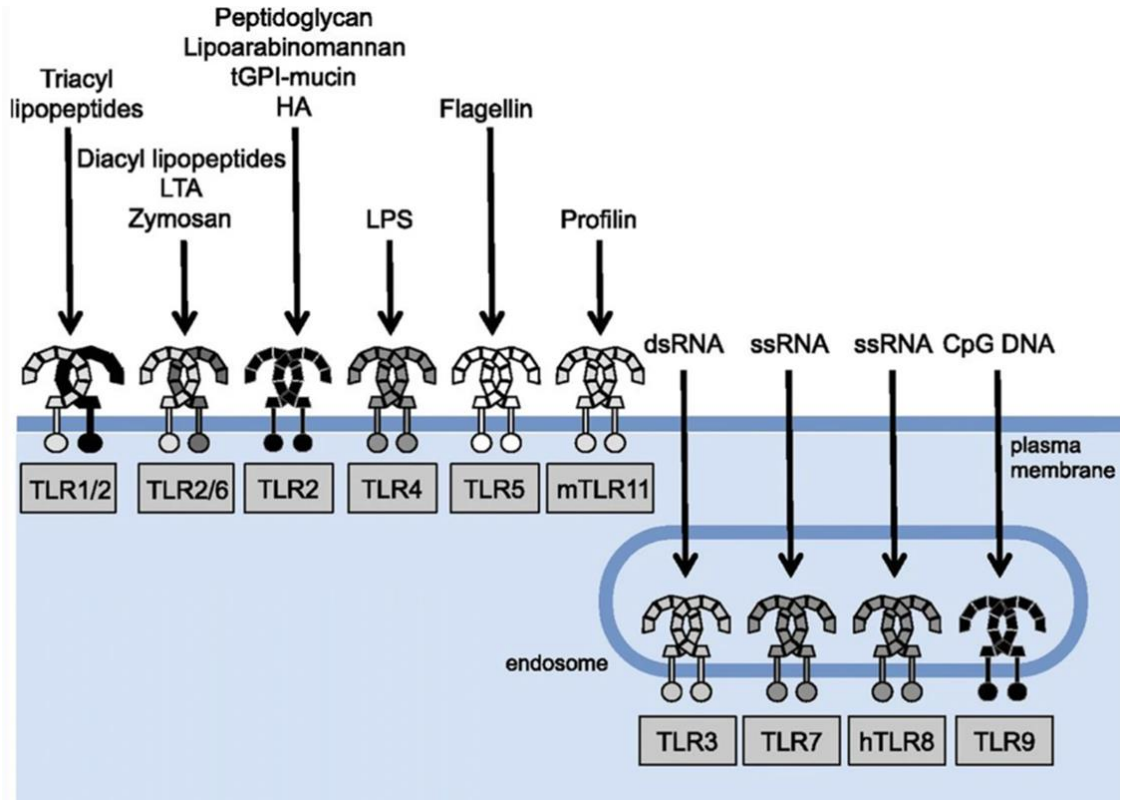

Fig. 1 TLR family members.
Schematic representation of the different TLRs, their localization and cognate ligands. TLRs: Toll-like receptors. From *El-Zayat et al. Bulletin of the National Research Centre, 2019.*

TLRs share a similar structure, including an ectodomain containing leucin-rich repeats (LLR), which mediates ligand recognition, a transmembrane domain, and an intracellular

Toll-interleukin 1 (IL-1) receptor (TIR) domain, that is necessary for intracellular signaling transduction.

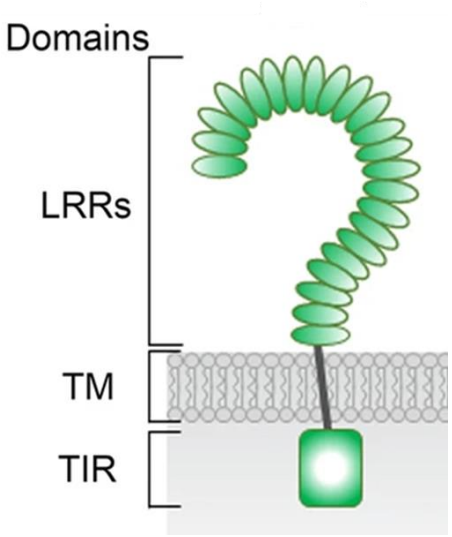

Fig. 2 TLR general structure.
Schematic representation of TLR structure. TLR: Toll-like receptor. Adapted from *Chen et al. Journal of Biomedical Science, 2019.*

TLRs can be expressed by immune cells, such as dendritic cells (DCs), macrophages, T and B lymphocytes, neutrophils, eosinophils, mast cells, monocytes, and non-immune cells, including chondrocytes, fibroblasts, and epithelial cells [4].

TLR	Expression on immune cells
TLR1	Most cell types including DCs and B cells
TLR2	PMLs, DCs, monocytes and T cells
TLR3	DCs, NK cells and T cells
TLR4	Macrophages, DCs and T cells
TLR5	Monocytes, DCs, NK cells and T cells
TLR6	B cells, DCs, monocytes and NK cells
TLR7	B cells, DCs, monocytes and T cells
TLR8	Monocytes, DCs, NK cells and T cells
TLR9	DCs, B cells, PMLs, macrophages, NK cells and microglial cells

Tab. 1 TLRs expression on immune cells.
Expression pattern of TLRs on different immune cells. DCs: dendritic cells; PMLs: peripheral mononuclear leucocytes; NK cells: natural killer cells. Adapted from *Liu et al. Immunology, 2007.*

The binding to their cognate ligands triggers intracellular signaling pathways leading to the production and secretion of several pro-inflammatory cytokines, chemokines, and interferons (IFNs), initiating the innate immune response against pathogens [5,6], that, in turn, promotes the activation of the adaptive immune system.

1.1.1 TLR localization and ligands

Based on their cellular localization, TLRs can be divided into two groups: surface TLRs, i.e. TLR1, TLR2, TLR4, TLR5, TLR6, and TLR11, and intracellular TLRs, comprising TLR7, TLR8, and TLR9, located in lysosomes, endosomes, and endolysosomes [7].

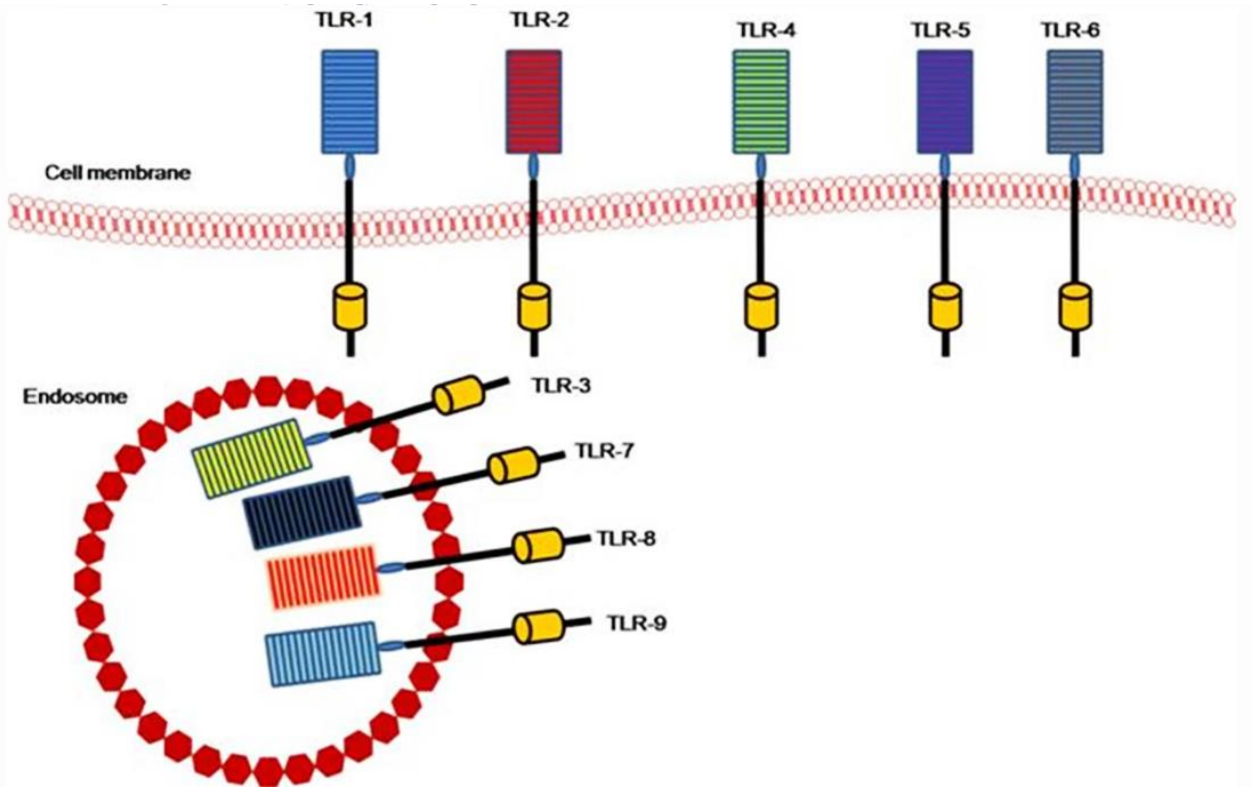

Fig. 3 TLR cellular localization.
Cellular localization of TLR family. TLR: Toll-like receptor. From *El-Zayat et al. Bulletin of the National Research Centre, 2019.*

Since the different localization pattern, the recognition of TLR ligands occurs in different cellular compartments, ranging from the plasma membrane to the endoplasmic reticulum. For instance, surface TLRs recognize peptidoglycans, lipopeptides and

lipopolysaccharides, whereas intracellular TLRs mostly bind microbial nucleic acids [8]. A detailed list of the different TLR ligands is provided in Table 2.

Receptor	Ligands
TLR1	Bacterial triacyl lipopeptides and proteins in parasites
TLR2	Bacterial diacyl lipopeptides, lipoteichoic acid from Gram-positive bacteria and zymosan from the cell wall of yeast
TLR3	Double-stranded RNA from viruses
TLR4	Endotoxin (LPS) from Gram-negative bacteria
TLR5	Flagellin from mobile bacteria
TLR6	Bacterial diacyl lipopeptides, lipoteichoic acid from Gram-positive bacteria and zymosan from the cell wall of yeast
TLR7	Single-stranded RNA from viruses
TLR8	Single-stranded RNA from viruses
TLR9	CpG DNA from bacteria or viruses
TLR10	Unknown

Table 2 TLR ligands.
List of the ligands of TLRs. TLR: Toll-like receptor; LPS: lipopolysaccharide; CpG DNA: cytidine-phosphate-guanosine DNA. Adapted from *Liu et al. Immunology, 2007*

1.1.2 TLR signaling pathways

TLR signaling is very complex and comprises different adaptor proteins. It can be generally classified into MyD88-dependent and MyD88-independent pathways, depending on the specific adaptor molecules required for inflammatory cytokine and IFN-1 induction [8]. However, the distinct intracellular signaling pathways triggered by TLRs result in similar downstream effects. For example, TLRs lead to the activation of the transcription factor Nuclear Factor-κB (NF-κB) that, after the translocation into the nucleus, promotes the expression of several genes involved in the inflammatory response.

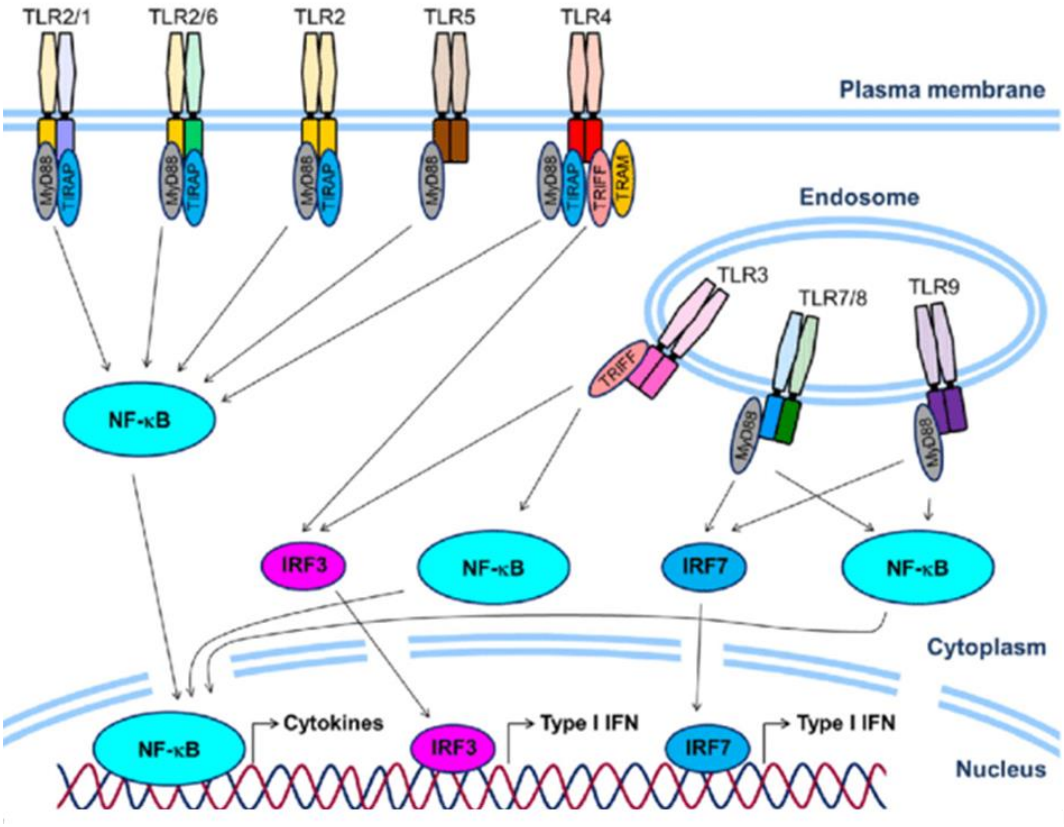

Fig. 4 TLR signaling.
Overview of TLR signaling. TLR: Toll-like receptor. From *Nishimoto et al. Inflammation and Regeneration, 2020.*

1.2 TLR9

1.2.1 TLR9 ligands and signaling pathway

TLR9 (CD289) is an intracellular TLR and its localization is functional for preventing the binding to host's nucleic acids, thus avoiding autoimmune responses. Indeed, post-translational modifications, such as the cleavage of specific aminoacidic sequences mediated by proteases, abrogate the possible translocation of this TLR on the cell surface [9–13]. TLR9 was found to possess five different isoforms, named TLR9-A, TLR9-B, TLR9-C, TLR9-D, and TLR9-E17. These different TLR9 variants, resulting from alternative splicing, exhibit distinct intracellular localization. For instance, TLR9-A, TLR9-C, TLR9-D, and TLR9-E were found in the endoplasmic reticulum, whereas TLR9-B localizes in mitochondria [14].

TLR9 is activated by unmethylated cytidine-phosphate-guanosine (CpG) DNA motifs, which are a characteristic of bacteria and viruses genomes but very rare in mammals. The recognition of CpG-DNA by dendritic cells (DCs), macrophages and B lymphocytes drives a potent pro-inflammatory response [8]. Upon activation, TLR9 triggers a signaling pathway involving several factors, including IRAK4, TRAF6 and Myd88, finally activating IRF5 and NF-κB. Moreover, TLR9 downstream signaling pathway leads to activation of MAPK and activator protein 1 (AP-1). The final outcome is represented by the induction of the transcription of cytokine genes, such as IL-6, IL-12, TNF together with costimulatory molecules as CD80 and CD86 [5].

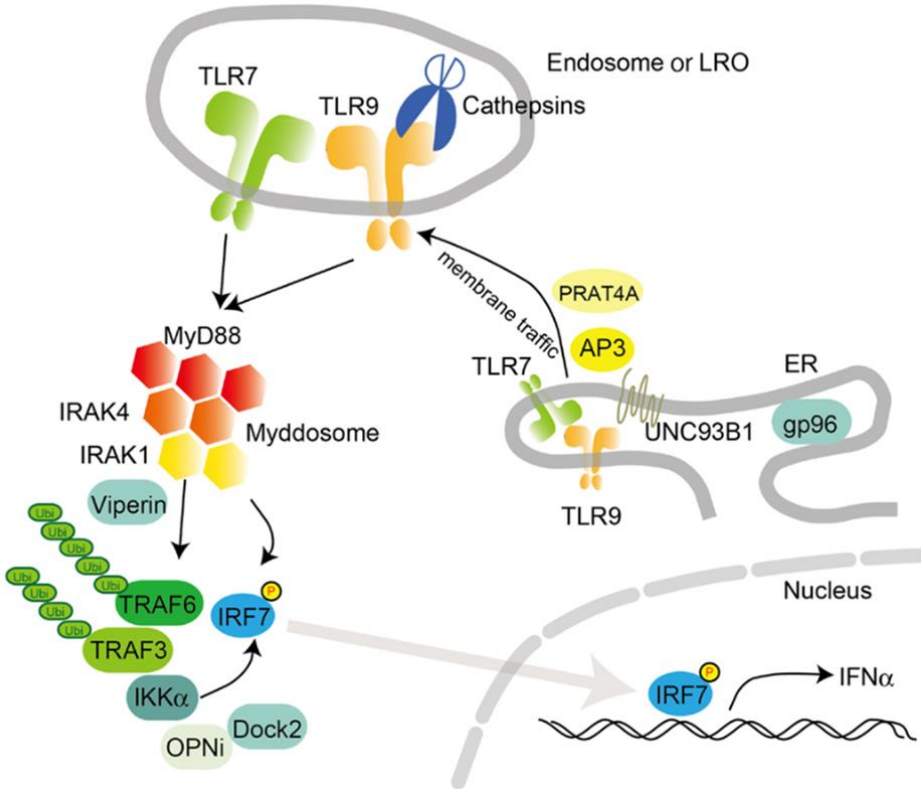

Fig. 5 TLR9 signaling pathway.
Schematic representation of TLR9 intracellular signaling. TLR9: Toll-like receptor 9. From *Kawasaki et al. Frontiers in Immunology, 2014.*

1.2.3 TLR9 agonists in cancer immunotherapy

As the other TLRs, TLR9 is expressed by immune cells, including B cells, dendritic cells, monocytes/macrophages, natural killer cells, T cells [15]. The immunological response

triggered by the binding of TLR9 with CpG-DNA gives rise to stimulation of both innate and adaptive immune response, resulting in NK cells, T and B cells, macrophages and DCs activation [16–18].

Exploiting the ability of TLR9 signaling to stimulate the immune system, it was speculated that TLR9 synthetic agonists could be utilized for the treatment of oncologic patients by enhancing the immune response against tumor cells. Indeed, several TLR9 agonists have been evaluated both as monotherapy and in combination with other pharmacological antitumor strategies, as chemotherapy, radiotherapy, and immunotherapy in clinical trials involving patients suffering from different types of cancers at advanced stage [19,20]. TLR9 agonists currently in clinical trials are listed in Table 3.

TLR9 Agonist	Study Phase	Histology
PF-3512676 (CPG 7909)	Phase I	Advanced BCC, CTCL, Advanced RCC or melanoma
MGN1703	Phase I	All solid tumors
CMP-001	Phase I	Advanced metastatic melanoma
PF-3512676 (CPG 7909)	Phase II	Advanced metastatic melanoma

Table 3 Clinical Trials of TLR9 agonists as monotherapy.
List of TLR9 agonists in clinical trials as monotherapy. BCC: basal cell carcinoma; CTCL: cutaneous T cell lymphoma; RCC: renal cell carcinoma. Adapted from *Karapetyan et al. OncoTargets and Therapy, 2020.*

Despite the promising premises, in clinical trials TLR9 agonists did not show any clinically meaningful efficacy, revealing only modest antitumor effects. Among patients enrolled in the clinical trials experiencing clinical benefits, the majority were classified as partial responders or stable disease state. Only a very limited percentage of patient achieved a complete and durable response [21,22]. The percentages of responding patients are reported in Table 4.

Percentage of responding patients	Tumor
11%	Cutaneous T cell lymphoma
25%	Basal cell carcinoma

Table 4 Efficacy outcomes of TLR agonists in clinical trials.
Percentages of patients responding to TLR9 agonists in clinical trials.

2. Programmed cell death-1 (PD-1) receptor

2.1 PD-1 structure and ligands

PD-1 is a receptor belonging to the B7/CD28/CTLA-4 family. It shows the molecular structure of type I transmembrane glycoprotein, consisting in an immunoglobulin extracellular domain, a transmembrane domain, and a tail extending to the cytoplasm. The cytoplasmic tail is composed by a tyrosine-based inhibitory motif (ITIM) and a tyrosine-based switch motif (ITSM), both responsible for the triggering of intracellular signaling pathway [23,24]. To date, two PD-1 ligands have been discovered, PD-L1 and PD-L2, also referred as B7-H1 or CD274, and B7-DC or CD273, respectively. Like PD-1, PD-Ls are members of B7/CD28/CTLA-4 family and show an immunoglobulin extracellular domain [25]. PD-L1 is constitutively expressed by hematopoietic and non-hematopoietic cells, whereas the expression of PD-L2 is restricted to Antigen Presenting Cells (APCs) and its expression is regulated by inflammatory stimuli, including interferons and several interleukins [26,27].

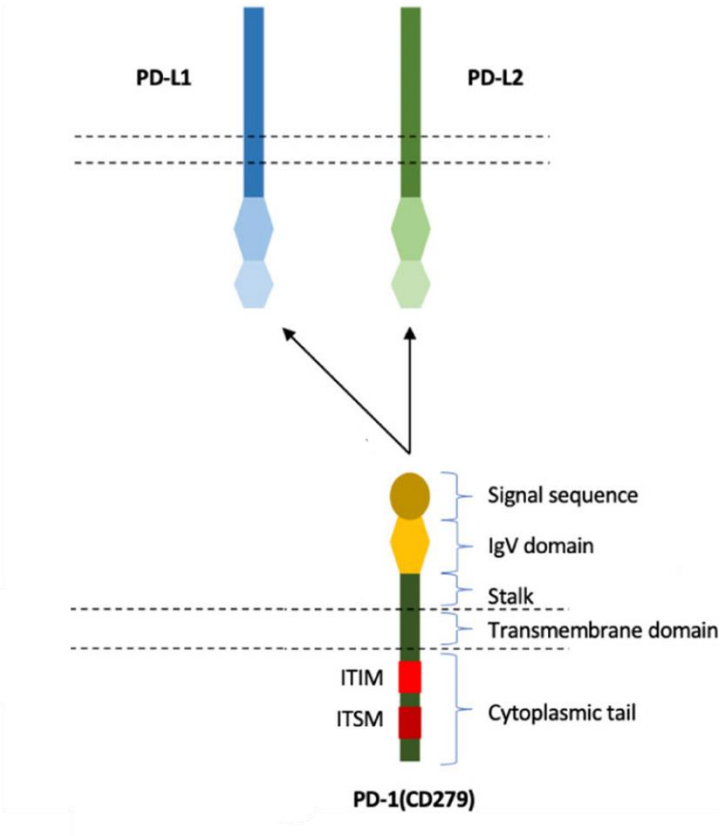

Fig. 6 Structure and ligands of PD-1 receptor.
Schematic view of PD-1 structure and its ligands. PD-1: Programmed cell death-1. From *Khan et al. Frontiers in Immunology, 2020.*

PD-1 can be found on the surface of a plethora of immune cells, belonging to both the innate and the adaptive immune system, as T cells, B cells, NK cells, monocytes, DCs and macrophages [28–31].

2.2 PD-1 signaling pathways

Upon binding to its ligands, PD-1 is phosphorylated on the tyrosine motifs of the ITSM domain by Scr homology region 2 domain-containing phosphatase-2 (SHP-2). The downstream effects of PD-1 ligation consist of the inhibition of phosphatidylinositol 3-kinase (PI3K)/protein kinase B (Akt), mammalian target of rapamycin (mTOR) and mitogen-activated protein kinase (MAPK) pathways [32]. It is also reported that, In T and myeloid cells, PD-1 signaling involves the blockade of phospholipase C_γ (PLC_γ) and extracellular-signal regulated kinase (ERK) pathways and the inhibition of janus kinase

(JAK)/STAT signaling cascade [33,34]. The blockade of these pathways inhibits immune cell functionality, proliferation, cytokine production and can lead to death of activated T cells. On the other hand, in tumor cells, as melanoma cells, the same signaling pathways are activated upon PD-1 interaction with its ligands [32,35,36], making cancer cells able to escape the local immune surveillance and finally promoting tumor growth.

A

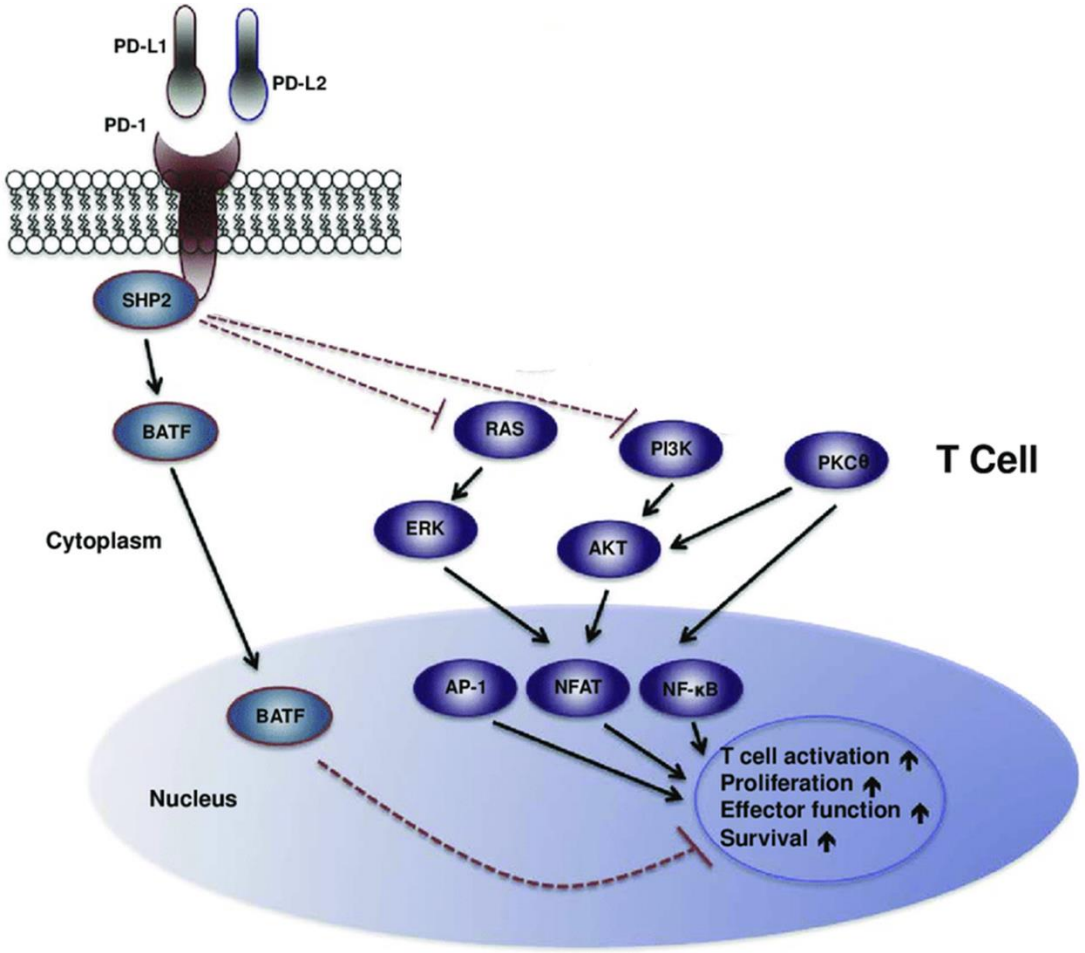

B

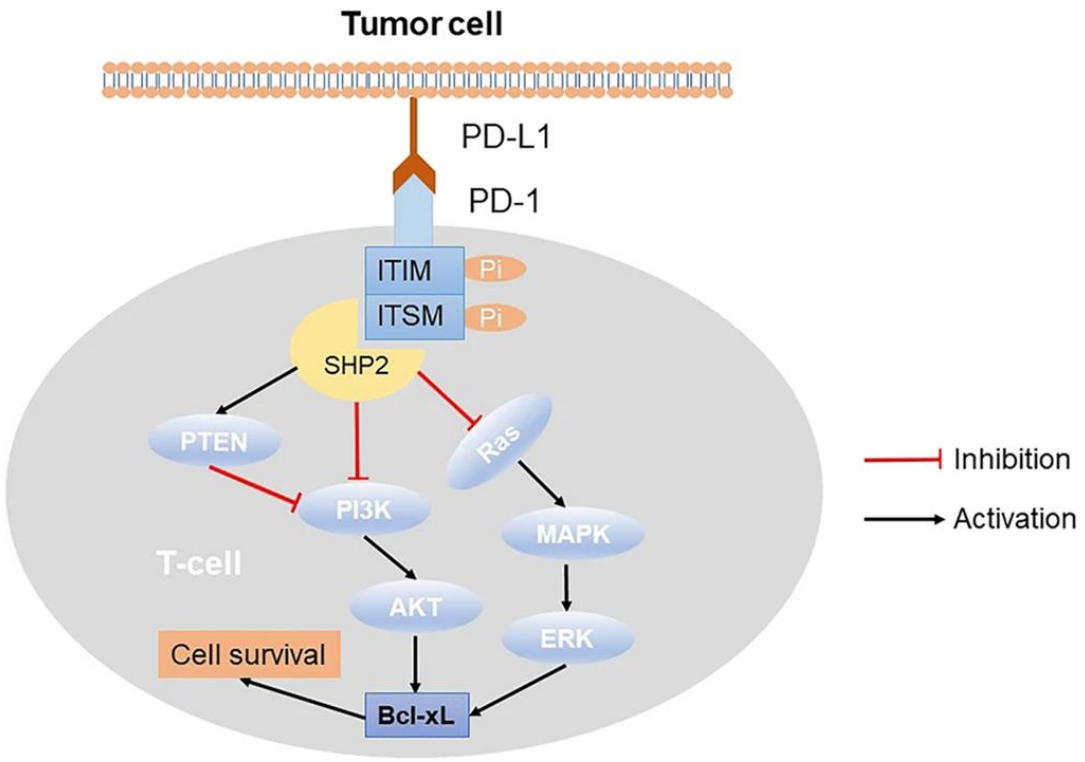

Fig. 7 PD-1 signaling in T cells and tumor cells.
Schematic representation of PD-1 signaling pathway. (A) PD-1 signaling in T cells. (B) PD-1 signaling in tumor cells. PD-1: Programmed cell death-1. Adapted from *Wu et al. Acta Pharmacologica Sinica, 2021; Wu et al. Computational and Structural Biotechnology Journal, 2019.*

2.3 Role of PD-1 in cancer

In physiological condition, PD-1 prevents an uncontrolled and harmful activation of the immune system and autoimmune reactions, suppressing both the innate and the adaptive immune response [37]. However, PD-1 engagement could be also exploited by cancer cells to escape the immune surveillance, facilitating tumor growth [38]. The expression of PD-1 ligands by tumors can activate PD-1 signaling, for example, in tumor infiltrating lymphocytes (TILs), determining T cell exhaustion eventually leading to an increased tumorigenesis and invasiveness [39,40]. Among PD-1^{+} immune cells infiltrating the tumor microenvironment, even tumor associated macrophages (TAMs), have been discovered to express PD-1 [41]. The engagement of PD-1 in TAMs reprograms macrophages towards a pro-tumor phenotype which cooperate to exacerbate the immune suppression [33,42].

Moreover, PD-1 ligation on TAMs stimulates the release of biochemical mediators that suppress T cell functions and lead to the restriction of T cell-mediated antitumor response [42].

2.4 Targeting PD-1/PD-Ls axis in cancer immunotherapy

Considering that PD-1/PD-Ls signaling pathway is responsible for the suppression of immune response and, consequently, tumor progression, the disruption of this axis has been recently targeted as a novel pharmacological approach in cancer treatment.

Today, there are several anti-PD-1 antibodies able to block the binding between PD-1 and PD-L1 utilized in the clinical practice. [43]. Nivolumab is an IgG4 anti-PD-1 antibody that has been approved for the treatment of metastatic melanoma, metastatic squamous non-small cell lung cancer (NSCLC), Hodgkin's lymphoma, and hepatocellular carcinoma [44–46]. Pembrolizumab is another anti-PD-1 antibody administered in metastatic melanoma, NSCLC, urothelial carcinoma, non-Hodgkin's lymphoma and head and neck squamous cell carcinoma patients [47–50]. Cemiplimab exhibits a high affinity for PD-1 and it is used in the immunotherapy of advanced cutaneous squamous cell carcinoma (CSCC) [51].

Results of different clinical trials highlighted the undoubted benefits of anti-PD-1 immunotherapy [52–54]. However, a considerable percentage of cancer patients did not take advantage from this regimen, and most of them develop resistance over time [55–58]. The efficacy outcomes of clinical trials are summarized in Table 5.

Anti-PD-1 antibody	Efficacy outcome	Tumor
Nivolumab	30% partial/complete responders	Malignant pleural mesothelioma
	38% resistant patients among initially responders	Melanoma
	65% resistant patients among initially responders	NSCLC
Pembrolizumab	11% partial/complete responders	Advanced gastric cancer

Table 5 Efficacy outcomes of anti-PD-1 antibodies in clinical trials.
Summary of efficacy outcomes of anti-PD-1 antibodies in clinical trials. NSCLC: non-small cell lung cancer.

2.4.1 Anti-PD-1 antibody and TLR9 agonist combinatorial treatment in cancer therapy

Considering that a considerable percentage of cancer patients failed to respond to anti-PD-1 antibody therapy, these agents have been tested in combination with other pharmacological approaches, such as TLR9 synthetic agonists. TLR9 stimulation combined with the blockade of PD-1 receptor has been studied in both preclinical and clinical trials [59]. In murine bladder cancer, longer survival was observed when animals were treated with CpG-ODN/anti-PD-1 antibody combination treatment [60]. In colon and head and neck cancer, CpG-ODN was able to revert resistance to anti-PD-1 antibody [61–63]. The encouraging results of such preclinical studies provided the rationale for clinical evaluation of combinatorial regimen. In advanced melanoma patients resistant to Pembrolizumab monotherapy, the association with CpG-ODN was able to produce a percentage of responding patient of 22% and triggered metastasis and tumor shrinkage [64]. In another clinical study, Pembrolizumab combined with TLR9 agonist produced 78% of responding patients. Moreover, compared to anti-PD-1 antibody monotherapy, the combination regimen increased the percentage of partial or complete response up to 13% in advanced melanoma patients [65].

3. Macrophages

3.1 Role of macrophages in innate immunity

Macrophages are considered the front-line cells of the innate immunity, since they recognize and rapidly respond to pathogen-associated molecular patterns (PAMPs) through pattern recognition receptors (PRRs), such as TLRs, providing a prompt immune response against pathogens [66]. The binding of PRRs with PAMPs leads macrophages to trigger a pro-inflammatory response, culminating with the release of antimicrobial factors,

that directly target the pathogen, and of chemokines and cytokines. Macrophage activation determines the recruitment of other immune cells to the site of the inflammation and orchestrates the adaptive immune response via stimulation of T and B lymphocytes activity. [67,68].

3.2 Phenotype heterogeneity of macrophages

Macrophages exhibit a variety of different phenotypes, each of them with peculiar biological functions and cellular morphology. These phenotypes are historically defined as M0 to M1 and M2 and this classification system is mainly based on the release of the inflammatory cytokines and other immunomodulatory molecules, together with the expression of specific transcriptional factors and the role played during inflammation process. The characteristics peculiar of each macrophage phenotype are summarized in Table 5.

M0 are reported as resting non-polarized macrophages that can give rise to a plethora of distinct macrophage subsets with broad spectrum of phenotypes upon exposure to different stimuli [69].

Phenotype	Stimuli	Secreted mediators	Functions
M1	IFN-γ, LPS, TNF-α, GM-CSF	TNF-α, IL-12, IL-1β, IL-6, IL-23, CCL2, CCL3, CCL4, CCL5, MMP1, MMP3, MMP9, iNOS	Pro-inflammation, host defense, tumor resistance, bacterial killing
M2a	IL-4, IL-13	IL-10, TGF-β, IL-1Ra, CCL17, CCL18, CCL22, CCL24	Anti-inflammatory, tissue repair, wound healing, allergy
M2b	Immune complexes, TLR ligands, IL-1β	TNF-α, IL-1β, IL-6, IL-10, CCL1	Immunoregulation, phagocytosis, high oxidative capacity
M2c	IL-10, TGF-β, glucocorticoids	IL-10, TGF-β, CCL16, CCL18, CXCL13	Immunoregulation, phagocytosis, matrix deposition, tissue remodeling

Tab. 6 Macrophage subsets and their characteristics.
Macrophage phenotypes, stimuli, secreted mediators and functions. IFN-γ: interferon γ; LPS: lipopolysaccharide; TNF-α: tumor necrosis factor α; GM-CSF: granulocyte-

macrophage colony-stimulating factor; IL-12: inerleukin 12; IL-1β: interleukin 1 β; IL-10: interleukin 10; IL-4: interleukin 4; IL-13: interleukin 13; IL-1Ra: interleukin 1 receptor agonist; CCL1: C-C motif chemokine ligand 1; CCL2: C-C motif chemokine ligand 2; CCL3: C-C motif chemokine ligand 3; CCL4: C-C motif chemokine ligand 4; CCL5: C-C motif chemokine ligand 5; CCL16: C-C motif chemokine ligand 16; CCL17: C-C motif chemokine ligand 17; CCL18: C-C motif chemokine ligand 18; CCL22: C-C motif chemokine ligand 22; CCL24: C-C motif chemokine ligand 24; MMP1: matrix metallopeptidase 1; MMP3: matrix metallopeptidase 3; MMP9: matrix metallopeptidase 9; iNOS: inducible nictrix oxide synthase; TGF- β: transforming growth factor β; TLR: toll-like receptor; CXCL13: chemokine C-X-C motif ligand 13.

3.2.1 M1: classically-activated macrophages

M1 macrophages or “classically activated macrophages” take part in antigen presentation and participate in antimicrobial, anti-tumor and inflammatory response. Upon stimulation via IFN-γ and TNF-α released by Th1 lymphocytes and NK cells, M1 macrophages produce inflammatory cytokines, as IL-6, IL-12 and TNF-α, to exert antitumor functions. The polarization of macrophages towards an M1 state is also possible following TLRs ligation [70].

3.2.2 M2: alternatively-activated macrophages

M2 macrophages are known as “alternatively activated macrophages” and exhibit biological functions diametrically opposed to M1 activity. This immunosuppressive, anti-inflammatory and pro-tumor phenotype of macrophages is triggered by IL-4 and IL-13, secreted by Th2 lymphocytes. Beside sharing the production of inflammatory cytokine as TNF and IL-12 with M1 macrophages, M2-polarized cells also secrete TGF-β, VEGF, matrix metalloproteinase 9 and IL-10.

Peculiar M2 marker genes include Arginase I (Arg I) [71], CD206 [72], IL1RN, FIZZ1 [73]. Within the M2 polarization state, further subtypes have been identified: M2a, M2b and M2c.

M2a macrophages show high anti-inflammatory activity and are commonly found in the tumor bed, thus being included in the so called “tumor-associated macrophages” (TAMs),

a particular subset of macrophages taking part in the complex immune infiltrate present in the tumor mass. The polarization towards an M2a phenotype predominantly results upon IL-4 and IL-13, that after the binding with IL-4Rα are able to activate and phosphorylate STAT6 [74]. Peroxisome proliferator activated receptor γ (PPARγ) and PPARδ are other transcription factors able to trigger the M2a phenotype [75,76].

The macrophage M2b subtype results from the combined stimulation of TLRs and Fc receptors by the Fc domain of immunoglobulins.

Finally, M2c macrophage derive from IL-10 stimulation [77–80].

AIM

TLR9 synthetic agonists are known to activate immune cells and have been extensively tested for the treatment of different types of tumor but no satisfied results have been achieved. Indeed, the induction of an immune response mediated by TLR9 stimulation is paralleled by the induction of negative feedback mechanisms, such as PD-1 induction, exploited to prevent uncontrolled and potentially harmful inflammatory reactions. PD-1 is reported to be expressed by adaptive and innate immune cells and it is associated with development of cellular dysfunction. Inhibiting PD-1 can restore the activity of immune system but only 30% of patients with advanced cancer can benefit of this kind of therapy.

Therefore, a combinatorial immunotherapeutic regimen based on the simultaneous activation of the immune system, by TLR9 agonist administration, and on the blocking of an immunosuppressive mechanism, by anti-PD-1 antibody treatment, has the potential to be effective. The efficacy of this combination therapy has been deeply investigated in several clinical and preclinical studies that mainly investigated the role played by the adaptive immune system. Considering that TLR9 agonists especially target innate immune cells and PD-1 can be also expressed by the innate immune system, the aim of the present study was to evaluate the contribution of the innate immune cells to the final outcome of this combinatorial therapy.

MATERIALS AND METHODS

1. Cell culture

IGROV-1 human ovarian cancer cell line (kind gift of Dr. J. Benard, Institute Gustave Roussy, Villejuif, France) and YAC-1 mouse lymphoma tumor cell lines (ATCC, Manassas, VA, USA) were cultured in RPMI 1640 medium with glutamine (Thermo Fisher Scientific Inc., Waltham, MA, USA) supplemented with 10% fetal bovine serum (FBS, Thermo Fisher Scientific Inc., Waltham, MA, USA). RAW264.7 macrophage-like cell line (ATCC, Manassas, VA, USA) was cultured in DMEM medium with glutamine (Thermo Fisher Scientific Inc., Waltham, MA, USA) supplemented with 10% FBS (Thermo Fisher Scientific Inc., Waltham, MA, USA). Cells were maintained at 37 °C in a 5% CO_2 atmosphere. Cell lines were tested for Mycoplasma using a specific kit (MycoAlert Mycoplasma Detection Kit, Lonza Group Ltd., Basel, Switzerland).

2. *In vivo* experiments

In vivo experiments were performed in the Animal Facility of the Fondazione IRCCS Istituto Nazionale dei Tumori (Milan, Italy) in a thermostatically maintained animal house following a 12 hours light/dark cycle. Mice were provided *ad libitum* access to food and water. Animal experiments were authorized by the Institutional Animal Welfare Body and the Italian Ministry of Health and performed in accordance with national law (D.lgs 26/2014) and the Guidelines for the Welfare of Animals in Experimental Neoplasia [81]. Athymic female nude mice (8-week-old; Charles River Laboratories, Calco, Italy) underwent intraperitoneal (i.p.) injection with IGROV-1 cells (2.5×10^6 cells/mouse) resuspended in 200μl of saline solution. After 7 days from tumor cell injection, mice were injected with 20 μg/mouse of purified phosphorothioated ODN1826

(5′-TCCATGACGTTCCTGACGTT-3′) containing CpG motifs (CpG-ODN; TriLink Biotechnologies, San Diego, CA, USA) delivered i.p. for 5 days/week for 3 consecutive weeks, with 200 µg/mouse of monoclonal rat or hamster anti-mouse PD-1 antibodies (clones RMP1-14 or J43 respectively; BioXCell, West Lebanon, NH, USA) administered i.p. twice a week for 3 consecutive weeks, alone or combined together. Control group received saline. The dose of CpG-ODN administered to mice was selected based on a dose-response curve evaluating the effects on cytokine production *in vivo* [82] and on previous *in vivo* experiments carried out in IGROV-1 i.p. xenograft model [83]. Macrophage depletion was performed before the initiation of CpG-ODN/anti-PD-1 immunotherapy. Specifically, mice xenografted with IGROV-1cells, were injected i.p. with 400 µL of liposomal clodronate (ClodronateLiposomes.com, Amsterdam, The Netherlands) three days after tumor cell injection and then treated as described above. The experimental group of mice treated with empty control liposomes was not included based on previously published data, obtained in IGROV-1 xenograft model, showing no effects of control liposomes on peritoneal macrophage population [84]. Animals were daily inspected and weighed three times/week. Ascites appearance was utilized as indicator of tumor growth and mice were sacrificed at the first evidence of ascites by cervical dislocation. The percentage of disease-free mice in each treatment group was calculated by the Kaplan–Meier product-limit method and compared with the log-rank (Mantel–Cox) test.

3. Fluorescence activated cell sorting (FACS) analysis

3.1 FACS analysis on mouse peritoneal cells

8-week-old female athymic nude mice (Charles River Laboratories, Calco, Italy) were treated with saline or 20 µg/mouse CpG-ODN by i.p. injection for 4 consecutive days. At

the end of treatment, mice were sacrificed by cervical dislocation and peritoneal cells were obtained by peritoneal lavage with cold phosphate buffered saline (PBS) supplemented with 3% FBS (Thermo Fisher Scientific Inc., Waltham, MA, USA) [85]. The obtained peritoneal cells were stained with anti-mouse CD45-FITC (eBioscience-Thermo Fisher Scientific Inc., Waltham, MA, USA) and anti-mouse PD-1-APC (eBioscience-Thermo Fisher Scientific Inc., Waltham, MA, USA) antibodies diluted in 1% bovin serum albumin (BSA)/PBS (Merk, Darmstadt, Germany), for 30 min at 4 °C. To avoid unspecific binding to mouse Fc receptors, cells were also incubated with a purified rat anti-mouse CD16/CD32 monoclonal antibody (clone 2.4G2; eBioscience-Thermo Fisher Scientific Inc., Waltham, MA, USA). After washing, samples were acquired using a FACSCanto flow cytometer (BD Biosciences, San Jose, CA, USA) and analyzed with FlowJo software (FlowJo LCC, Ashland, OR, USA). Analyses were performed by gating live $CD45^+$ cells after doublet exclusion.

3.2 FACS analysis on RAW264.7 macrophage cell line

RAW264.7 macrophages (8×10^5 cells/well) were seeded in 12-well plates (Corning, Glendale, AZ, USA) and stimulated with 1 µM CpG-ODN or left untreated for 6 hours. At the end of the treatment, RAW264.7 cells were detached from plates utilizing TrypLE Select enzyme (Thermo Fisher Scientific Inc., Waltham, MA, USA) and incubated with 10 µg/mL anti-mouse PD-1 antibody (clone RMP1-14; BioXCell, West Lebanon, NH, USA) for 30 min at 4 °C. After washing, the cells were then exposed to a FITC anti-rat IgG (H+L) antibody (KPL, SeraCare Life Sciences, Milford, MA, USA), for 30 min at 4 °C. After washing, PD-1 expression in RAW264.7 macrophages was evaluated using a FACSCanto flow cytometer (BD Biosciences, San Jose, CA, USA) and analyzed with FlowJo software (FlowJo LCC, Ashland, OR, USA).

To evaluate CD80, CD86 and CD206 expression in RAW264.7 cell line, cells were cultured and treated as described above. Cells were then incubated with the following antibodies: anti-mouse CD80-PE (clone 16-10A1; BD Pharmingen, San Diego, CA, USA), anti-mouse CD86-APC-R700 (clone GL1; BD Biosciences, San Jose, CA, USA) or with anti-mouse CD206-PE (clone C068C2; Elabscience, Houston, TX, USA, clone C068C2) for 30 min at 4 °C. RAW264.7 were also incubated with a purified rat anti-mouse CD16/CD32 monoclonal antibody (eBioscience-Thermo Fisher Scientific Inc., Waltham, MA, USA) to prevent unspecific binding to mouse Fc receptors. After washing, samples were acquired by a BD FACSCelesta Cell Analyzer (BD Biosciences, San Jose, CA, USA) and analyzed with FlowJo software (FlowJo LCC, Ashland, OR, USA). Analyses were performed by gating live cells after doublet exclusion.

4. Immunofluorescence analysis

IGROV-1 tumors were fixed in 10% formalin, paraffin-embedded and cut by a rotator microtome (Leyca Biosystems, IL, USA) to obtain 4 μm thick sections [86]. After dewaxing and rehydration in a descending scale of ethanol, sections were processed for immunofluorescence analysis. For immunofluorescence, 0.01 M citrate buffer pH 6 was used for antigen retrieval, in autoclave at 90°C for 20 min. For autofluorescence quenching, sections were incubated with 1 M $NaBH_4$ for 10 min at RT. After saturation of unspecific binding sites with 3% BSA/PBS (Merk, Darmstadt, Germany) for 1 hour at RT, samples were stained with rat anti-mouse CD206 (BioLegend, San Diego, CA, USA) or anti-mouse IL-10-FITC conjugated (BD Biosciences, San Jose, CA, USA) at a dilution of 1:50, overnight at 4 °C. For CD206 immunostaining, goat anti-rat AlexaFluor 488 (Thermo Fisher Scientific Inc., Waltham, MA, USA) was utilized 1 hour at too temperature (RT) as a secondary antibody. Nuclei were counterstained with 4′,6-Diamidino-2-Phenylindole

Dihydrochloride (DAPI; Thermo Fisher Scientific Inc., Waltham, MA, USA) for 10 min at RT. Slides were mounted by ProLong Gold Antifade Mountant (Thermo Fisher Scientific Inc., Waltham, MA, USA). Analysis were performed by a Leica TCS SP8 X laser scanning confocal microscope (Leica Microsystems GmbH, Mannheim, Germany). The quantitative analysis of CD206 and IL-10 immunostaining was carried out using ImageJ 1.53, measuring the positive area on five randomly selected fields for each sample acquired with constant parameters [87].

5. *In vitro* studies on RAW264.7 macrophage cell line

RAW264.7 macrophages (8 x 10^5 cells/well) were seeded in 12-well plates (Corning, Glendale, AZ, USA) and treated for 6 hours with 1 µM CpG-ODN (TriLink Biotechnologies, San Diego, CA, USA), 10 µg/ml anti-mouse PD-1 antibody (clone RMP1-14; BioXCell, West Lebanon, NH, USA), 10 µg/ml anti-mouse PD-1 antibody Fc silent (clone RMP1-14; Absolute Antibody, Redcar, Cleveland, UK), 10 µg/ml anti-mouse PD-1 antibody $F(ab)_2$ (clone RMP1-14, BioXCell, West Lebanon, NH, USA produced as described in the work of Lo Russo et al. [71], rat anti-mouse CD16/CD32 monoclonal antibody (clone 2.4G2; eBioscience-Thermo Fisher Scientific Inc., Waltham, MA, USA) or rat IgG2a isotype control antibody (clone 2A3; BioXCell, West Lebanon, NH, USA). Untreated cells served as controls. Each experimental condition was run in triplicate and experiments were carried out at least three times.

6. Gene expression profile and bioinformatic analysis

Microarray analysis was performed at the Genomic Core Facility of the Fondazione IRCCS Istituto Nazionale dei Tumori (Milan, Italy). RAW264.7 cells (8 x 10^5 cells/well) were

seeded in 12-well plates (Corning, Glendale, AZ, USA) and treated for 6 hours with 1 µM CpG-ODN (TriLink Biotechnologies, San Diego, CA, USA), 10 µg/ml anti-mouse PD-1 antibody (clone RMP1-14; BioXCell, West Lebanon, NH, USA) alone or in combination. Untreated cells served as controls. Each experimental condition was run in triplicate. At the end of treatment, mRNA extraction was carried out using the RNeasy Mini Kit (Qiagen, Valencia, CA, USA), according to manufacturer's instructions. After RNA quality check by 4200TapeStation (Agilent Technologies, Santa Clara, CA, USA) and quantification by Qubit Fluorometer (ThermoFisher Scientific, Waltham, MA, USA), RNA expression was evaluated using Clariom S Assay, mouse (ThermoFisher Scientific, Waltham, MA, USA) according to the manufacturer's instructions. Raw data from Clariom S Assay .CEL files were imported in the Transcriptomic Analysis Console (TAC, version 4.0.2.15; Thermo Fisher Scientific Inc.) and normalized using the robust multichip average (RMA) algorithm. Principal Component Analysis (PCA) analysis was generated by TAC software (Thermo Fisher Scientific Inc.). Enrichment analysis was performed using Gene Set Enrichment Analysis (GSEA) Desktop Application v4.2.3.0 (http://www.broadinstitute.org/gsea/index.jsp) with the Reactome collection, retrieved from the molecular signature database (https://www.gsea-msigdb.org/gsea/msigdb/genesets.jsp?collection=CP:REACTOME). Pathways with FDR q value < 0.05 were considered statistically significant.

7. Quantitative real-time PCR analysis

RAW264.7 cells (8 x 10^5 cells/well) were seeded in 12-well plates (Corning, Glendale, AZ, USA) and treated for 6 hours with 1 µM CpG-ODN (TriLink Biotechnologies, San Diego, CA, USA) alone or in combination with 10 µg/ml anti-mouse PD-1 antibody (clone RMP1-14; BioXCell, West Lebanon, NH, USA), or 10 µg/ml anti-mouse PD-1 antibody $F(ab)_2$

(clone RMP1-14; BioXCell, West Lebanon, NH, USA), or 10 µg/ml anti-mouse PD-1 antibody Fc silent (clone RMP1-14; Absolute Antibody, Redcar, Cleveland, UK), or rat IgG2a isotype control antibody (clone 2A3; BioXCell, West Lebanon, NH, USA). Anti-mouse PD-1 antibody $F(ab)_2$ was produced as described in the work of Lo Russo et al. [71]. In some experiments, in addition to the aforementioned treatments, cells were also incubated with rat anti-mouse CD16/CD32 monoclonal antibody (clone 2.4G2; eBioscience-Thermo Fisher Scientific Inc., Waltham, MA, USA). Untreated cells served as controls. Each experimental condition was run in triplicate and experiments were carried out at least three times. At the end of treatment, mRNA from RAW264.7 was extracted by Direct-zol RNA MicroPrep kit (Zymo Research, Irvine, CA, USA) and reverse-transcribed using a High-Capacity RNA-to-cDNA kit (Applied Biosystems-Thermo Fisher Scientific Inc., Waltham, MA, USA). Real-time PCR was performed with TaqMan Fast Universal PCR Master Mix (Applied Biosystems-Thermo Fisher Scientific Inc., Waltham, MA, USA) on a StepOne real-time PCR system (Applied Biosystems-Thermo Fisher Scientific Inc., Waltham, MA, USA). The utilized TaqMan gene expression assays (Applied Biosystems-Thermo Fisher Scientific Inc., Waltham, MA, USA) are reported in Table 7. The expression of each gene was normalized on β2m expression and real-time PCR data were analyzed by the comparative $2^{-\Delta\Delta Ct}$ method [88].

Gene symbol	Assay ID
β2m	Mm00437762_m1
Ccl1	Mm00441236_m1
Ccl2	Mm00441242_m1
Cd80	Mm00711660_m1
Cd86	Mm00444540_m1
Il-1β	Mm00434228_m1
Il-6	Mm00446190_m1
Il-10	Mm01288386_m1
IL-12b	Mm00434174_m1
Irf4	Mm00516431_m1
Irf5	Mm00496477_m1
Mertk	Mm00434920_m1
Nos2	Mm00440502_m1
Socs1	Mm00782550_s1
Socs2	Mm05820064_g1
Stat1	Mm01257286_m1
Stat6	Mm01160477_m1
Tnf-α	Mm00443258_m1
Trim21	Mm00447364_m1

Table 7 TaqMan gene expression assays for real-time PCR analysis.
List of TaqMan gene expression assays utilized for real-time PCR analysis.

8. Multiplex ELISA assay

For Multiplex ELISA assay, Bio-Plex Pro Mouse Cytokine 23-plex Assay kit (Bio-Rad Laboratories, Hercules, CA, USA) was used for the simultaneous quantification of IL-1α, IL-1β, IL-2, IL-3, IL-4, IL-5, IL-6, IL-9, IL-10, IL-12 (p40), IL-12 (p70), IL-13, IL-17A, Eotaxin, G-CSF, GM-CSF, IFN-γ, KC, MCP-1 (MCAF), MIP-1α, MIP-1β, RANTES, TNF-α. RAW264.7 cells (8 x 10^5 cells/well) were seeded in 12-well plates (Corning, Glendale, AZ, USA) and treated for 6 hours with 1 μM CpG-ODN (TriLink Biotechnologies, San Diego, CA, USA), 10 μg/ml anti-mouse PD-1 antibody (clone RMP1-14; BioXCell, West Lebanon, NH, USA) alone or in combination. At the end of treatment, medium was replaced with 1.5

ml of fresh medium without FBS (DMEM). Supernatants were collected 24 hours later. Untreated cells served as controls. Each experimental condition was run in quadruplicate. For BioPlex analysis, BSA (0.5% final concentration) was added to each supernatant. Samples were incubated on 96-well plate with polystyrene-beads coated with specific antibodies for 30 min at RT, and then exposed to detection antibodies for 30 min at RT prior incubation with Streptavidin-PE for 10 min at RT. Capture lysates were analyzed on the Bio-Plex200 system and all samples were assayed in duplicate. Results were expressed as observed concentrations (pg/ml). The observed concentrations that were below or above the out of range were considered as the first and the last concentration detected in the standard curves related to each cytokine, respectively. The final data were collectively visualized by Principal Component Analysis (PCA) performed using ClustVis 2.0 (https://biit.cs.ut.ee/clustvis/) [89].

9. Metabolomic analysis

Metabolomic analysis were conducted on supernatants of RAW264.7 after determining the protein concentration by Bradford's method. The untargeted metabolic analysis was performed in the UNITECH OMICs facility at Università degli Studi di Milano (Milan, Italy) using ExionLCTM AD system (SCIEX) connected to TripleTOFTM 6600 system (SCIEX) equipped with Turbo VTM Ion Source with ESI Probe. Chromatographic separation was achieved on a CORTECS UPLC T3 (Waters), 150 mm (length) x 2.1 mm (ID) x 1.6 m (particle size) using mobile phase A (0,1% formic acid in water) and mobile phase B (0,1% formic acid in acetonitrile) at a flow rate of 400 µl/min. The elution program is summarized in Table 8. The column and autosampler temperatures were set at 40°C and 10°C respectively. The sample injection volume was 15 µl. MS spectra were collected over an

m/z range of 50-1500 Da in positive and negative polarity, operating in Information Dependent Acquisition (IDA) mode. Collision energy was set at 30 (CES 15). Final data were analyzed by the software SCIEX OS 2.2 (SCIEXTM) integrated with the metabolomic database LibraryView 2.0 to compare the observed MS/MS spectrum to the database MS/MS spectra. The ratio peak area / IS area was normalized on protein concentration. The final data underwent PCA using Partek software (Partek).

N.	Time	Flow (µl/min)	%A	%B
1	0.00	Run		
2	0.00	400	99.0	1.0
3	2.00	400	99.0	1.0
4	6.00	400	75.0	25.0
5	10.00	400	5.0	95.0
6	15.00	400	5.0	95.0
7	15.20	400	99.0	1.0
8	20.00	400	99.0	1.0
9	20.00	Stop run		

Tab. 8 Program elution for high resolution mass spectrometry analysis (UHPLC-HRMS).

Program elution followed for UHPLC-HRMS in metabolomic analysis. A: mobile phase A; B: mobile phase B.

10. Generation of bone-marrow-derived macrophages (BMDMs) and isolation of NK cells

After sacrifice, femur and tibia of 8-week-old female healthy athymic nude mice (Charles River Laboratories, Calco, Italy) were dissected and all the tissue around the bones was removed. Each bone end was cut off and the bone marrow was isolated by perfusion with cold HBSS (Euroclone, Pero, MI, Italy). Erythtrocytes were lysed using ACK lysing buffer (Thermo Fisher Scientific Inc., Waltham, MA, USA) and after washing in PBS and filtering,

bone marrow cells were cultured in Iscove's Modified Dulbecco's Medium (IMDM, Thermo Fisher Scientific Inc., Waltham, MA, USA) supplemented with 10% FBS (Thermo Fisher Scientific Inc., Waltham, MA, USA) and 1% penicillin and streptomycin (Thermo Fisher Scientific Inc., Waltham, MA, USA) in 5% CO_2 at 37°C. After 24 h (day 0), the medium was replaced with fresh medium containing 20 ng/ml murine macrophage-colony stimulating factor (mM-CSF, PeproTech, Cranbury, NJ, USA). On day 3, the culture medium was replaced again with fresh medium supplemented with mM-CSF and differentiated BMDMs were finally harvested on day 7.

For NK isolation, spleen was dissected from the abdominal cavity of 8-week-old female healthy athymic nude mice (Charles River Laboratories, Calco, Italy) and gently flushed in HBSS to obtain splenocytes. To remove red cells, a red cell lysis buffer (RBC; Euroclone, Pero, MI, Italy) was used and NK cells were then isolated by a mouse NK cell isolation kit according to manufacturer's instructions (Miltenyi Biotec, Bergisch Gladbach, Germany).

11. *In vitro* cytotoxicity assay

BMDMs (8 x 10^5 cells/well) were seeded in 24-well plates (Corning, Glendale, AZ, USA) and treated with 1 µM CpG-ODN, 10 µg/ml anti-mouse PD-1 antibody alone or in combination. Untreated BMDMs served as control group. Each experimental group was run in triplicate. After 6 hours of treatment, medium was removed and spleen-derived NK cells were added to each BMDM well at the ratio of 1:1. NK cells were harvested 36 hours later and their cytotoxic activity was assayed. Specifically, YAC-1 target cells were labeled with 100 µCi ^{51}Cr (PerkinElmer, Waltham, MA, USA) for 1 hour at 37°C. After 3 washes with 5% FBS/PBS, YAC-1 cells were resuspended in IMDM supplemented with 10% FBS. NK cells were co-incubated for 4 hours at 37°C with labeled YAC-1 cells at the effector/target ratio of 50:1 in quadruplicate 96-well U bottomed plates (Corning, Glendale,

AZ, USA). At the end of the co-incubation, the supernatant radioactivity was measured using a Trilux Beta scintillation counter (PerkinElmer, Waltham, MA, USA). Results were expressed as percentage of lysis, calculated as [(experimental cpm - spontaneous cpm) / (maximum cpm-spontaneous cpm)] x 100.

12. Proteasome inhibition and Trim21 silencing on RAW264.7

RAW264.7 cells (8 x 10^5 cells/well) were seeded in 12-well plates (Corning, Glendale, AZ, USA) and treated for 6 hours as described above, in presence or not of the proteasome inhibitor MG132 (20 μM; Merck, Darmstadt, Germany). MG132 was added 30 min before the treatment with the immunotherapeutic drugs. At the end of the treatments, real-time PCR analysis were carried out as described above.

For Trim21 gene silencing, RAW264.7 (3 x 10^5 cells/well) were seeded in 12-well plates (Corning, Glendale, AZ, USA) and transfected with 50 nM ON-TARGETplus Mouse Trim21 siRNA or ON-TARGETplus Non-targeting Pool, as control, (Horizon Discovery, Cambridge, GB) in 1 ml of complete medium (DMEM supplemented with 10% FBS) for each well, according to the manufacturer's protocol. After 24 hours, cells were treated with CpG-ODNs and/or anti-PD-1 antibody, as above, for 6 hours. Each experimental condition was run in quadruplicate. At the end of treatment, real-time PCR analysis were carried out as previously described.

13. Western Blot analysis

Proteins were extracted from RAW264.7 silenced or not for Trim21 using TNTG buffer (50 mM Tris-HCl pH 7.5, 150 mM NaCl, 100 mM NaF, 10 mM sodium pyrophosphate, 10%

glycerol, 1% Triton X-100), supplemented with complete Mini Protease Inhibitor Cocktail (Merck, Darmstadt, Germany) and activated by 2 mM orthovanadate (Merck, Darmstadt, Germany). Bradford assay with CoomassiePlus Protein Assay Reagent (Thermo Fisher Scientific, Waltham, MA, USA) was used to quantify the protein extracts at the Ultrospec 2100 pro (GE Healthcare, Chicago, IL, USA) spectrophotometer. Proteins (30 µg) were fractionated on NuPAGE 10% gel (ThermoFisher Scientific, Waltham, MA, USA) and blotted onto nitrocellulose filters (American Biosciences, Buckinghamshire, UK) for 2 hours at constant 250 mA at 4°C. Filters were incubated at RT for 1 hour in TBS containing 0.1% Tween-20 (Merck, Darmstadt, Germany) and 5% skim milk powder (Genespin, Milan, Italy) to block aspecific binding sites, followed by rabbit anti-TRIM21 antibody (dilution 1:1000; Abcam, Cambridge, UK) incubation in 5% milk/TBS/0.1% Tween-20 solution, overnight at 4°C. Anti-rabbit secondary peroxidase-linked antibodies (dilution 1: 10000; Vector Laboratories, Bulringame, CA, USA) and mouse anti-β-actin peroxidase antibody (dilution 1:25000; Merck, Darmstadt, Germany) were finally used 1 hour at RT in 5% milk/TBS/0.1% Tween-20 solution and bands were visualized using ECL Western Blotting Detection Reagents (American Biosciences, Blauvelt, NY, USA). Quantification was performed by Quantity One 4.6.6 software (Bio-Rad, Hercules, CA, USA).

14. Statistical analysis

All the data are presented as mean ± SEM and statistical analysis were performed by GraphPad Prism (GraphPad Software, San Diego, CA, USA). Before performing statistical analysis, normal distribution of data was verified by normality tests. For comparisons between two experimental groups, a two-tailed unpaired Student's *t*-test was used for data with normal distribution, whilst the Mann-Whitney U test was applied for data without normal distribution. To compare three or more experimental groups, the one-way ANOVA

followed by Tukey's post-hoc multiple comparison test was used for parametric data, whereas the Kruskal-Wallis test followed by Dunn.'s post-hoc multiple comparison test was applied for non-parametric data. Differences were considered significant when $p < 0.05$.

RESULTS

1. TLR9 stimulation triggered by CpG-ODN treatment increases PD-1 expression on peritoneal immune cells

To verify PD-1 up-regulation after TLR9 stimulation in peritoneal immune cells, as already described in other tissues [90,91], flow-cytometry analysis was performed on $CD45^+$ cells isolated from the peritoneum of healthy athymic nude mice treated for 4 consecutive days with CpG-ODN. PD-1 expression was found to be increased in CpG-ODN-treated mice compared to control group (Fig. 8).

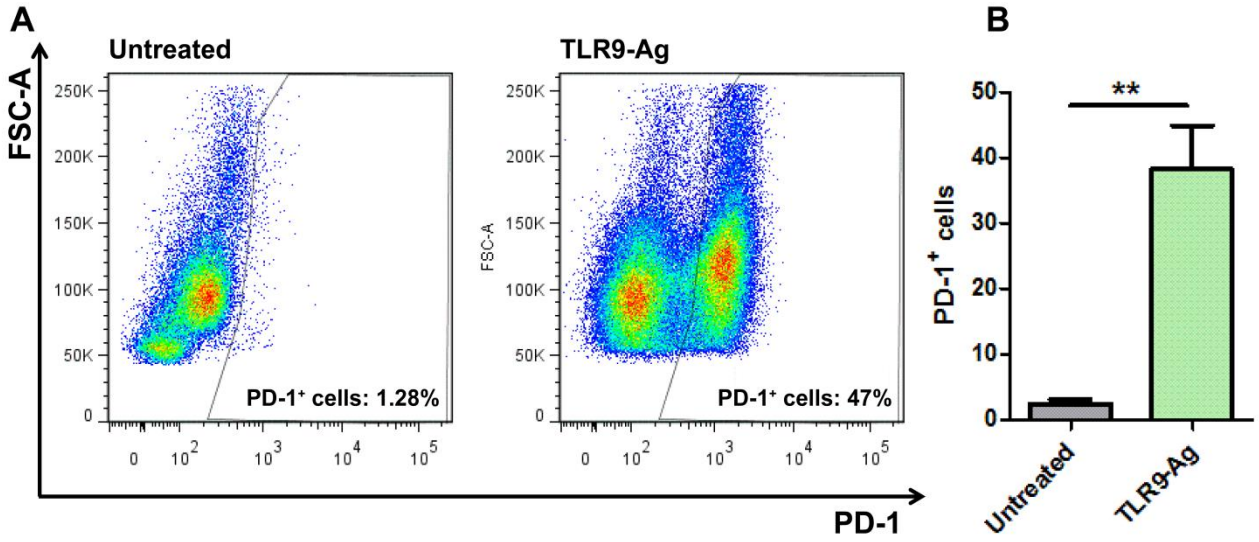

Fig. 8 FACS analysis for PD-1 expression on peritoneal immune cells of healthy athymic nude mice after treatment with CpG-ODN. Representative scatter dot plots (A) and quantification (B) of the percentage of PD-1+ cells, gated on CD45+ live cells, obtained by peritoneal lavage from healthy athymic nude mice (n=3 mice/group) treated with saline or with 20 µg/mouse CpG-ODN for 4 consecutive days. Data are expressed as mean ± SEM. ** $p<0.01$ by two-tailed unpaired Student's t-test. TLR9-Ag: TLR9 agonist (CpG oligodeoxynucletotides).

2. Effect of CpG-ODN and anti-PD-1 antibody combination in the treatment of IGROV-1 tumor-bearing mice

The efficacy of CpG-ODN/anti-PD-1 combination was tested in athymic nude mice peritoneally xenografted with IGROV-1 human ovarian cancer cells and treated with CpG-

ODN, anti-PD-1 antibody (clone RMP1-14) or their combination starting seven days after tumor cell injection. As already reported [84,92,93], tumor growth, evaluated as ascites appearance, was delayed in mice treated with TLR9 agonist alone compared to all the other experimental groups (TLR9-Ag group vs. Untreated group, p=0.0004 by the log-rank test; TLR9-Ag group vs. Anti-PD-1 Ab group, p=0.0005 by the log-rank test; TLR9-Ag group vs. Combination group, p=0.0079 by the log-rank test). Anti-PD-1 antibody, as single agent, didn't exert any antitumor activity, since the timing of ascites onset was comparable to that observed in control group (Anti-PD-1 Ab group vs. Untreated group, p=0.34 by the log-rank test). Interestingly, mice that received the combination therapy showed an acceleration of tumor development, observed as earlier ascites appearance compared to CpG-ODN-treated group. (Fig. 9).

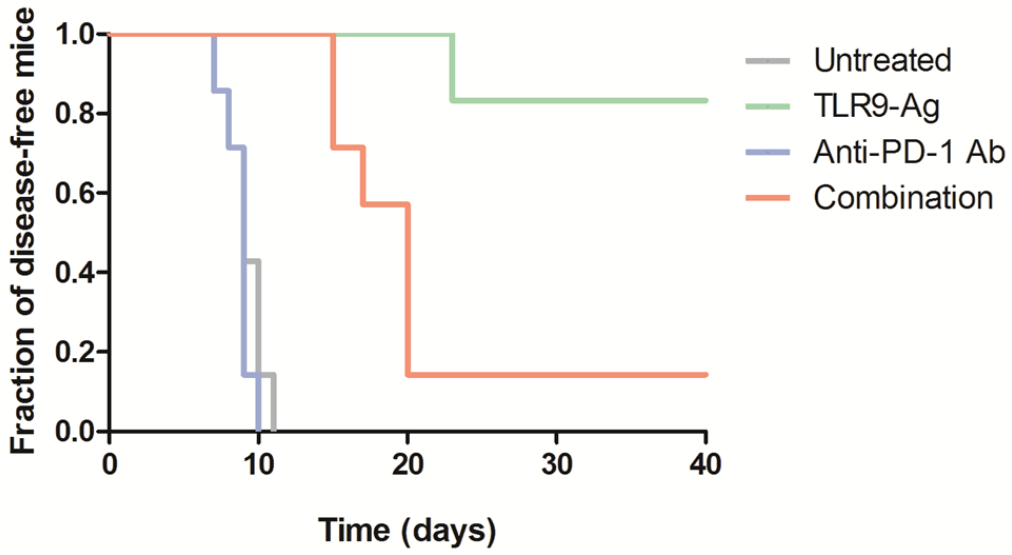

Fig. 9 Kaplan-Meier plot of disease-free mice injected with IGROV-1 cells and treated with CpG-ODN and/or anti-PD-1 antibody clone RMP1-14.
Kaplan-Meier plot of disease-free mice (n=8 mice/group) xenografted with IGROV-1 ovarian tumor cells and treated with CpG-ODN, anti-PD-1 antibody alone or in combination. Tumor-bearing mice were i.p. treated with 20 µg/mouse CpG-ODN (5 days/week for 3 weeks, starting 7 days from tumor cell injection), 200 µg/mouse anti-PD-1 antibody clone RMP1-14 (2 times/week for 3 weeks, starting 7 days from tumor cell injection), alone or in combination. Untreated group received saline. TLR9-Ag: TLR9 agonist (CpG oligodeoxynucletotides); anti-PD-1 Ab: anti-PD-1 antibody; Combination: CpG-ODN+anti-PD-1 antibody. Time on x-axis indicates the days from tumor cell injection.

The same experiment was then repeated using another anti-PD-1 antibody clone (J43). Again, a reduction of CpG-ODN anti-tumor efficacy was observed when co-administered with anti-PD-1 antibody compared to the monotherapy, corroborating the previous observations (Fig. 10).

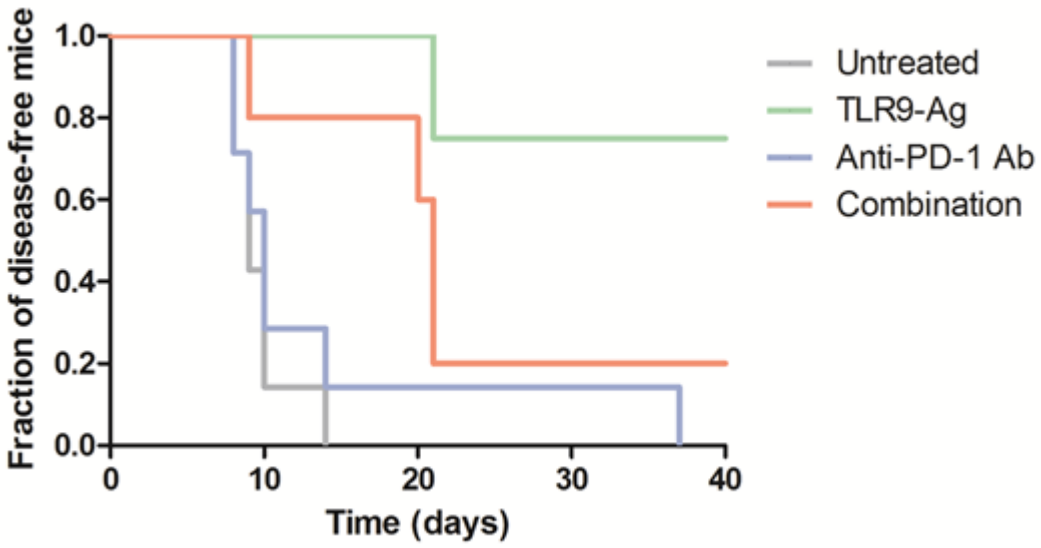

Fig. 10 Kaplan-Meier plot of disease-free mice injected with IGROV-1 cells and treated with CpG-ODN and/or anti-PD-1 antibody clone J43.
Kaplan-Meier plot of disease-free mice (n=8 mice/group) xenografted with IGROV-1 ovarian tumor cells and treated with CpG-ODN, anti-PD-1 antibody alone or in combination. Tumor-bearing mice were i.p. treated with 20 µg/mouse CpG-ODN (5 days/week for 3 weeks, starting 7 days from tumor cell injection), 200 µg/mouse anti-PD-1 Ab clone RMP1-14 (2 times/week for 3 weeks, starting 7 days from tumor cell injection), alone or in combination. Untreated group received saline. TLR9-Ag: TLR9 agonist (CpG oligodeoxynucletotides); anti-PD-1 Ab: anti-PD-1 antibody; Combination: CpG-ODN+anti-PD-1 antibody. Time on x-axis indicates the days from tumor cell injection.

3. CpG-ODN/anti-PD-1 antibody treatment increases M2-like macrophage infiltration in the tumor microenvironment

Macrophages with an M2-like phenotype are reported to be associated with a peculiar detrimental response, called hyperprogressive disease, that is characterized by an acceleration of tumor growth following anti-PD-1 antibody treatment [71]. To investigate

whether macrophages are also involved in the observed reduction of CpG-ODN efficacy upon anti-PD-1 antibody administration, immunofluorescence analysis were carried out on tumor sections to evaluate the expression of CD206 and IL-10, well-known M2 markers [72,94]. $CD206^{+}$ and $IL\text{-}10^{+}$ elements were clearly detectable in the tumor stroma of mice treated with the combinatorial regimen, whilst in the experimental group receiving the TLR9 agonist alone CD206 and IL-10 related immunostaining signals were barely observed (Fig. 11 A and 12 A). Immunofluorescence quantitative analysis showed a statistically significant increase of positive area for both CD206 (Fig. 11 B) and IL-10 (Fig. 12 B) after the combination compared to CpG-ODN-treated group, suggesting a possible M2-like phenotype for macrophages infiltrated in the tumor.

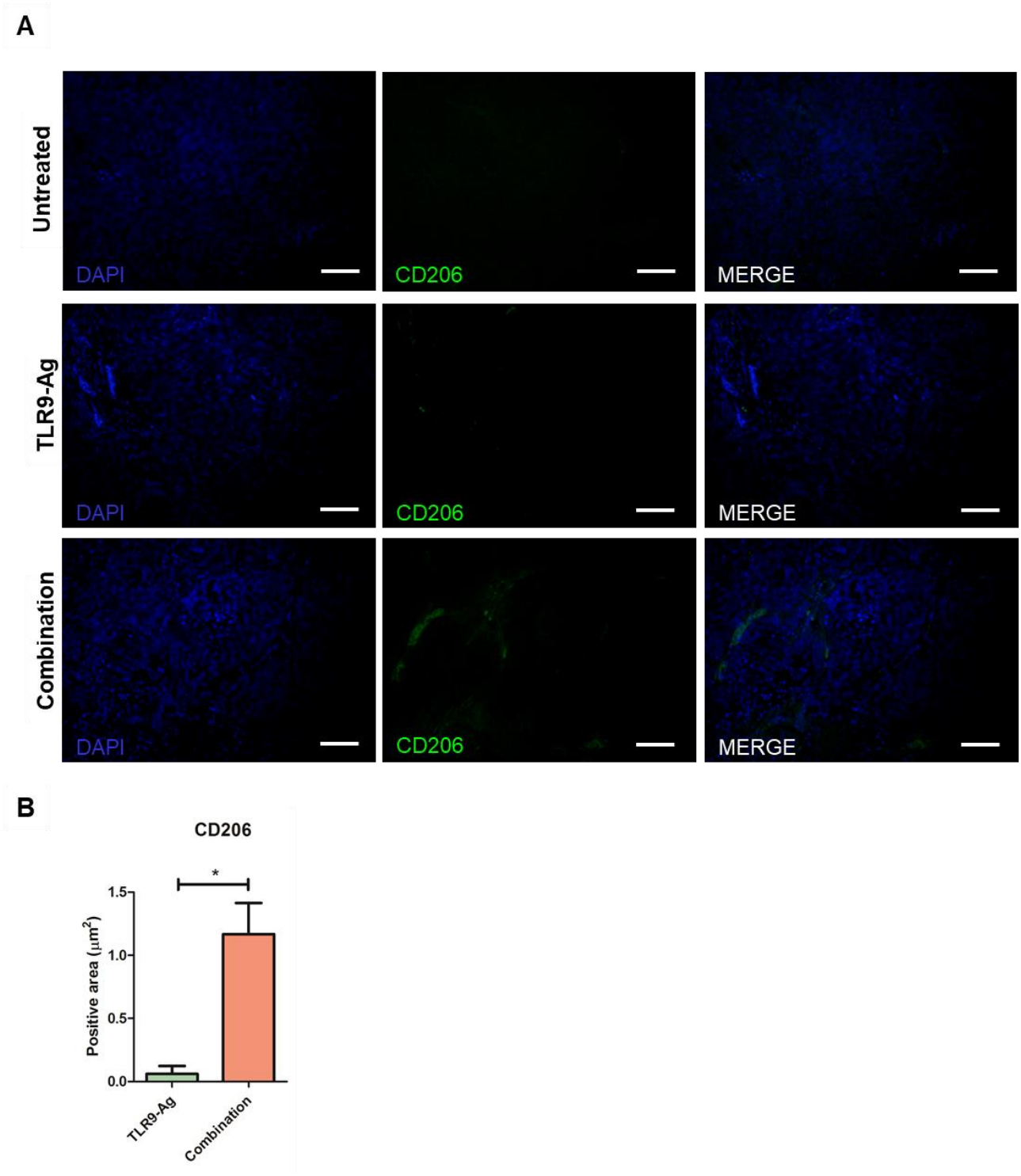

Fig. 11 CD206 immunofluorescence analysis on IGROV-1 tumors *in vivo* treated with CpG-ODN alone or in combination with anti-PD-1 antibody. Immunofluorescence and quantitative analysis of CD206 expression in tumor samples obtained from athymic nude mice xenografted with IGROV-1 cells and treated with 20 µg/mouse CpG-ODN alone (5 days/week for 3 weeks) or in combination with 200 µg/mouse monoclonal anti-mouse PD-1 antibody clone RMP1-14 (2 times/week for 3 weeks) starting 7 days from tumor cell injection. Untreated group received saline. (A) Representative photomicrographs of CD206 immunostaining (green). Nuclei were counterstained with DAPI (blue). (B) Quantitative analysis of CD206 positive area

measured on five random fields for each tumor sample (n=8) acquired with constant parameters. CD206: cluster of differentiation 206; DAPI: 4′,6-diamidino-2-phenylindole; TLR9-Ag: TLR9 agonist (CpG oligodeoxynucletotides); Combination: CpG-ODN+anti-PD-1 antibody. Data are expressed as mean ± SEM. * p<0.05 by Mann-Whitney U test. Bars: 40 µm.

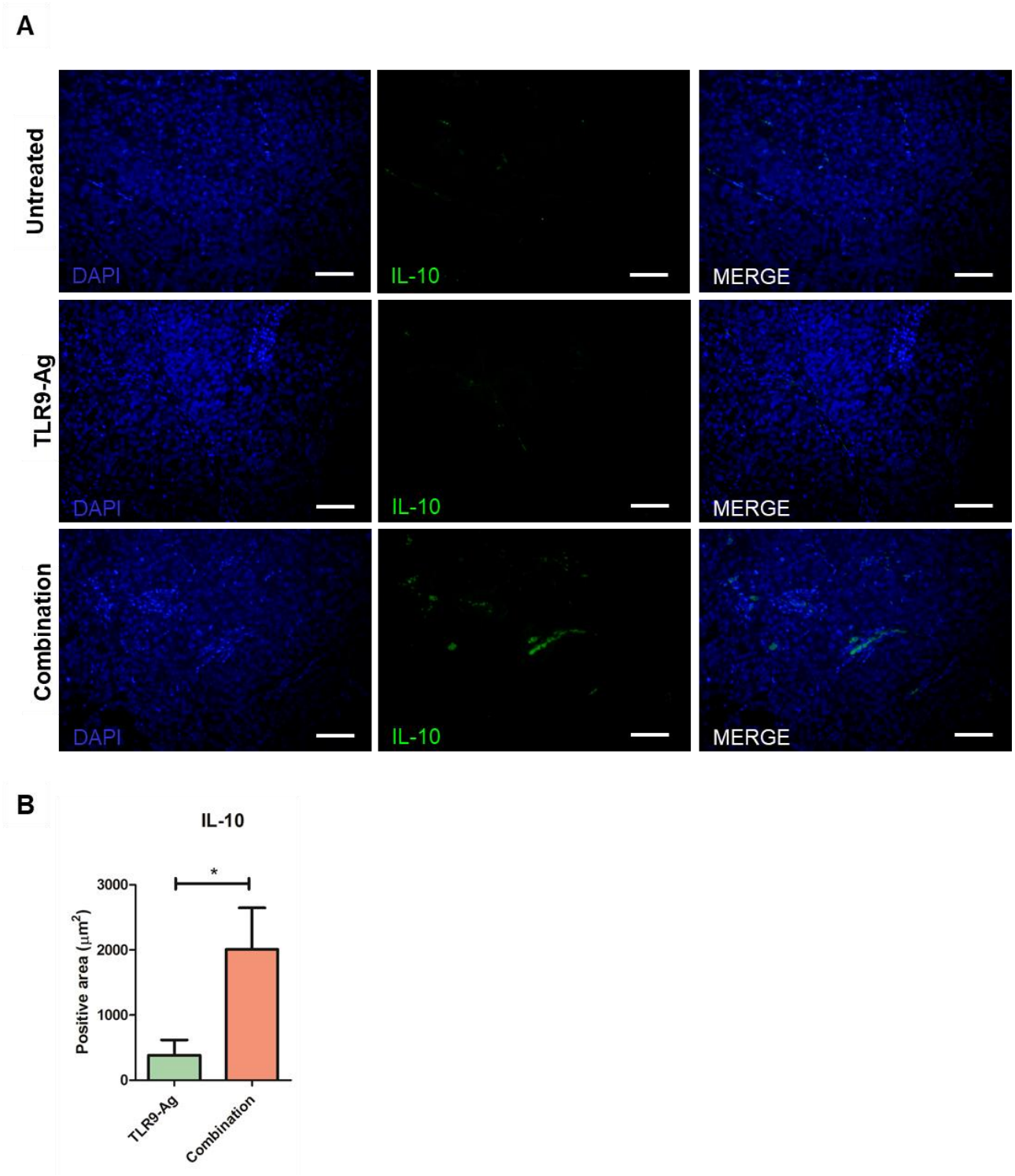

Fig. 12 IL-10 immunofluorescence analysis on IGROV-1 tumors *in vivo* treated with CpG-ODN alone or in combination with anti-PD-1 antibody.
Immunofluorescence and quantitative analysis of IL-10 expression in tumor samples obtained from athymic nude mice xenografted with IGROV-1 cells and treated with 20 µg/mouse CpG-ODN alone (5 days/week for 3 weeks) or in combination with 200 µg/mouse monoclonal anti-mouse PD-1 antibody clone RMP1-14 (2 times/week for 3 weeks) starting 7 days from tumor cell injection. Untreated group received saline. (A) Representative photomicrographs of IL-10 immunostaining (green). Nuclei were counterstained with DAPI (blue). (B) Quantitative analysis of IL-10 positive area measured on five random fields for each tumor sample (n=8) acquired with constant parameters. IL-10: interleukin 10; DAPI: 4′,6-diamidino-2-phenylindole; TLR9-Ag: TLR9 agonist (CpG oligodeoxynucletotides); Combination: CpG-ODN+anti-PD-1 antibody. Data are expressed as mean ± SEM. * $p<0.05$ by Mann-Whitney U test. Bars: 40 µm.

4. The impairment of antitumor activity of CpG-ODN after anti-PD-1 antibody co-administration is mediated by macrophages

To ascertain the role of macrophages in the impairment of antitumor efficacy of CpG-ODN in the dual treatment with anti-PD-1 antibody, macrophages were *in vivo* depleted by clodronate encapsulated in liposomes in athymic nude mice bearing IGROV-1 human ovarian cancer xenografts and treated as above. Clodronate administration slightly reduced the antitumor activity of CpG-ODN, but ascites was not significantly delayed after macrophage depletion (Clodronate+TLR9-Ag group vs TLR9-Ag group, p=0.2743 by the log-rank test). Interestingly, macrophage depletion nullified the negative effect of anti-PD-1 antibody on CpG-ODN efficacy, since the percentage of disease-free mice in the combination group was perfectly comparable to that of TLR9 agonist-treated animals (Clodronate+TLR9-Ag group vs Clodronate+Combination group, p=0.8056 by the log-rank test). As in the previous experiment, in anti-PD-1 Ab and in untreated group the time of appearance of ascites was extremely similar (Fig. 13).

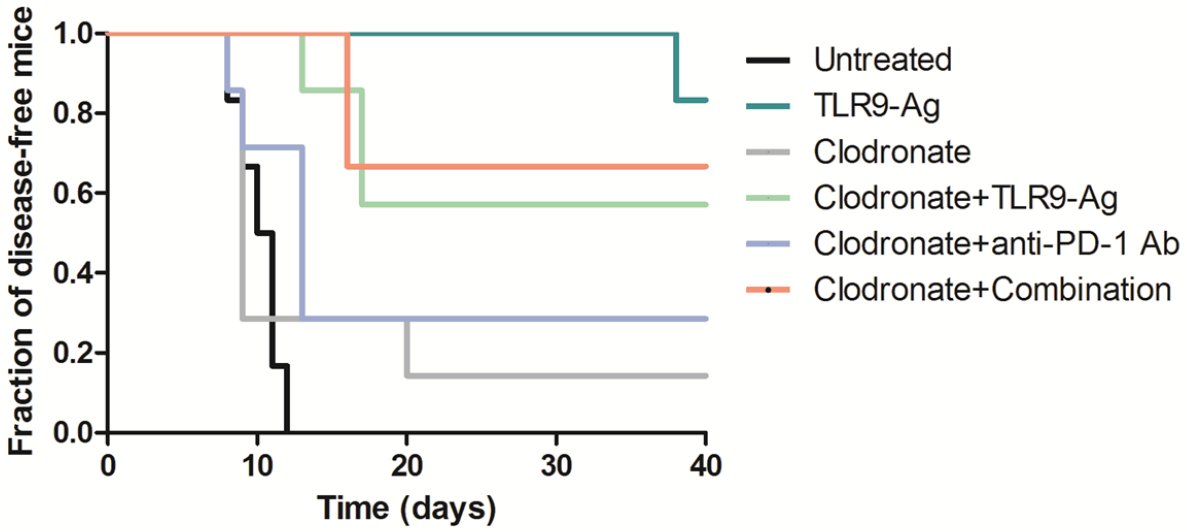

Fig. 13 Kaplan-Meier plot of disease-free mice injected with IGROV-1 cells and treated with CpG-ODN and/or anti-PD-1 antibody after macrophage depletion.
Kaplan-Meier plot of disease-free IGROV-1-tumor bearing mice (n=8 mice/group) treated with CpG-ODN, anti-PD-1 Ab, alone or in combination, after macrophage depletion. Mice were xenografted with IGROV-1 human ovarian cancer cells and were i.p. treated with clodronate delivered by liposomes 3 days after tumor cell injection. Four days after, animals were i.p. injected with 20 µg/mouse CpG-ODN (5 days/week for 3 weeks), 200 µg/mouse anti-PD-1 Ab clone RMP1-14 (2 times/week for 3 weeks), alone or in combination. Untreated group received saline. TLR9-Ag: TLR9 agonist (CpG oligodeoxynucletotides); anti-PD-1 Ab: anti-PD-1 antibody; Combination: CpG-ODN+anti-PD-1 antibody. Time on x-axis indicates the days from tumor cell injection.

5. Effects of CpG-ODN/anti-PD-1 antibody combinatorial treatment on macrophage phenotype

Since our *in vivo* experiments highlighted the role of macrophages in reducing the effect of CpG-ODN/anti-PD-1 antibody treatment and that M2 macrophages are reported to impair immunotherapy efficacy [95], *in vitro* experiments were carried to evaluate the phenotype acquired by macrophages after exposure to both drugs. RAW264.7 murine macrophage cell line was incubated with CpG-ODN, anti-PD-1 antibody or their combination for 6 hours. Control cells were left untreated. At the end of the treatment, mRNA was extracted and a comprehensive gene expression profile was performed. Principal component analysis performed on normalized data revealed the existence of four separate clusters

corresponding to the different four experimental groups. Interestingly, it is possible to appreciate that, while macrophages treated with single agents are in close proximity, RAW264.7 incubated with both CpG-ODN and anti-PD-1 antibody segregated apart from all the other experimental groups (Fig. 14).

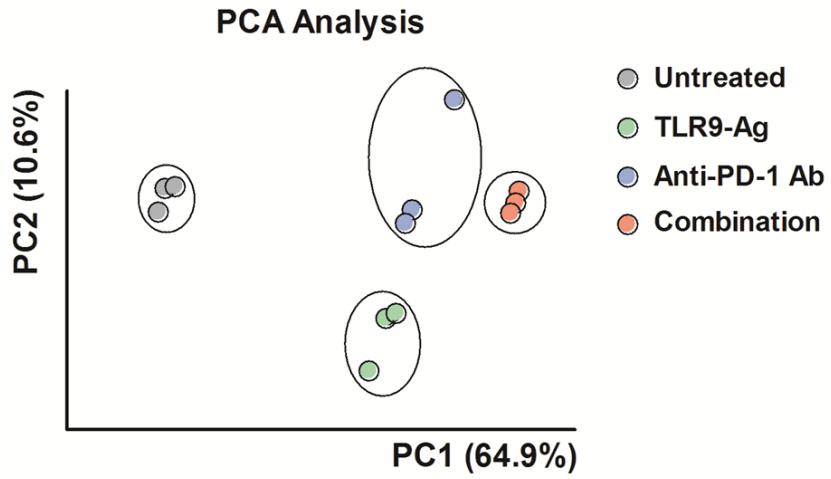

Fig. 14 Principal Component Analysis (PCA) on normalized gene expression profile data of RAW264.7 macrophages treated with CpG-ODN and anti-PD-1 antibody alone or in combination.
PCA based on transcriptional profile data performed on RAW264.7 macrophages exposed to CpG-ODN (1 µM), anti-PD-1 antibody clone RMP1-14 (10 µg/ml) or their combination for 6 hours. Controls were left untreated. Each group was run in triplicate. PCA: principal component analysis; TLR9-Ag: TLR9 agonist (CpG oligodeoxynucletotides); anti-PD-1 Ab: anti-PD-1 antibody; Combination: CpG-ODN+anti-PD-1 antibody.

Functional analysis, by GSEA, was conducted on the global gene expression profiling data. The combination group was compared to the single agents and to the control group.

A

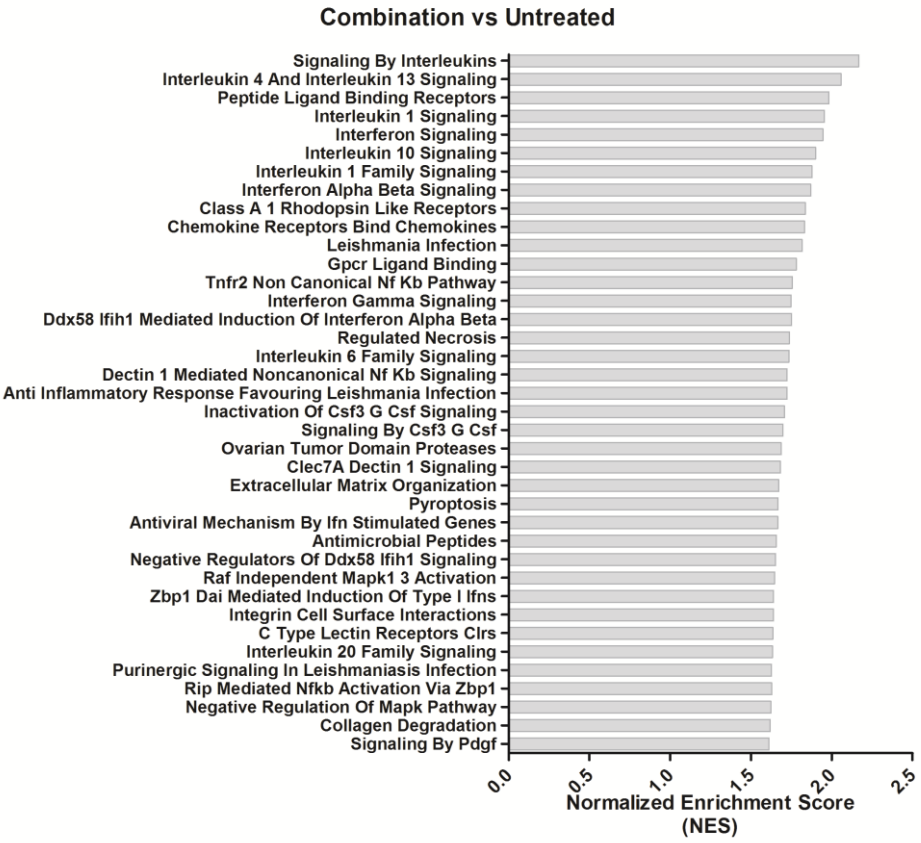
Combination vs Untreated
Signaling By Interleukins
Interleukin 4 And Interleukin 13 Signaling
Peptide Ligand Binding Receptors
Interleukin 1 Signaling
Interferon Signaling
Interleukin 10 Signaling
Interleukin 1 Family Signaling
Interferon Alpha Beta Signaling
Class A 1 Rhodopsin Like Receptors
Chemokine Receptors Bind Chemokines
Leishmania Infection
Gpcr Ligand Binding
Tnfr2 Non Canonical Nf Kb Pathway
Interferon Gamma Signaling
Ddx58 Ifih1 Mediated Induction Of Interferon Alpha Beta
Regulated Necrosis
Interleukin 6 Family Signaling
Dectin 1 Mediated Noncanonical Nf Kb Signaling
Anti Inflammatory Response Favouring Leishmania Infection
Inactivation Of Csf3 G Csf Signaling
Signaling By Csf3 G Csf
Ovarian Tumor Domain Proteases
Clec7A Dectin 1 Signaling
Extracellular Matrix Organization
Pyroptosis
Antiviral Mechanism By Ifn Stimulated Genes
Antimicrobial Peptides
Negative Regulators Of Ddx58 Ifih1 Signaling
Raf Independent Mapk1 3 Activation
Zbp1 Dai Mediated Induction Of Type I Ifns
Integrin Cell Surface Interactions
C Type Lectin Receptors Clrs
Interleukin 20 Family Signaling
Purinergic Signaling In Leishmaniasis Infection
Rip Mediated Nfkb Activation Via Zbp1
Negative Regulation Of Mapk Pathway
Collagen Degradation
Signaling By Pdgf
0.0
0.5
1.0
1.5
2.0
2.5
Normalized Enrichment Score
(NES)

B

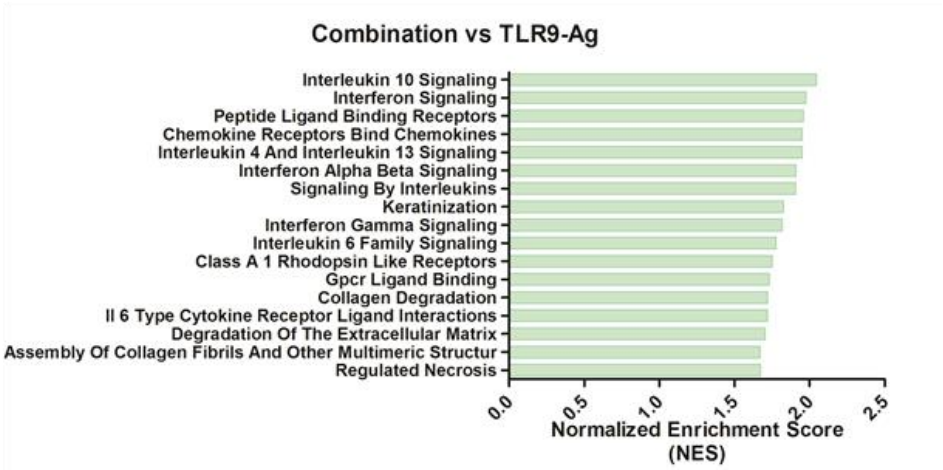
Combination vs TLR9-Ag
Interleukin 10 Signaling
Interferon Signaling
Peptide Ligand Binding Receptors
Chemokine Receptors Bind Chemokines
Interleukin 4 And Interleukin 13 Signaling
Interferon Alpha Beta Signaling
Signaling By Interleukins
Keratinization
Interferon Gamma Signaling
Interleukin 6 Family Signaling
Class A 1 Rhodopsin Like Receptors
Gpcr Ligand Binding
Collagen Degradation
Il 6 Type Cytokine Receptor Ligand Interactions
Degradation Of The Extracellular Matrix
Assembly Of Collagen Fibrils And Other Multimeric Structur
Regulated Necrosis
0.0
0.5
1.0
1.5
2.0
2.5
Normalized Enrichment Score
(NES)

C

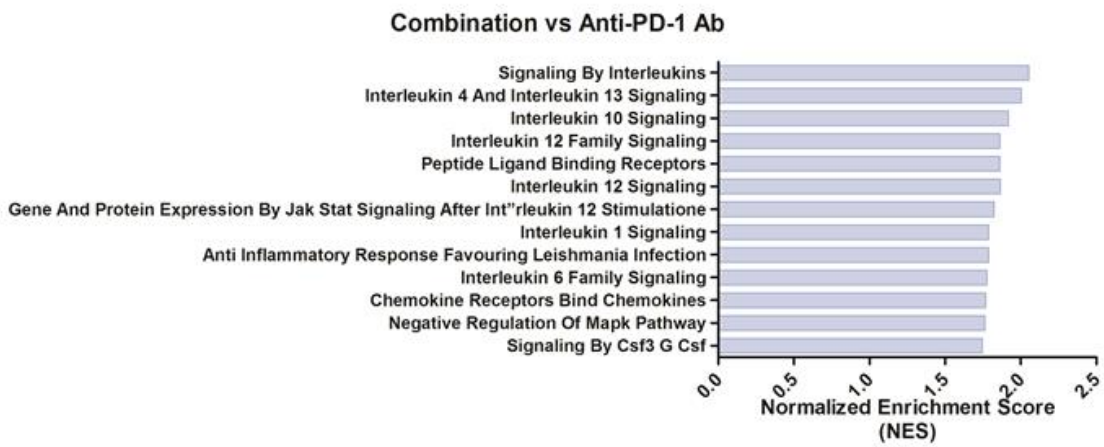
Combination vs Anti-PD-1 Ab
Signaling By Interleukins
Interleukin 4 And Interleukin 13 Signaling
Interleukin 10 Signaling
Interleukin 12 Family Signaling
Peptide Ligand Binding Receptors
Interleukin 12 Signaling
Gene And Protein Expression By Jak Stat Signaling After Int"rleukin 12 Stimulatione
Interleukin 1 Signaling
Anti Inflammatory Response Favouring Leishmania Infection
Interleukin 6 Family Signaling
Chemokine Receptors Bind Chemokines
Negative Regulation Of Mapk Pathway
Signaling By Csf3 G Csf
0.0
0.5
1.0
1.5
2.0
2.5
Normalized Enrichment Score
(NES)

Fig. 15 Pathway analysis by GSEA on RAW264.7 cells gene expression profiling after CpG-ODN, anti-PD-1 antibody treatment or their combination.
Barplots of the normalized enrichment score (NES) of the significant pathways enriched in the combination group compared to the (A) untreated group (grey barplots), (B) TLR9-Ag group (green barplots) or (C) anti-PD-1 Ab group (blue barplot). Pathways with FDR<0.05 were considered statistically significant. TLR9-Ag: TLR9 agonist (CpG oligodeoxynucletotides); anti-PD-1 Ab: anti-PD-1 antibody; Combination: CpG-ODN+anti-PD-1 antibody.

When considering all the comparisons, gene sets related to IL-6, IL-4, IL-13 and IL-10 signaling were always significantly enriched in RAW264.7 exposed to both CpG-ODN and anti-PD-1 antibody (Fig. 15 and Tab. 9). Moreover, IL-12 signaling pathway was also enriched in the combination group when compared to RAW264.7 incubated with anti-PD-1 Ab alone. These data suggest that macrophages exposed to the combination regimen exhibit a possible “mixed” polarization status, intermediate between M1 and M2 phenotype.

Common pathways between the comparisons
Interleukin 10 Signaling
Interleukin 4 and Interleukin 13 Signaling
Interleukin 6 Family Signaling
Signaling by Interleukins
Peptide ligand binding receptors
Chemokine receptors bind chemokines

Tab. 9 Common pathways emerging from GSEA analysis by comparing the gene expression profile of combination-treated macrophages to all the other experimental groups.
Combination: CpG-ODN+anti-PD-1 antibody.

To validate gene profiling data, real-time PCR analysis were performed on RAW264.7 and the expression of both M1- and M2-specific genes [96] was evaluated. mRNA levels of Il-12b, Il-6, Tnf-α and Ccl2, M1 markers, and Irf4, Ccl1 and Nos2, M2-related genes, were significantly increased in the combination group compared to monotherapies. Similarly, the

expression of the activation markers Cd80 and Cd86 resulted increased in the double treatment compared to single treatment groups (Fig. 16).

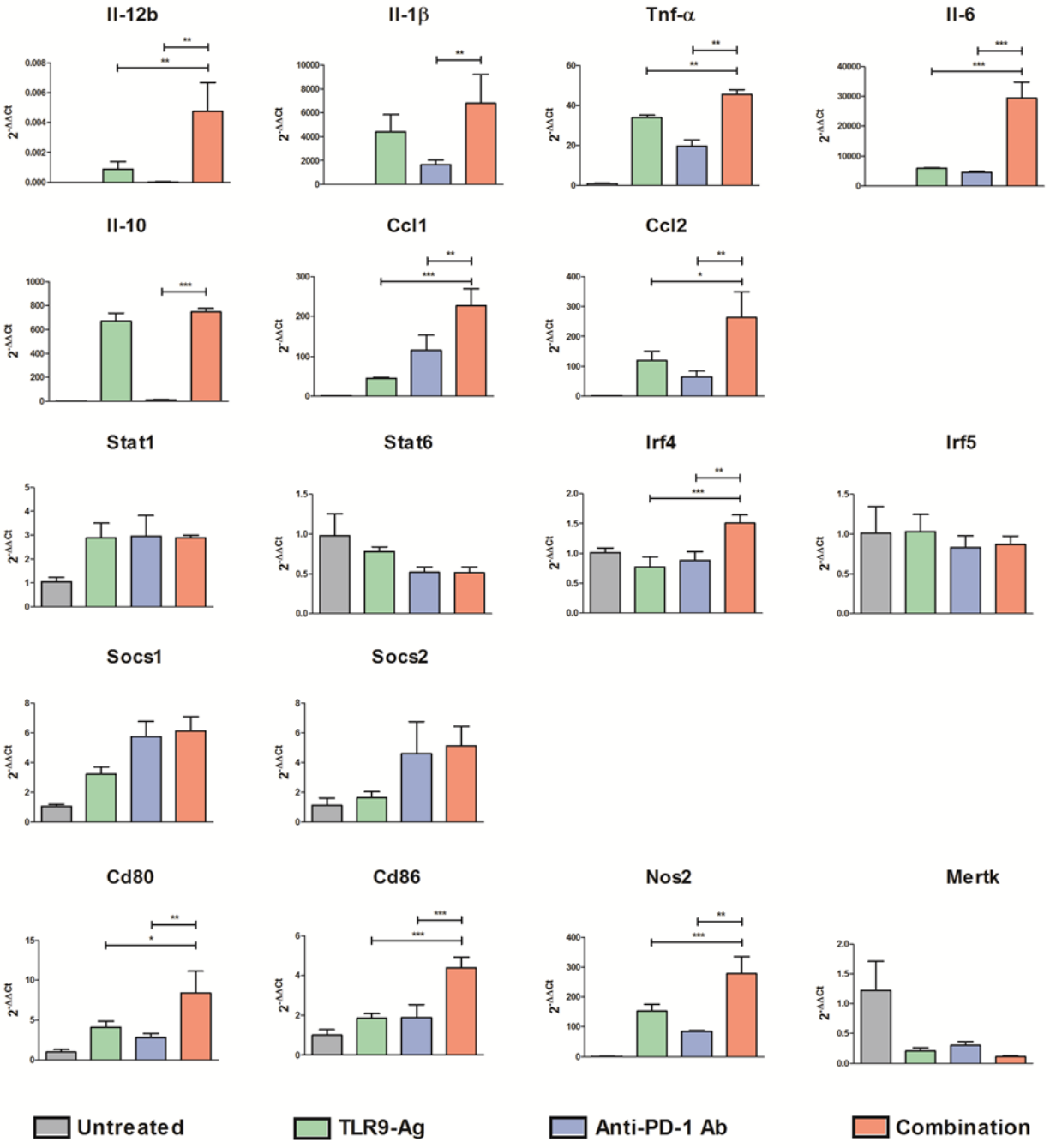

Fig. 16 Real-time PCR analysis on RAW264.7 macrophages treated with CpG-ODN and anti-PD-1 antibody alone or in combination.

Real-time PCR analysis were performed on RAW264.7 incubated with 1 µM CpG-ODN and/or 10 µg/ml anti-mouse PD-1 antibody (clone RMP1-14) for 6 hours. Controls were left untreated. The data are normalized to β2M expression as housekeeping reference gene

and analyzed by the comparative $2^{-\Delta\Delta Ct}$ method. The data are presented as mean ± SEM. Each group was run in triplicate; data represent one of three *in vitro* experiments showing similar results. Il-12b: interleukin 12 b; Il-1β: interleukin 1β; Tnf-α: tumor necrosis factor α; Il-6: interleukin 6; Il-10: interleukin 10; Ccl1: C-C motif chemokine ligand 1; Ccl2: C-C motif chemokine ligand 2; Stat1: signal transducer and activator of transcription 1; Stat6: signal transducer and activator of transcription 6; Irf4: interferon regulatory factor 4; Irf5: interferon regulatory factor 5; Socs1: suppressor of cytokine signaling 1; Socs2: suppressor of cytokine signaling 2; Cd80: cluster of differentiation 80; Cd86: cluster of differentiation 86; Nos2: nitric oxide synthase 2; Mertk: MER proto-oncogene tyrosine kinase; CpG-ODN: CpG oligodeoxynucleotides; anti-PD-1 Ab: anti-PD-1 antibody; Combination: CpG-ODN+anti-PD-1 antibody. * $p<0.05$; ** $p<0.01$; *** $p<0.001$ by one-way ANOVA followed by Tukey's multiple comparison test for parametric data or by Kruskal-Wallis test followed by Dunn's multiple comparison test for non-parametric data.

Flow cytometry analysis confirmed CD80 and CD86 upregulation at the protein level. Specifically, an augmented percentage of $CD80^+$ macrophage expression was found in the combination group compared to single treatments (Fig. 17 A). Regarding CD86, it was highly expressed by all the cells in every experimental groups, but the double treatment determined a rise of the fluorescence intensity compared to the other groups (Fig. 17 B). Moreover, FACS analysis showed an increase of the percentage of $CD206^+$ cells after exposure to both the immunotherapeutic drugs (Fig. 17 C).

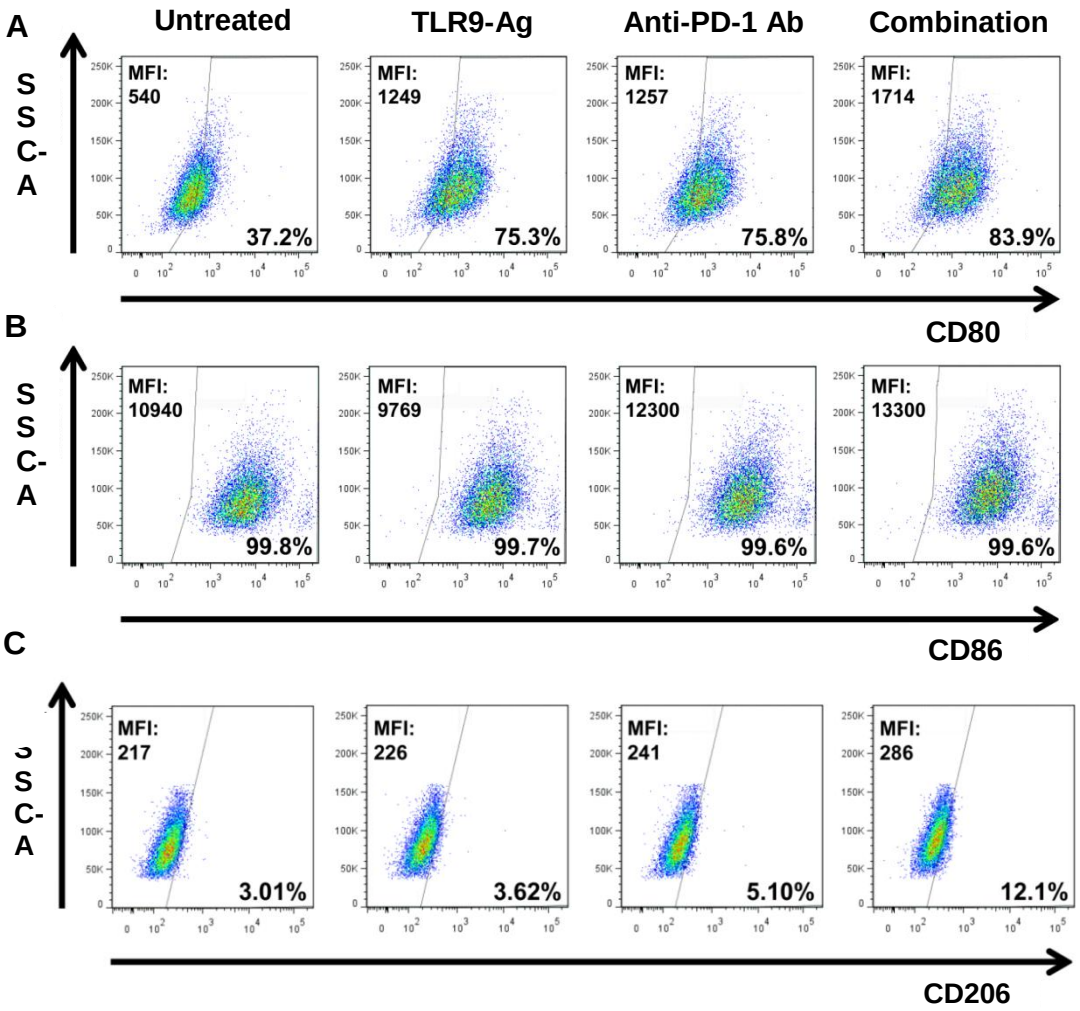

Fig. 17 FACS analysis for CD80, CD86 and CD206 on RAW264.7 after incubation with CpG-ODN and/or anti-PD-1 antibody.

CD80, CD86 and CD206 FACS analysis on RAW264.7 incubated with 1 µM CpG-ODN, 10 µg/ml anti-mouse PD-1 antibody clone RMP1-14 or their combination for 6 hours. Controls were left untreated. Representative scatter dot plot images showing the percentage of $CD80^+$ (A), $CD86^+$ (B) and $CD206^+$ (C) RAW264.7 cells in the different experimental conditions. Each group was run in triplicate; data represent one of three *in vitro* experiments showing similar results. Mean Fluorescence Intensity (MFI) for each experimental group was also indicated. FACS: Fluorescence-activated cell sorting; CD80: cluster of differentiation 80; CD86: cluster of differentiation 86; CD206: cluster of differentiation 206; TLR9-Ag: TLR9 agonist (CpG oligodeoxynucletotides); anti-PD-1 Ab: anti-PD-1 antibody; Combination: CpG-ODN+anti-PD-1 antibody.

The release of cytokines important for macrophage activation and function [97] was quantified by multiplex ELISA assays on RAW264.7 supernatants after the aforementioned *in vitro* treatments. When multiplex ELISA data were collectively considered by PCA

analysis, it is possible to identify 4 different clusters, closely resembling those observed for genomic data. (Fig. 18 A).

Measurement of cytokine release showed a statistically significant increase of IL-4, IL-6 and IL-12b and a parallel reduction of TNF-α release in RAW264.7 exposed to concomitant CpG-ODN and anti-PD-1 antibody administration compared to that incubated with single agents. Moreover, IL-10 levels were higher in CpG-ODN/anti-PD-1 antibody-treated macrophages compared to anti-PD-1 group. IL-1β and IL-12a concentration in the supernatant was increased in the combination group compared to the CpG-ODN group. (Fig. 18 B).

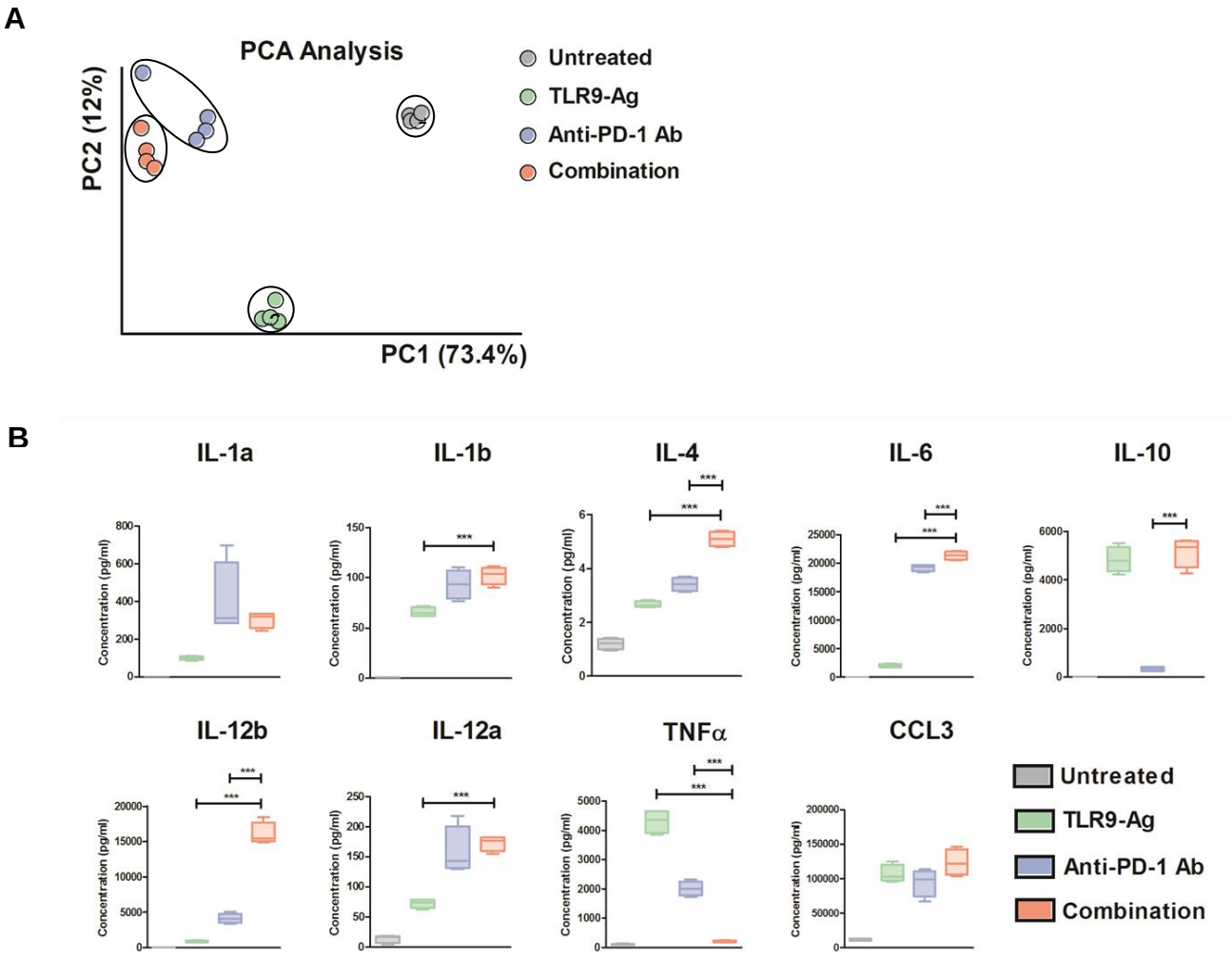

Fig. 18 Multiplex ELISA assay on RAW264.7 treated with CpG-ODN and anti-PD-1 antibody alone or in combination

Multiplex ELISA assay on supernatants of RAW 264.7 incubated with CpG-ODN, anti-PD-1 antibody or their combination for 6 hours. (A) PCA conducted on Multiplex ELISA assay data of RAW264.7 incubated with 1 µM CpG-ODN and/or 10 µg/ml anti-mouse PD-1 antibody for 6h. (B) Multiplex ELISA assay performed on supernatants of RAW264.7 incubated with 1 µM CpG-ODN and/or 10 µg/ml anti-mouse PD-1 antibody clone RMP1-14 for 6h. Controls were left untreated. The data are presented as mean ± SEM. Each group was run in quadruplicate. PCA: principal component analysis; IL-1a: interleukin 1a; IL-1b: interleukin 1b; IL-4: interleukin 4; IL-6: interleukin 6; IL-10: interleukin 10; IL-12b: interleukin 12 b; IL-12a: interleukin 12a; TNFα: tumor necrosis factor α; CCL3: C-C motif chemokine ligand 3; TLR9-Ag: TLR9 agonist (CpG oligodeoxynucletotides); anti-PD-1 Ab: anti-PD-1 antibody; Combination: CpG-ODN+anti-PD-1 antibody. *** $p<0.001$ by one-way ANOVA followed by Tukey's multiple comparison test for parametric data or by Kruskal-Wallis test followed by Dunn's multiple comparison test for non-parametric data.

Macrophage polarization toward a particular phenotype is a complex biological process that produces profound changes in the cellular machinery, affecting several biological processes such as metabolic pathways. Therefore, macrophage metabolic profile can mirror the phenotype acquired by these immune cells [98]. Moreover, metabolites secreted by macrophages can exert profound effects on the surrounding environment [99]. To better characterize the secretome profile of macrophages exposed to both CpG-ODN and anti-PD-1 antibody, mass spectrometry was carried out on RAW264.7 supernatants. The overall tendency of metabolites consisted in an increase of molecule levels after the incubation with the combination regimen compared to single agent exposure. Particularly, the release of polyamines belonging to arginine catabolism, as spermidine and betaine, together with the levels of aminoacids like alanine, valine, histidine, and carnitine derivatives such as acetylcarnitine and propionylcarnitine were found augmented in the combination group compared to single agent-exposed RAW264.7 supernatants (Fig. 19 A and 19 B).

A

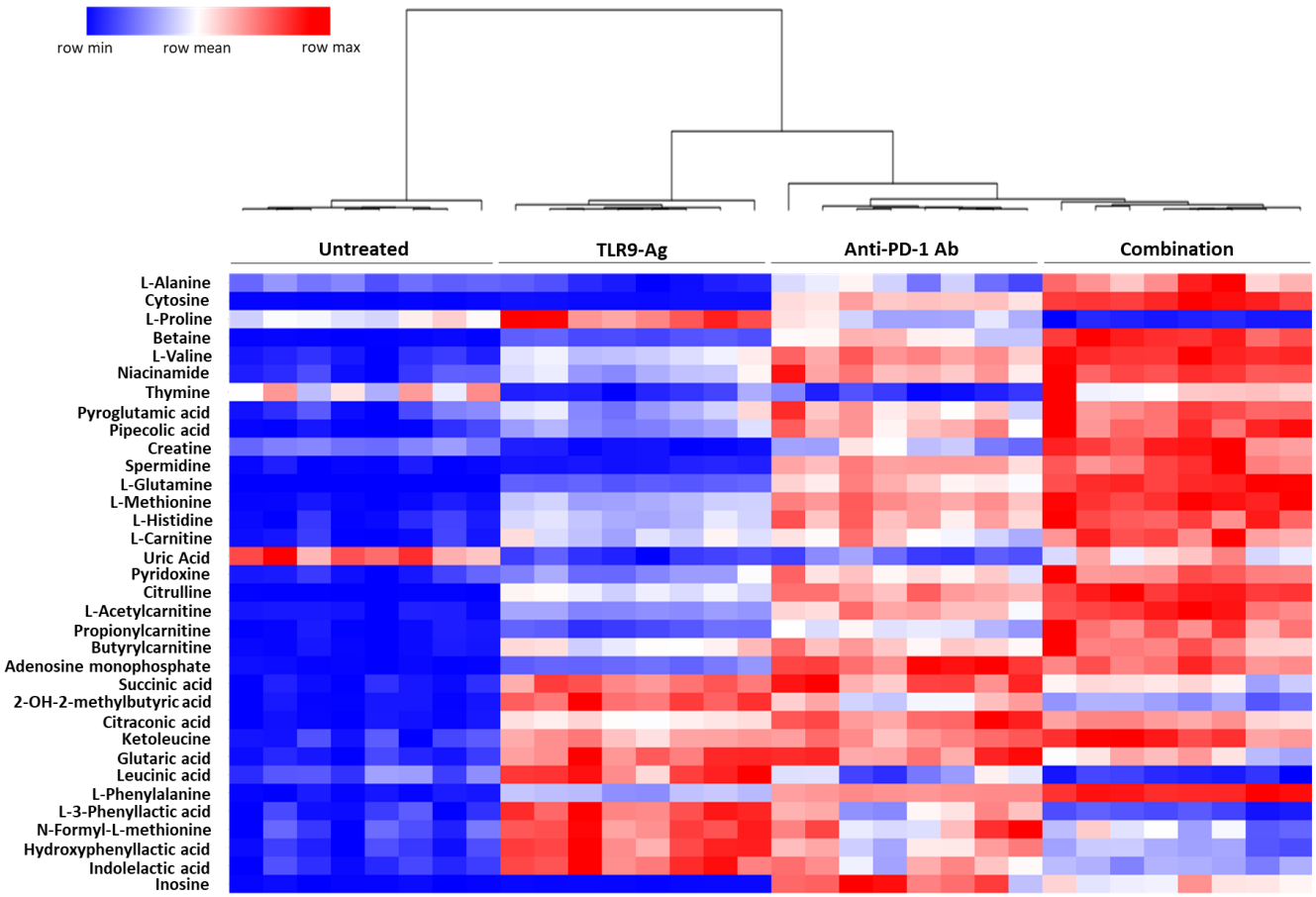
row min
row mean
row max
Untreated
TLR9-Ag
Anti-PD-1 Ab
Combination
L-Alanine
Cytosine
L-Proline
Betaine
L-Valine
Niacinamide
Thymine
Pyroglutamic acid
Pipecolic acid
Creatine
Spermidine
L-Glutamine
L-Methionine
L-Histidine
L-Carnitine
Uric Acid
Pyridoxine
Citrulline
L-Acetylcarnitine
Propionylcarnitine
Butyrylcarnitine
Adenosine monophosphate
Succinic acid
2-OH-2-methylbutyric acid
Citraconic acid
Ketoleucine
Glutaric acid
Leucinic acid
L-Phenylalanine
L-3-Phenyllactic acid
N-Formyl-L-methionine
Hydroxyphenyllactic acid
Indolelactic acid
Inosine

B

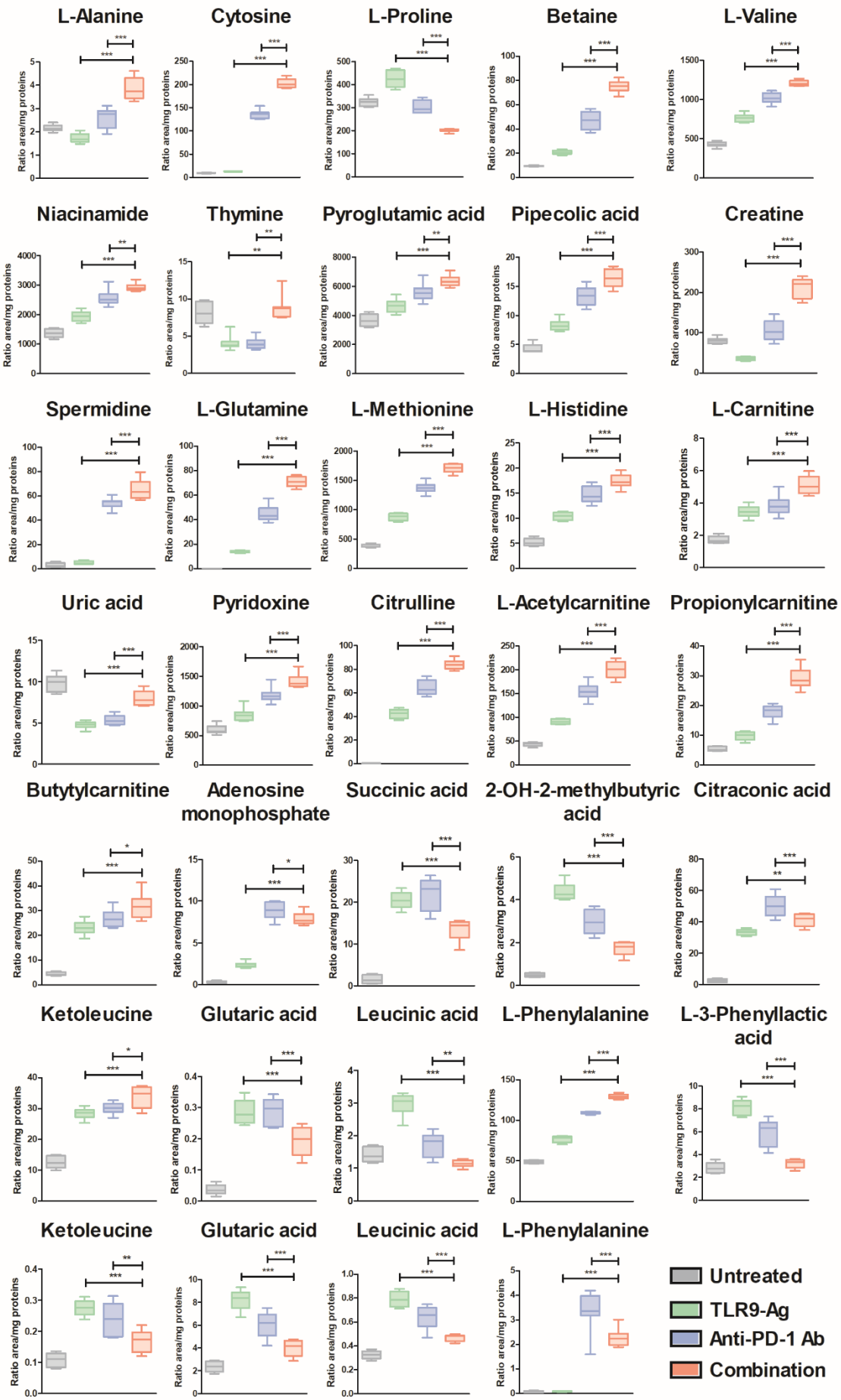
L-Alanine
Cytosine
L-Proline
Betaine
L-Valine
Niacinamide
Thymine
Pyroglutamic acid
Pipecolic acid
Creatine
Spermidine
L-Glutamine
L-Methionine
L-Histidine
L-Carnitine
Uric acid
Pyridoxine
Citrulline
L-Acetylcarnitine
Propionylcarnitine
Butytylcarnitine
Adenosine monophosphate
Succinic acid
2-OH-2-methylbutyric acid
Citraconic acid
Ketoleucine
Glutaric acid
Leucinic acid
L-Phenylalanine
L-3-Phenyllactic acid
Ketoleucine
Glutaric acid
Leucinic acid
L-Phenylalanine
Ratio area/mg proteins
Untreated
TLR9-Ag
Anti-PD-1 Ab
Combination

Fig. 19 Metabolomic analysis on RAW264.7 treated with CpG-ODN and anti-PD-1 antibody alone or in combination.
Mass spectrometry analysis on supernatants of RAW 264.7 incubated with 1 µM CpG-ODN and/or 10 µg/ml anti-mouse PD-1 antibody clone RMP1-14 for 6 hours. Controls were left untreated. (A) Hierarchical clustering and (B) box plot graphs of metabolites resulted significantly differently expressed in Combination compared to either TLR9-Ag and anti-PD-1 Ab groups. Results are expressed as the ratio peak area / intern standard (IS) area normalized on protein concentration (mg). Each group was run in quadruplicate. FAD: flavin adenine di nucleotide; DOPA: dihydroxyphenylalanine; TLR9-Ag: TLR9 agonist (CpG oligodeoxynucletotides); anti-PD-1 Ab: anti-PD-1 antibody; Combination: CpG-ODN+anti-PD-1 antibody. * $p<0.05$; ** $p<0.01$; *** $p<0.001$ by one-way ANOVA followed by Tukey's multiple comparison test for parametric data or by Kruskal-Wallis test followed by Dunn's multiple comparison test for non-parametric data.

6. CpG-ODN/anti-PD-1 antibody dual treatment affects macrophage functionality

It has been reported that macrophages are able to influence NK cytotoxic activity. This ability can be exploited as a mirror of macrophage phenotype. Indeed, M1 macrophages promote while M2 macrophages dampen NK cell cytotoxicity. [100,101]. To investigate if changes in the gene expression profile observed in RAW264.7 exposed to CpG-ODN/anti-PD-1 antibody combination could have repercussions also on cell functionality, the cytotoxic activity of NK cells was evaluated after co-culture with macrophages, previously treated with the different immunotherapeutic drugs. BMDMs were incubated with CpG-ODN, anti-PD-1 antibody or their combinations, and co-cultured with untouched NK cells. At the end of the incubation time, the cytotoxicity of NK cells was assayed by evaluating the lysis percentage of YAC-1 target cells. NK cells, receiving single agents, had higher cytotoxic activity compared to the untreated group. The effects of the association between CpG-ODN and anti-PD-1 antibody on macrophages resulted in low level of NK cytotoxicity, since the percentage of YAC-1 lysis was comparable to untreated group (Fig. 20).

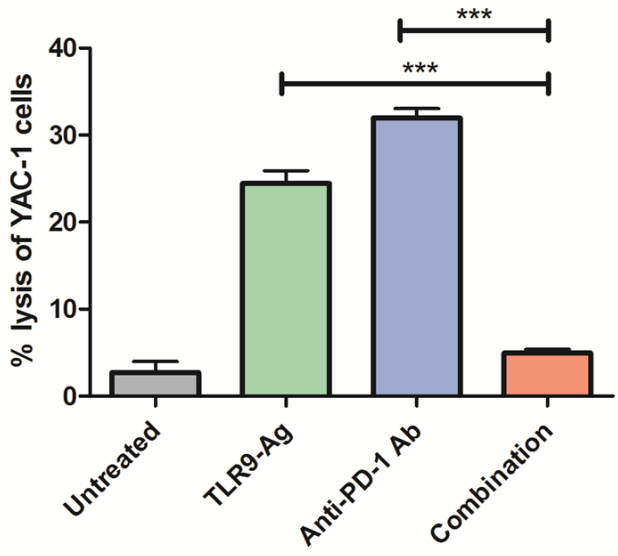

Fig. 20 Cytotoxicity assay on NK cells co-cultured with *in vitro* stimulated BMDMs. ^{51}Cr-release assay on NK cells co-cultured with BMDMs previously stimulated with 1 µM CpG-ODN and/or 10 µg/ml anti-mouse PD-1 antibody clone RMP1-14 for 6 hours. At the end of the treatment, NK cells isolated from mice spleens were co-cultured with stimulated BMDMs for 36 hours. Cytotoxic activity was evaluated against YAC-1 target cells by ^{51}Cr release assay. Results are expressed as the lysis percentage of ^{51}Cr-labeled YAC-1 cells by NK cells. Each group was run in triplicate; data represent one of three *in vitro* experiments that showed similar results. NK cells: natural killer cells; BMDMs: bone marrow-derived macrophages; TLR9-Ag: TLR9 agonist (CpG oligodeoxynucletotides); anti-PD-1 Ab: anti-PD-1 antibody; Combination: CpG-ODN+anti-PD-1 antibody. The data are presented as the mean ± SEM. ***p<0.001 by one-way ANOVA followed by Tukey's multiple comparison test.

7. Effects of anti-PD-1 antibody Fc domain on CpG-ODN antitumor activity in macrophages

Blocking PD-1 can impact on macrophage behavior [41]. Moreover, it has been reported that anti-PD-1 antibody Fc domain may reprogram macrophage toward a phenotype able to promote tumor growth [71]. *In vitro* experiments were then carried out to investigate if changes in gene expression observed in the combination treatment group were related to the direct binding to PD-1 or to the interaction with the Fc domain of anti-PD-1 antibody on these cells. Therefore, RAW264.7 were treated as above, but for these experiments two different forms of anti-PD-1 antibody were utilized: anti-PD-1 antibody $F(ab)_2$, lacking the

Fc domain but still able to bind PD-1 [71] and anti-PD-1 antibody “Fc Silent” possessing a point mutation in the Fc domain that abrogates the binding to all the Fc receptors. Real-time PCR analysis were performed on genes that showed a statistically significant modulation in combinatorial treatment compared to single agents, as indicated in Figure 16. When the two anti-PD1 antibody variants were utilized for macrophage treatment, no gene was found differentially modulated in the combination group compared to CpG-ODN-treated group (Fig. 21 and 22).

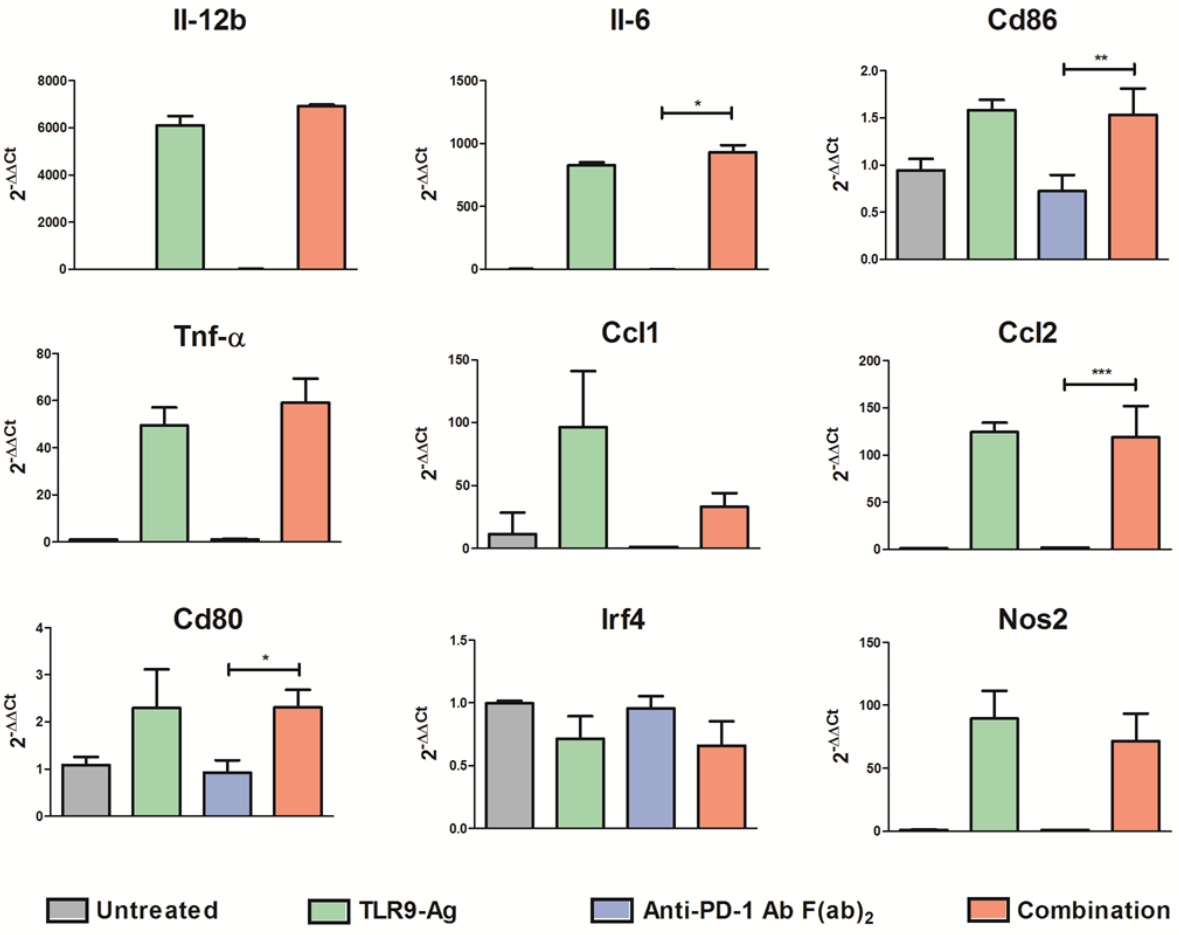

Fig. 21 Real-time PCR analysis on RAW264.7 macrophages treated with CpG-ODN and anti-PD-1 antibody F(ab)$_2$ alone or in combination.
Real-time PCR analysis on RAW264.7 incubated with 1 µM CpG-ODN and/or 10 µg/ml anti-mouse PD-1 antibody F(ab)$_2$ for 6 hours. Controls were left untreated. The data are normalized to β2M expression as housekeeping reference gene and analyzed by the comparative $2^{-\Delta\Delta Ct}$ method. The data are presented as mean ± SEM. Each group was run in triplicate; data represent one of three *in vitro* experiments that showed similar results. Il-

12b: interleukin 12 b; Tnf-α: tumor necrosis factor α; Il-6: interleukin 6; Ccl1: C-C motif chemokine ligand 1; Ccl2: C-C motif chemokine ligand 2; Irf4: interferon regulatory factor 4; Cd80: cluster of differentiation 80; Cd86: cluster of differentiation 86; Nos2: nitric oxide synthase 2; CpG-ODN: CpG oligodeoxynucleotides; anti-PD-1 Ab: anti-PD-1 antibody; Combination: CpG-ODN+anti-PD-1 antibody. * p<0.05; ** p<0.01; *** p<0.001 by one-way ANOVA followed by Tukey's multiple comparison test for parametric data or by Kruskal-Wallis test followed by Dunn's multiple comparison test for non-parametric data.

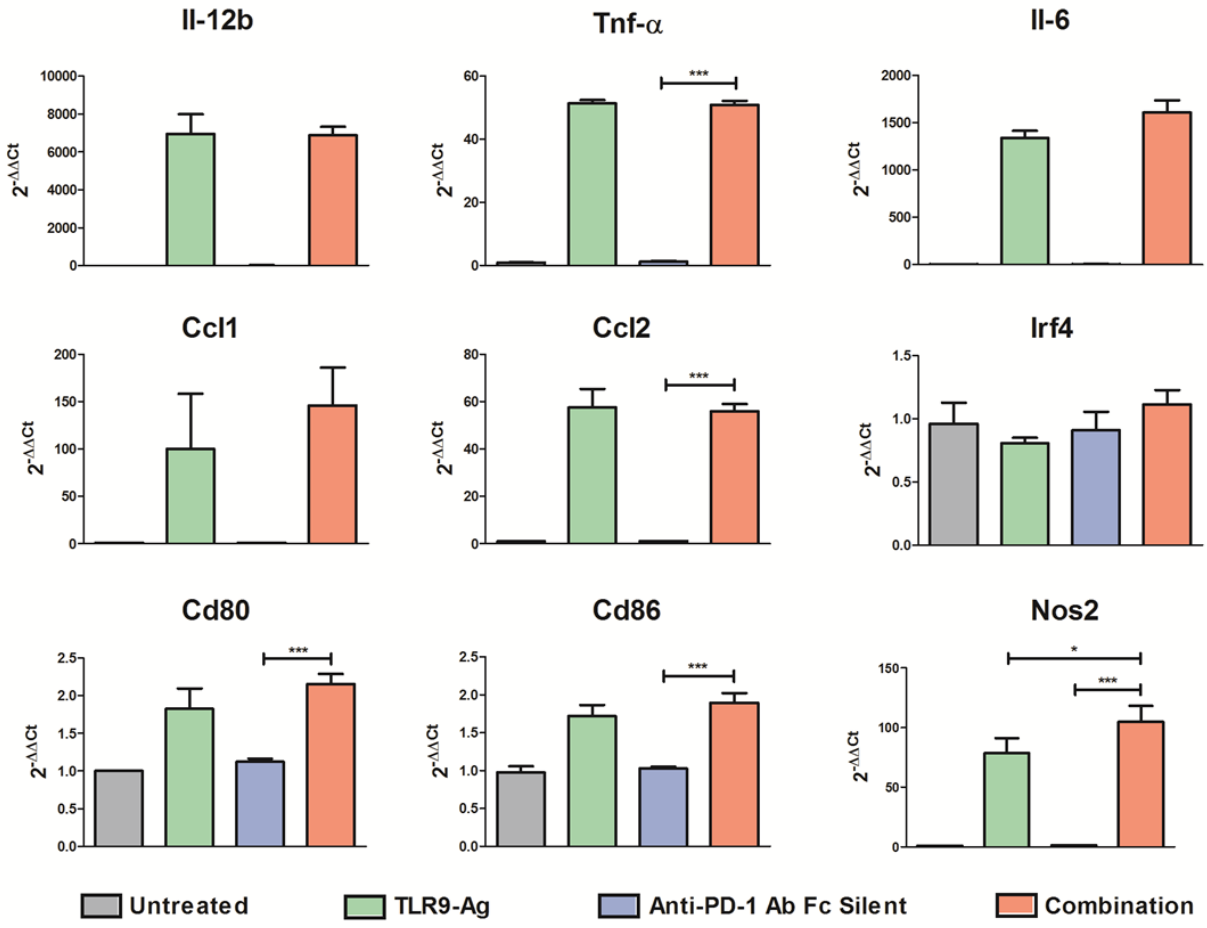

Fig. 22 Real-time PCR analysis on RAW264.7 macrophages treated with CpG-ODN and anti-PD-1 antibody "Fc Silent" alone or in combination.

Real-time PCR analysis on RAW264.7 incubated with 1 µM CpG-ODN and/or 10 µg/ml "Fc silent" anti-mouse PD-1 antibody for 6 hours. Controls were left untreated. The data are normalized to β2M expression as housekeeping reference gene and analyzed by the comparative $2^{-\Delta\Delta Ct}$ method. The data are presented as mean ± SEM. Each group was run in triplicate; data represent one of three *in vitro* experiments that showed similar results. Il-12b: interleukin 12 b; Tnf-α: tumor necrosis factor α; Il-6: interleukin 6; Ccl1: C-C motif chemokine ligand 1; Ccl2: C-C motif chemokine ligand 2; Irf4: interferon regulatory factor 4; Cd80: cluster of differentiation 80; Cd86: cluster of differentiation 86; Nos2: nitric oxide synthase 2; CpG-ODN: CpG oligodeoxynucleotides; anti-PD-1 Ab: anti-PD-1 antibody;

Combination: CpG-ODN+anti-PD-1 antibody. * $p<0.05$; *** $p<0.001$ by one-way ANOVA followed by Tukey's multiple comparison test for parametric data or by Kruskal-Wallis test followed by Dunn's multiple comparison test for non-parametric data.

Since these results suggest that the direct blocking of PD-1 alone was not sufficient for macrophage reprogramming, it was investigated whether the Fc domain of the antibody alone may trigger the phenotype shift in macrophage phenotype. For this reason, it was utilized a rat IgG2a isotype-matched control antibody, which maintains the ability to bind Fc receptors but can't recognize PD-1. The abrogation of PD-1 binding resulted in no modulation of any gene in the combination group compared to TLR9 agonist-stimulated cells (Fig. 23). These findings indicate that not only the recognition of Fc domain by Fc receptors expressed by macrophages but also the direct binding to PD-1 are both necessary to produce macrophage polarization observed in the double treatment.

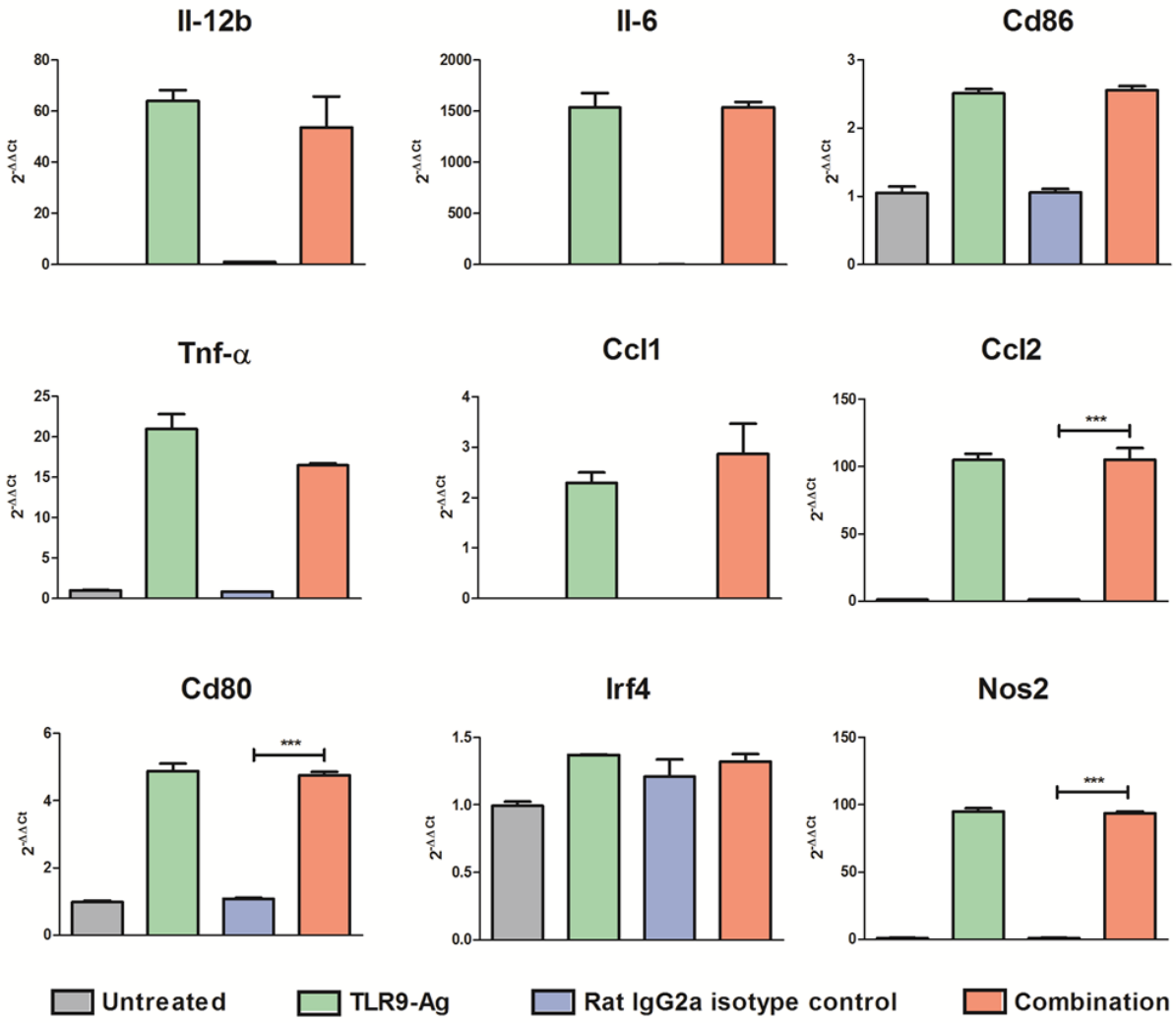

Fig. 23 Real-time PCR analysis on RAW264.7 macrophages treated with CpG-ODN and rat IgG2a isotype control antibody alone or in combination. Real-time PCR analysis on RAW264.7 incubated with 1 µM CpG-ODN and/or 10 µg/ml rat IgG2a isotype control antibody for 6 hours. Controls were left untreated. The data are normalized to β2M expression as housekeeping reference gene and analyzed by the comparative $2^{-\Delta\Delta Ct}$ method. Each group was run in triplicate; data represent one of three *in vitro* experiments that showed similar results. The data are presented as mean ± SEM. Il-12b: interleukin 12 b; Tnf-α: tumor necrosis factor α; Il-6: interleukin 6; Ccl1: C-C motif chemokine ligand 1; Ccl2: C-C motif chemokine ligand 2; Irf4: interferon regulatory factor 4; Cd80: cluster of differentiation 80; Cd86: cluster of differentiation 86; Nos2: nitric oxide synthase 2; CpG-ODN: CpG oligodeoxynucleotides; anti-PD-1 Ab: anti-PD-1 antibody; Combination: CpG-ODN+anti-PD-1 antibody. *** $p<0.001$ by one-way ANOVA followed by Tukey's multiple comparison test for parametric data or by Kruskal-Wallis test followed by Dunn's multiple comparison test for non-parametric data.

Since the Fc domain of the utilized anti-PD-1 antibody for is reported to be recognized by the Fc receptors FcγR2b (CD32) and FcγR3 (CD16) [102,103], *in vitro* experiments were carried out to ascertain if the effects of the anti-PD-1 antibody Fc domain can be mediated by the binding to these FcγRs. Therefore, RAW264.7 were previously treated with an anti-

CD16/32 blocking antibody and then exposed to CpG-ODN, anti-PD-1 antibody or their combination for 6 hours. Blockade of CD16 and CD32b did not abrogate the up-modulation of Il-12b, Il-6 and Cd86 genes in the combination treatment compared to single agents (Fig. 24), as observed in the first *in vitro* experiment (Fig. 16).

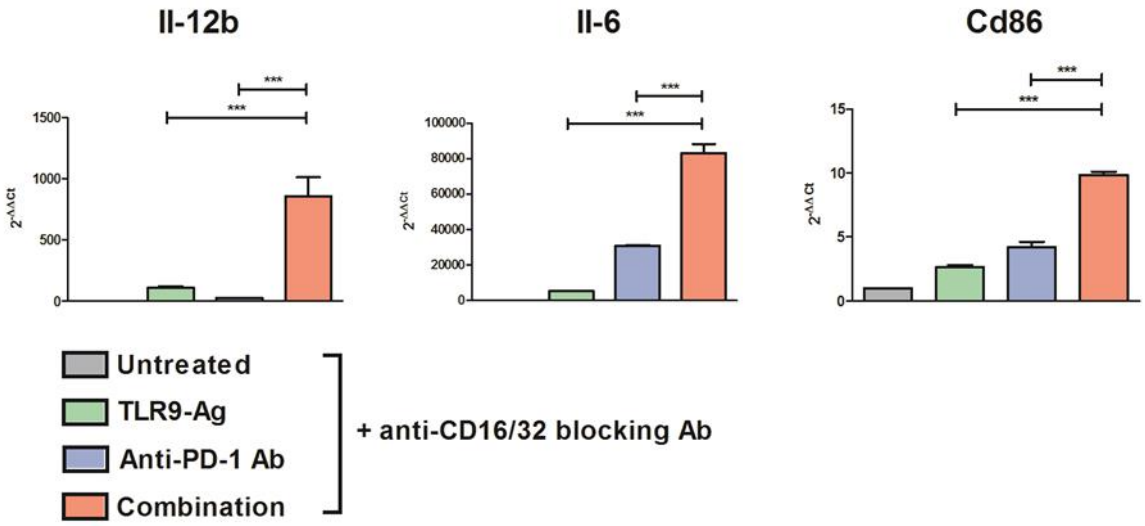

Fig. 24 Real-time PCR analysis on RAW264.7 macrophages treated with CpG-ODN and anti-PD-1 antibody alone or in combination after CD16/32 blockade.
Real-time PCR analysis on RAW264.7 pre-treated with 10 µg/ml rat anti-mouse CD16/32 blocking antibody for 30 min and incubated with 1 µM CpG-ODN and/or 10 µg/ml anti-mouse PD-1 antibody for 6 hours. Controls were left untreated. The data are normalized to β2M expression as housekeeping reference gene and analyzed by the comparative $2^{-\Delta\Delta Ct}$ method. The data are presented as mean ± SEM. Each group was run in triplicate; data represent one of three *in vitro* experiments that showed similar results. CD16/32: cluster of differentiation 16/32; Il-12b: interleukin 12 b; Il-6: interleukin 6; Cd86: 86; Nos2: nitric oxide synthase 2; CpG-ODN: CpG oligodeoxynucleotides; anti-PD-1 Ab: anti-PD-1 antibody; Combination: CpG-ODN+anti-PD-1 antibody. *** $p<0.001$ by one-way ANOVA followed by Tukey's multiple comparison test for parametric data or by Kruskal-Wallis test followed by Dunn's multiple comparison test for non-parametric data.

To exclude the possibility that even small amount of PD-1 receptors, remained available after CD16/32 blockade, may mediate the effect observed in macrophages, decreasing anti-PD-1 antibody concentrations were used. Il-6 expression progressively decreased by reducing anti-PD-1 antibody concentration (Fig. 25). This result suggests the effect of the anti-PD-1 antibody on macrophages is dose-dependent.

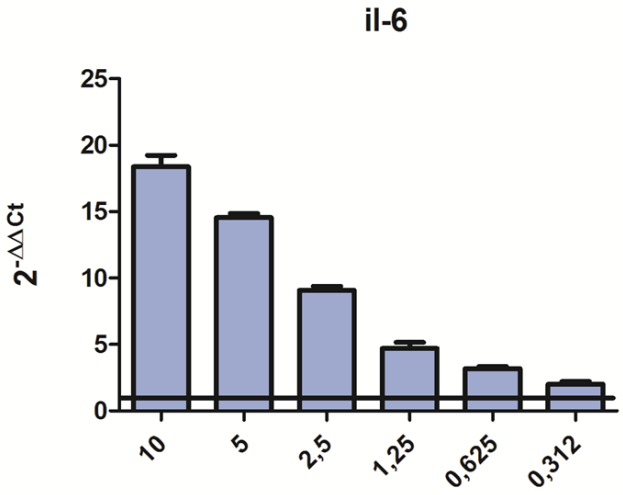

Fig. 25 Real-time PCR analysis on RAW264.7 macrophages treated with CpG-ODN in combination with decreasing concentrations of anti-PD-1 antibody.
Real-time PCR analysis on RAW264.7 incubated with 1 μM CpG-ODN alone or in combination with decreasing concentrations of anti-mouse PD-1 antibody (ranging from 10 to 0.312 μg/ml) for 6 hours. The black line represents the mRNA level of il-6 in RAW264.7 treated with CpG-ODN alone that was used as reference gene. The data are normalized to β2M expression as housekeeping reference gene and analyzed by the comparative $2^{-\Delta\Delta Ct}$ method. The data are presented as mean ± SEM. Numbers on X axis indicate anti-PD-1 antibody concentrations (μg/ml). Each group was run in triplicate; data represent one of three *in vitro* experiments that showed similar results. Il-6: interleukin 6; CpG-ODN: CpG oligodeoxynucleotides; anti-PD-1 Ab: anti-PD-1 antibody.

8. TRIM21 triggers macrophage phenotype reprogramming upon coadministration with CpG-ODN

The Fc domain of the antibodies can be recognized not only by FcγRs located on cell membrane, but also by the intracellular Fc receptor TRIM21, which belongs to the ubiquitination-proteasome system [104]. To ascertain whether TRIM21 can be involved in mediating the effects observed in the combination group, the ubiquitination-proteasome pathway was firstly inhibited. It was found that the increased expression of genes previously observed in the combination group was completely abrogated by ubiquitin-proteasome inhibition, with the exception of Irf4 that remained unchanged (Fig. 26).

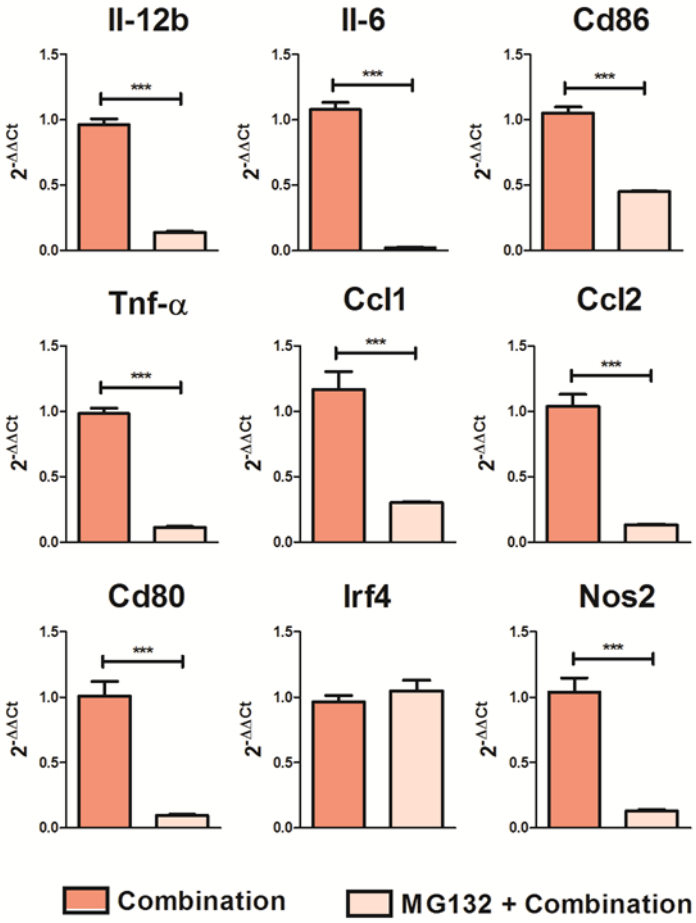

Fig. 26 Real-time PCR analysis on RAW264.7 macrophages treated with CpG-ODN and anti-PD-1 antibody combination after inhibition of ubiquitin-proteasome pathway by MG132.
Real-time PCR analysis on RAW264.7 pre-treated with 20 μM proteasome inhibitor MG132 for 30 min and then exposed to 1 μM CpG-ODN and 10 μg/ml anti-mouse PD-1 antibody for 6 hours. The data are normalized to β2M expression as housekeeping reference gene and analyzed by the comparative $2^{-\Delta\Delta Ct}$ method. The data are presented as mean ± SEM. Each group was run in triplicate; data represent one of three *in vitro* experiments that showed similar results. Il-12b: interleukin 12 b; Tnf-α: tumor necrosis factor α; Il-6: interleukin 6; Ccl1: C-C motif chemokine ligand 1; Ccl2: C-C motif chemokine ligand 2; Irf4: interferon regulatory factor 4; Cd80: cluster of differentiation 80; Cd86: cluster of differentiation 86; Nos2: nitric oxide synthase 2; Combination: CpG-ODN+anti-PD-1 antibody. *** $p<0.001$ by two-tailed unpaired Student's *t*-test for parametric data or the Mann-Whitney U test for one-way non-parametric data.

Subsequently, Trim21 gene was silenced in RAW264.7 24 hours before the exposure to the combinatorial treatment. Both real-time PCR (Fig. 27 A) and Western Blot analysis (Fig. 27 B) confirmed Trim21 silencing. A statistically significant reduction of Il-12b, Ccl1

and Irf4 mRNA expression was observed in Trim21-silenced RAW264.7 cells compared to macrophages transfected with control siRNA (Fig. 27 C).

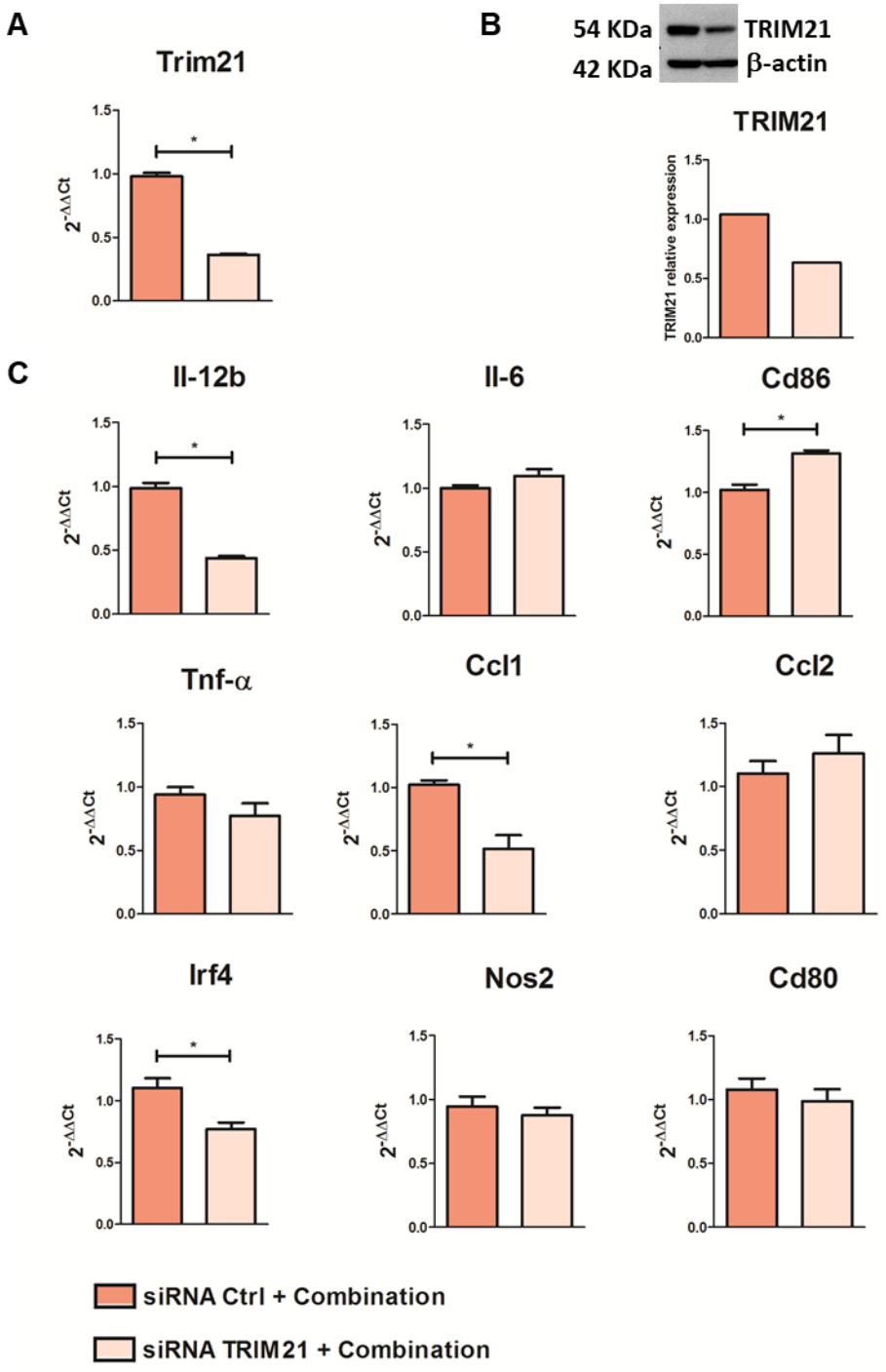

Fig. 27 Real-time PCR analysis on RAW264.7 macrophages silenced for Trim21 gene and treated with CpG-ODN/anti-PD-1 antibody combination.
Real-time PCR analysis on RAW264.7 silenced inTrim21 gene and incubated with 1 µM CpG-ODN and 10 µg/ml anti-mouse PD-1 antibody clone RMP1-14 for 6 hours. The data are normalized to β2M expression as housekeeping reference gene and analyzed by the comparative $2^{-\Delta\Delta Ct}$ method. The data are presented as mean ± SEM. Each group was run

in triplicate; data represent one of three *in vitro* experiments showing similar results. Trim21: Tripartite motif containing-21; Il-12b: interleukin 12 b; Tnf-α: tumor necrosis factor α; Il-6: interleukin 6; Ccl1: C-C motif chemokine ligand 1; Ccl2: C-C motif chemokine ligand 2; Irf4: interferon regulatory factor 4; Cd80: cluster of differentiation 80; Cd86: cluster of differentiation 86; Nos2: nitric oxide synthase 2; Combination: CpG-ODN+anti-PD-1 antibody. * $p<0.05$; ** $p<0.01$; *** $p<0.001$ by two-tailed unpaired Student's *t*-test for parametric data or the Mann-Whitney U test for one-way non-parametric data.

Taken together, these results show that the anti-PD-1 antibody dampens CpG-ODN antitumor activity by the Fc domain-TRIM21 interaction, which triggers the polarization of macrophages towards a mixed phenotype, since the up-regulation of both M1 and M2 markers. Mixed phenotype macrophages are able to exert pro-tumor and immunosuppressive functions, finally facilitating tumor growth.

DISCUSSION

The antitumor activity of TLR9 synthetic agonists have been demonstrated in mouse models [83,105] and in human settings for the treatment of advanced stage solid tumors [22,106–108]. The results of different clinical trials highlighted the poor efficacy of CpG-ODN when delivered as monotherapy. There are different reasons to explain these data; for example, it should be considered that the anticancer activity of these oligos is strictly dependent to the route of administration. Indeed, several preclinical studies revealed that the only strategy to achieve the full potential of CpG-ODN is represented by the locoregional delivery, not possible for the majority of cancer types [83,84]. Moreover, the activation of TLR9 by its cognate ligands triggers a series of feedback regulatory mechanisms to avoid uncontrolled inflammatory reactions. For instance, it has been reported that CpG-ODN stimulation leads to PD-1 upregulation in NK cells [109], B lymphocytes [91], monocytes and macrophages [90]. Accordingly, in the present study we found that PD-1 expression is increased on peritoneal immune cells after *in vivo* TLR9 triggering.

Therefore, the stimulation of the innate immunity by TLR9 agonists together with anti-PD-1 antibodies may represent a successful combinatorial immunotherapeutic strategy. TLR9 activation determines the activation of the immune response and PD-1 blockade prevents the occurrence of immunosuppressive mechanisms.

Ovarian cancer is described to partially benefit to TLR9 agonist administration, although never reaching a complete and durable cure [92], and it is characterized by a very limited responsiveness to anti-PD-1 antibody therapy [110,111], making this tumor type a good model to investigate the effects of this combination treatment.

We xenografted IGROV-1 human ovarian cancer cells in athymic nude mice, a mouse model lacking of T lymphocytes. The use of this mouse model allows to focus on the contribution of the innate arm of the immune system, since the role of the adaptive

immune cells in the context of CpG-ODN/anti-PD-1 antibody treatment has been already thoroughly investigated [60,62,63].

Unexpectedly, our results indicate that CpG-ODN/anti-PD-1 antibody combination showed an antitumor effect greatly reduced compared to CpG-ODN alone, independently of the clone of the anti-PD-1 antibody utilized. These data suggest the acquisition of pro-tumor and immunosuppressive activity by innate immunity following the exposure to both the immunotherapeutic agents. Analysis of the tumor immune contexture revealed the upregulation of the M2-related macrophage markers [112,113] CD206 and IL-10 in the tumor stroma of mice treated with the combination compared to CpG-ODN monotherapy, indicating the possible involvement of these innate immune cells in the reduced anti-tumor activity observed in the combination group. Accordingly, *in vivo* macrophage depletion and functional *in vitro* assays clearly indicated that macrophages are responsible for the impairment of TLR9 agonist antitumor efficacy upon combination with anti-PD-1 antibody.

Macrophages infiltrating the tumor microenvironment usually promote and sustain tumor growth. This ability is strictly dependent to their phenotype, that can be shaped by a plethora of different signals, such as factors released by tumor or immune cells or, in our specific case, by immunotherapeutic drugs.

By gene expression analysis, we observed that macrophages exposed *in vitro* to both immunotherapeutic drugs exhibited a peculiar gene expression profile completely different from the transcriptional profile of macrophages incubated with single agents. This result indicates that TLR9 activation and PD-1 blockade cooperate in reprogramming macrophage phenotype. Moreover, we found a statistically significant enrichment of both M1- and M2-associated pathways in RAW264.7 treated with CpG-ODN/anti-PD-1 antibody combination, suggesting a possible acquisition of a “mixed phenotype”. In tumors, macrophages are rarely polarized towards an M1 or M2 “pure” phenotype but, on the contrary, often show both M1 and M2 features [114–117]. Our results perfectly fit with this

view, since double treated-macrophages seem to express markers of both these opposite polarization statuses. For instance, mRNA levels of the M1-associated cytokines Il-12b and Tnfα [118,119] were increased in the combination regimen. Moreover, the mRNA expression of Il-6, which is a pro-inflammatory cytokine reported to be associated to both M1 and M2 macrophages [120,121], resulted up-regulated after exposure to both agents. Ccl1 and Ccl2 genes, reported to be associated to pro-tumor TAMs [43,113,122], rose after CpG-ODN/anti-PD-1 antibody exposure. When considering the transcription factors important to regulate macrophage phenotype switch, a marked boost of mRNA expression was observed only for the M2-related transcription factor Irf4 [123] but not for Irf5, which is peculiar of M1 macrophages [124]. Furthermore, the augmented mRNA expression of Nos2 is in line with the idea of a mixed phenotype, since this gene can be produced by both M1 and M2 macrophages [125]. Finally, the expression of Cd80 and Cd86 activation markers, which augmented in combination-treated RAW264.7 cells at both mRNA and protein level, suggests a very strong activation status of these macrophages. The Multiplex ELISA assays confirmed that the combination of CpG-ODN and anti-PD-1 antibody induces a mixed phenotype in macrophages, characterized by the secretion of M1- and M2-associated cytokines. Mass spectrometry analysis further shows that macrophages treated with the combination secrete different immunomodulatory factors. For example, betaine, found increased in RAW264.7 supernatants after combinatorial regimen exposure, is an essential biochemical molecule of the methionine/homocysteine cycle [126] and it is reported to exert pro-tumor and anti-tumor effects. Particularly, betaine can inhibit TLR signaling and the secretion of pro-inflammatory cytokines [127]. On the other hand, betaine has been recently considered as anti-inflammatory agent for the prevention of the occurrence of colon cancer [128] and, indeed, higher betaine intake results in lower cancer incidence [129]. Increased levels of polyamines belonging to arginine catabolism were also detected in supernatants of RAW264.7 incubated with CpG-ODN/anti-PD-1 Ab

combination compared to macrophages exposed to single agents. Polyamines, such as spermidine [130], derive from arginine conversion by Arginase I enzyme and represent essential molecules for cell proliferation and differentiation [131]. Moreover, polyamines participate in the regulation of inflammatory processes down-regulating the production of pro-inflammatory cytokines, as IL-12a, TNF-α, IL-6 and IL-1β, finally inducing macrophage polarization towards the M2 anti-inflammatory phenotype [132,133]. In line with the idea that macrophages incubated with both CpG-ODN and anti-PD-1 antibody may acquire a mixed phenotype, it is not surprising that increased amounts of spermidine were detected in the supernatants of the combination group compared to single agent groups, characteristic of M2 macrophages. However, at the same time, we observed an augmented level of citrulline in CpG-ODN/anti-PD-1 antibody treated macrophages. The catabolism of arginine in citrulline is mediated by iNOS that is an enzyme typical of M1 macrophages [134]. RAW264.7 macrophages treated with the combination regimen showed augmented citrulline level compared to the other experimental groups. Taken together, these results corroborate the acquisition of a mixed phenotype by combination-treated macrophages.

Even though the results obtained so far clearly point to a macrophage activation status in which M1- and M2-related features coexist, *in vivo* and *in vitro* functional experiments suggest that there is an imbalance towards an M2 phenotype, since these macrophages exhibit immunosuppressive functions and are able to promote tumor growth.

Our *in vivo* data indicate that, as expected, CpG-ODN exerted a good anti-tumor activity. Indeed, mice receiving TLR9 agonist showed a delay in tumor ascites appearance. Therefore, we hypothesized that the reduction in CpG-ODN efficacy observed in the combination group could be ascribed to anti-PD-1 antibody. Therefore, we attempted to unravel the mechanism through which anti-PD-1 antibody is able to dampen CpG-ODN antitumor activity. It has been reported that blocking PD-1 on macrophages can promote a

shift from a pro- to an anti-tumor state by increasing their phagocytic capability [41]. On the contrary, these innate immune cells can also increase the immune tolerance in the tumor microenvironment by secreting the immunoregulatory cytokine IL-10 upon interaction with anti-PD-1 antibody [71,90]. To ascertain the consequences of blocking PD-1 on macrophages in our experimental setting, *in vitro* experiments were performed using $F(ab)_2$ and Fc silent anti-PD-1 antibodies, that only retain the ability to recognize and bind PD-1 without interference of the antibody Fc domain, well known to mediate important biological functions [135]. Interestingly, the up-regulation of genes, found to be increased in the combination group in the previous experiment, was completely lost when using $F(ab)_2$ and Fc silent anti-PD-1 antibodies. Similarly, treatment of macrophages with anti-rat IgG2a isotype control, which possesses the same Fc domain of the anti-PD-1 antibody clone RMP1-14 but is not able to bind the PD-1 receptor, did not produce any modification in macrophage gene profile when combined to CpG-ODN, compared to TLR9 agonist alone. These results indicate that the antigen-binding site and the Fc domain of anti-PD-1 antibody, taken individually, are not sufficient but are equally important to influence macrophage gene expression upon combination with CpG-ODN. Most likely, the binding of the antibody to its target is a necessary prerequisite to induce the correct three-dimensional arrangement in order to allow the Fc domain to bind Fc receptors on macrophages, finally producing the observed biological effects. Indeed, the importance of Fc domain-FcRs interaction in determining functional and therapeutic activities of anti-PD-1 antibodies has been already demonstrated [71,135]. As mentioned, anti-PD-1 Fc domain was found to be one of the causes of hyperprogressive disease in NSCLC [71]. Based on these considerations, we can speculate that the binding of anti-PD-1 Fc portion to macrophage Fc receptors together with TLR9 activation may lead to the acquisition of a M2b phenotype by macrophages. Indeed, M2b macrophages are generated by the simultaneous stimulation of an antibody Fc domain and TLR agonists and represent a

subtype of M2 regulatory/immunosuppressive macrophages secreting both pro- and anti-inflammatory cytokines and associated with cancer progression [120].

Considering that the clone RMP1-14 of anti-PD-1 antibody is demonstrated to only interact with FcγR2b (CD32b) and FcγR3 (CD16) [102,103], we evaluated whether these FcγRs may participate in macrophage phenotype modulation observed in the combination treatment group. Unexpectedly, the blockade of both CD32b and CD16 by increasing concentrations of anti-CD16/32 blocking antibody did not abrogate the effect of CpG-ODN/anti-PD-1 antibody combination on macrophages. Furthermore, treatment of RAW264.7 cells with CpG-ODN in combination with decreasing concentrations of anti-PD-1 antibody ruled out the possibility that a small amount of the aforementioned receptors remained available following CD16/32 blockade, since the reprogramming of macrophages appears to be dose dependent. Excluding a direct involvement of FcγR2b and FcγR3, our results raise the question about which FcγRs are able to induce the macrophage shift in the combination group. Arlaukas et al. showed that the anti-PD-1 antibody, initially bound to PD-1 expressing cells, was actively uptaken by TAMs, internalized through the anti-PD-1 antibody Fc domain and subsequently degraded [136]. However, the Authors did not provide information about the fate of the antibody once entered into macrophage cytoplasm and the functional consequences of this internalization process.

It has been demonstrated that the Fc domain of antibodies can be recognized not only by the binding to classical cell-surface FcγRs, but also by the cytosolic IgG receptor tripartite motif- containing 21 (TRIM21) [137,138]. This intracellular immunoglobulin receptor binds IgG antibodies with higher affinity than FcγRs and is constitutively expressed by a plethora of cell subsets, including macrophages [139]. TRIM21 has been primarily studied for its role in antiviral response recruiting the proteasome machinery for neutralization and destruction of antibody-coated viral particles. TRIM21 signaling pathways involve the activation of different transcription factors, as NF-κB, eventually determining the release of

pro-inflammatory cytokines, such as IL-6, TNF and CXCL10 [140]. Based on these premises, we speculated that the degradation of anti-PD-1 antibody in macrophage cytosol might be mediated by TRIM21 and the proteasome system. To investigate this possibility, macrophages were treated as described above in presence of ubiquitin-proteasome inhibitor MG132. The inhibition of the proteasome machinery abrogated the mRNA upregulation observed in the combination group. Moreover, Trim21 silencing produced similar results, although not all the genes were significantly downregulated. The apparent discrepancy between the gene modulations obtained by these two experimental approaches could be related to the involvement of other biological regulators that, together with TRIM21, regulate macrophage phenotypic switch. Moreover, it is not surprising that the inhibition of the proteasome machinery resulted in a more marked downregulation of the same genes compared to Trim21-silenced macrophages, since the ubiquitin-proteasome pathway has broader biological functions compared to TRIM21 alone [141] and it also plays an important role in mediating the signal transduction of several TLRs, including TLR9 [142]. Indeed, it has been also demonstrated that the inhibition of the proteasome system in RAW264.7 cells abrogates the CpG-ODN-induced inflammatory gene expression [143], as we observed in our experimental setting. Thus, it is plausible that the inhibition of the ubiquitin-proteasome system in macrophages may also negatively impact on TLR9 signaling, resulting in a more marked effect on the genes upregulated by the CpG-ODN/anti-PD-1 antibody combination treatment.

CONCLUSIONS

Taken together, our results demonstrated that macrophages are the innate immune cells responsible for the impairment of CpG-ODN antitumor efficacy when combined to anti-PD-1 antibody. The treatment with both agents triggers a phenotype shift of macrophages towards a mixed state, characterized by an upregulation of both M1- and M2-associated genes, although the final outcome of macrophage functionality is characterized by immunosuppressive and protumor activity. Finally, we elucidated the mechanism through which the anti-PD-1 antibody dampens CpG-ODN antitumor efficacy, demonstrating that both the direct blockade of the inhibitory receptor PD-1 and the binding of the Fc domain with the intracellular Fc receptor TRIM21 are pivotal to determine the phenotype reprogramming in macrophages. Since immunotherapies based on TLR9 stimulation and PD-1 blockade are already under investigation in several clinical trials, the impact of this combination on macrophages should be taken into serious consideration in order to prevent undesirable adverse effects, especially in tumors where the presence of both resident and recruited macrophages is particularly abundant, such as ovarian, lung and hepatocellular carcinoma [144,145]. Moreover, the activation of TLRs cannot only be achieved by microbial products or synthetic agonists but also by molecules present in the tumor microenvironment, released by tumor of immune/stromal cells. Therefore, macrophages in which TLR signaling was activated by those factors could undergo a phenotype reprogramming also in the context of anti-PD-1 antibody monotherapy, determining an acceleration of tumor growth, as already described for hyperprogressive disease.

BILBIOGRAPHY

[1] L.S. Miller, Toll-Like Receptors in Skin, Adv. Dermatol. 24 (2008) 71–87. https://doi.org/10.1016/j.yadr.2008.09.004.

[2] G. Liu, Y. Zhao, Toll-like receptors and immune regulation: Their direct and indirect modulation on regulatory CD4+ CD25+ T cells, Immunology. 122 (2007) 149–156. https://doi.org/10.1111/j.1365-2567.2007.02651.x.

[3] L. Nie, S.Y. Cai, J.Z. Shao, J. Chen, Toll-Like Receptors, Associated Biological Roles, and Signaling Networks in Non-Mammals, Front. Immunol. 9 (2018). https://doi.org/10.3389/fimmu.2018.01523.

[4] K.C.M. Santegoets, L. Van Bon, W.B. Van Den Berg, M.H. Wenink, T.R.D.J. Radstake, Toll-like receptors in rheumatic diseases: Are we paying a high price for our defense against bugs?, FEBS Lett. (2011). https://doi.org/10.1016/j.febslet.2011.04.028.

[5] S. Akira, K. Takeda, Toll-like receptor signalling, Nat. Rev. Immunol. (2004). https://doi.org/10.1038/nri1391.

[6] T. Kawai, S. Akira, TLR signaling, Semin. Immunol. 19 (2007) 24–32. https://doi.org/10.1016/j.smim.2006.12.004.

[7] T. Kawai, S. Akira, The role of pattern-recognition receptors in innate immunity: Update on toll-like receptors, Nat. Immunol. (2010). https://doi.org/10.1038/ni.1863.

[8] S. Akira, S. Uematsu, O. Takeuchi, Pathogen recognition and innate immunity, Cell. (2006). https://doi.org/10.1016/j.cell.2006.02.015.

[9] G.M. Barton, J.C. Kagan, R. Medzhitov, Intracellular localization of Toll-like receptor 9 prevents recognition of self DNA but facilitates access to viral DNA, Nat. Immunol. 7 (2006) 49–56. https://doi.org/10.1038/ni1280.

[10] B. Park, M.M. Brinkmann, E. Spooner, C.C. Lee, Y.M. Kim, H.L. Ploegh, Proteolytic cleavage in an endolysosomal compartment is required for Toll-like receptor 9

activation, Nat. Immunol. 9 (2008) 1407–1414.

[11] S.E. Ewald, B.L. Lee, L. Lau, K.E. Wickliffe, G.P. Shi, H.A. Chapman, G.M. Barton, The ectodomain of Toll-like receptor 9 is cleaved to generate a functional receptor, Nature. 456 (2008) 658–662.

[12] F. Matsumoto, S.I. Saitoh, R. Fukui, T. Kobayashi, N. Tanimura, K. Konno, Y. Kusumoto, S. Akashi-Takamura, K. Miyake, Cathepsins are required for Toll-like receptor 9 responses, Biochem. Biophys. Res. Commun. 367 (2008) 693–699. https://doi.org/10.1016/j.bbrc.2007.12.130.

[13] M. Asagiri, T. Hirai, T. Kunigami, S. Kamano, H. Gober, K. Okamoto, K. Nishikawa, E. Latz, D.T. Golenbock, K. Aoki, K. Ohya, Y. Imai, Y. Morishita, K. Miyazono, Cathepsin K–Dependent Toll-Like Receptor 9 Signaling Revealed in Experimental Arthritis, (2008) 624–627.

[14] K.J. McKelvey, J. Highton, P.A. Hessian, Cell-specific expression of TLR9 isoforms in inflammation, J. Autoimmun. 36 (2011) 76–86. https://doi.org/10.1016/j.jaut.2010.11.001.

[15] A.M. Hosseini, J. Majidi, B. Baradaran, M. Yousefi, Toll-like receptors in the pathogenesis of autoimmune diseases, Adv. Pharm. Bull. 5 (2015) 605–614. https://doi.org/10.15171/apb.2015.082.

[16] A.A. Ashkar and K.L. Rosenthal, Toll-like Receptor 9, CpG DNA and Innate Immunity, Curr. Mol. Med. 2 (2002) 546–556.

[17] A.M. Krieg, CpG motifs in bacterial DNA and their immune effects, Annu. Rev. Immunol. 20 (2002) 709–760. https://doi.org/10.1146/annurev.immunol.20.100301.064842.

[18] M.J. McCluskie, R.D. Weeratna, Novel adjuvant systems, Curr. Drug Targets - Infect. Disord. 1 (2001) 263–271.

[19] S. Agrawal, E.R. Kandimalla, Intratumoural immunotherapy: activation of nucleic

acid sensing pattern recognition receptors, Immuno-Oncology Technol. 3 (2019) 15–23. https://doi.org/10.1016/j.iotech.2019.10.001.

[20] O. Hamid, R. Ismail, I. Puzanov, Intratumoral Immunotherapy—Update 2019, Oncologist. 25 (2020) e423–e438. https://doi.org/10.1634/theoncologist.2019-0438.

[21] Y.H. Kim, M. Girardi, M. Duvic, T. Kuzel, B.K. Link, L. Pinter-Brown, A.H. Rook, Phase i trial of a Toll-like receptor 9 agonist, PF-3512676 (CPG 7909), in patients with treatment-refractory, cutaneous T-cell lymphoma, J. Am. Acad. Dermatol. 63 (2010) 975–983. https://doi.org/10.1016/j.jaad.2009.12.052.

[22] M.A. Hofmann, C. Kors, H. Audring, P. Walden, W. Sterry, U. Trefzer, Phase 1 Evaluation of Intralesionally Injected TLR9-agonist PF-3512676 in Patients With Basal Cell Carcinoma or Metastatic Melanoma, J. Immunother. 31 (2008) 520–527.

[23] T. Okazaki, A. Maeda, H. Nishimura, T. Kurosaki, T. Honjo, PD-1 immunoreceptor inhibits B cell receptor-mediated signaling by recruiting src homology 2-domain-containing tyrosine phosphatase 2 to phosphotyrosine, Proc. Natl. Acad. Sci. U. S. A. 98 (2001) 13866–13871. https://doi.org/10.1073/pnas.231486598.

[24] J.M. Chemnitz, R.V. Parry, K.E. Nichols, C.H. June, J.L. Riley, SHP-1 and SHP-2 Associate with Immunoreceptor Tyrosine-Based Switch Motif of Programmed Death 1 upon Primary Human T Cell Stimulation, but Only Receptor Ligation Prevents T Cell Activation, J. Immunol. 173 (2004) 945–954. https://doi.org/10.4049/jimmunol.173.2.945.

[25] L. Strauss, M.A.A. Mahmoud, J.D. Weaver, N.M. Tijaro-Ovalle, A. Christofides, Q. Wang, R. Pal, M. Yuan, J. Asara, N. Patsoukis, V.A. Boussiotis, Targeted deletion of PD-1 in myeloid cells induces antitumor immunity, Sci. Immunol. 5 (2020) 1–27. https://doi.org/10.1126/sciimmunol.aay1863.

[26] M.J. Butte, M.E. Keir, T.B. Phamduy, A.H. Sharpe, G.J. Freeman, H. Sharpe, PD-L1 interacts specifically with B7-1 to inhibit T cell proliferation, Immunity. 27 (2009) 111–

122. https://doi.org/10.1016/j.immuni.2007.05.016.PD-L1.

[27] L.M. Francisco, P.T. Sage, A.H. Sharpe, The PD-1 Pathway in Tolerance and Autoimmunity, Immunol. Rev. 236 (2010) 219–242.

[28] H. Nishimura, M. Nose, H. Hiai, N. Minato, T. Honjo, Development of lupus-like autoimmune diseases by disruption of the PD-1 gene encoding an ITIM motif-carrying immunoreceptor, Immunity. 11 (1999) 141–151. https://doi.org/10.1016/S1074-7613(00)80089-8.

[29] A.H. Sharpe, K.E. Pauken, The diverse functions of the PD1 inhibitory pathway, Nat. Rev. Immunol. 18 (2018) 153–167. https://doi.org/10.1038/nri.2017.108.

[30] Y.J. Lim, J. Koh, K. Kim, E.K. Chie, B. Kim, K.B. Lee, J.Y. Jang, S.W. Kim, D.Y. Oh, Y.J. Bang, S.W. Ha, High ratio of programmed cell death protein 1 (PD-1)+/CD8+ tumor-infiltrating lymphocytes identifies a poor prognostic subset of extrahepatic bile duct cancer undergoing surgery plus adjuvant chemoradiotherapy, Radiother. Oncol. 117 (2015) 165–170. https://doi.org/10.1016/j.radonc.2015.07.003.

[31] X. Huang, F. Venet, Y.L. Wang, A. Lepape, Z. Yuan, Y. Chen, R. Swan, H. Kherouf, G. Monneret, C.S. Chung, A. Ayala, PD-1 expression by macrophages plays a pathologic role in altering microbial clearance and the innate inflammatory response to sepsis, Proc. Natl. Acad. Sci. U. S. A. 106 (2009) 6303–6308. https://doi.org/10.1073/pnas.0809422106.

[32] N. Patsoukis, Q. Wang, L. Strauss, V.A. Boussiotis, Revisiting the PD-1 pathway, 1 (2020).

[33] J. Cai, D. Wang, G. Zhang, X. Guo, The role of PD-1/PD-L1 axis in treg development and function: Implications for cancer immunotherapy, Onco. Targets. Ther. 12 (2019) 8437–8445. https://doi.org/10.2147/OTT.S221340.

[34] R.V. Parry, J.M. Chemnitz, K.A. Frauwirth, A.R. Lanfranco, I. Braunstein, S.V. Kobayashi, P.S. Linsley, C.B. Thompson, J.L. Riley, CTLA-4 and PD-1 Receptors

Inhibit T-Cell Activation by Distinct Mechanisms, Mol. Cell. Biol. 25 (2005) 9543–9553. https://doi.org/10.1128/mcb.25.21.9543-9553.2005.

[35] M.E. Keir, M.J. Butte, G.J. Freeman, A.H. Sharpe, PD-1 and its ligands in tolerance and immunity, Annu. Rev. Immunol. 26 (2008) 677–704. https://doi.org/10.1146/annurev.immunol.26.021607.090331.

[36] S. Kleffel, C. Posch, S.R. Barthel, H. Mueller, E. Guenova, C.P. Elco, N. Lee, R. Vikram, Q. Zhan, C.G. Lian, R. Thomi, W. Hoetzenecker, R. Dummer, M.C.M. Jr, K.T. Flaherty, M.H. Frank, G.F. Murphy, A.H. Sharpe, T.S. Kupper, T. Schatton, Melanoma cell-intrinsic PD-1 receptor functions promote tumor growth, 162 (2016) 1242–1256. https://doi.org/10.1016/j.cell.2015.08.052.Melanoma.

[37] Y. Han, D. Liu, L. Li, PD-1/PD-L1 pathway: current researches in cancer., Am. J. Cancer Res. 10 (2020) 727–742. http://www.ncbi.nlm.nih.gov/pubmed/32266087.

[38] A. Salmaninejad, V. Khoramshahi, A. Azani, E. Soltaninejad, S. Aslani, M.R. Zamani, M. Zal, A. Nesaei, S.M. Hosseini, PD-1 and cancer: molecular mechanisms and polymorphisms, Immunogenetics. 70 (2018) 73–86. https://doi.org/10.1007/s00251-017-1015-5.

[39] K.E. Pauken and E.J. Wherry, Overcoming T cell exhaustion in infection and cancer, Trends Immunol. 36 (2015) 265–276. https://doi.org/10.1016/j.it.2015.02.008.Overcoming.

[40] F. Schütz, S. Stefanovic, L. Mayer, A. Von Au, C. Domschke, C. Sohn, PD-1/PD-L1 Pathway in Breast Cancer, Oncol. Res. Treat. 40 (2017) 294–297. https://doi.org/10.1159/000464353.

[41] S.R. Gordon, R.L. Maute, B.W. Dulken, G. Hutter, B.M. George, M.N. McCracken, R. Gupta, J.M. Tsai, R. Sinha, D. Corey, A.M. Ring, A.J. Connolly, I.L. Weissman, PD-1 expression by tumour-associated macrophages inhibits phagocytosis and tumour immunity, Nature. 545 (2017) 495–499.

https://doi.org/10.1038/nature22396.PD-1.

[42] D. Lu, Z. Ni, X. Liu, S. Feng, X. Dong, X. Shi, J. Zhai, S. Mai, J. Jiang, Z. Wang, H. Wu, K. Cai, Beyond T Cells: Understanding the Role of PD-1/PD-L1 in Tumor-Associated Macrophages, J. Immunol. Res. (2019).

[43] Y. Jiang, M. Chen, H. Nie, Y. Yuan, PD-1 and PD-L1 in cancer immunotherapy: clinical implications and future considerations, Hum. Vaccines Immunother. 15 (2019) 1111–1122. https://doi.org/10.1080/21645515.2019.1571892.

[44] C. Robert, G.V. Long, B. Brady, C. Dutriaux, M. Maio, L. Mortier, J.C. Hassel, P. Rutkowski, C. McNeil, E. Kalinka-Warzocha, K.J. Savage, M.M. Hernberg, C. Lebbé, J. Charles, C. Mihalcioiu, V. Chiarion-Sileni, C. Mauch, F. Cognetti, A. Arance, H. Schmidt, D. Schadendorf, H. Gogas, L. Lundgren-Eriksson, C. Horak, B. Sharkey, I.M. Waxman, V. Atkinson, P.A. Ascierto, Nivolumab in Previously Untreated Melanoma without BRAF Mutation , N. Engl. J. Med. 372 (2015) 320–330. https://doi.org/10.1056/nejmoa1412082.

[45] J. Brahmer, K.L. Reckamp, P. Baas, L. Crinò, W.E.E. Eberhardt, E. Poddubskaya, S. Antonia, A. Pluzanski, E.E. Vokes, E. Holgado, D. Waterhouse, N. Ready, J. Gainor, O. Arén Frontera, L. Havel, M. Steins, M.C. Garassino, J.G. Aerts, M. Domine, L. Paz-Ares, M. Reck, C. Baudelet, C.T. Harbison, B. Lestini, D.R. Spigel, Nivolumab versus Docetaxel in Advanced Squamous-Cell Non–Small-Cell Lung Cancer, N. Engl. J. Med. 373 (2015) 123–135. https://doi.org/10.1056/nejmoa1504627.

[46] K.V. Lepik, N.V. Mikhailova, E.V. Kondakova, L.A. Tsvetkova, Y.R. Zalyalov, E.S. Borzenkova, I.S. Moiseev, V.V. Baykov, B.A. Afanasyev, Efficacy and safety of nivolumab in the treatment of relapsed/refractory classical Hodgkin’s lymphoma: Pavlov First Saint Petersburg State Medical University experience, 13 (2018).

[47] C. Robert, J. Schachter, G. V. Long, A. Arance, J.J. Grob, L. Mortier, A. Daud, M.S.

Carlino, C. McNeil, M. Lotem, J. Larkin, P. Lorigan, B. Neyns, C.U. Blank, O. Hamid, C. Mateus, R. Shapira-Frommer, M. Kosh, H. Zhou, N. Ibrahim, S. Ebbinghaus, A. Ribas, Pembrolizumab versus Ipilimumab in Advanced Melanoma, N. Engl. J. Med. 372 (2015) 2521–2532. https://doi.org/10.1056/nejmoa1503093.

[48] A. Ribas, O. Hamid, A. Daud, F.S. Hodi, J.D. Wolchok, R. Kefford, A.M. Joshua, A. Patnaik, W.J. Hwu, J.S. Weber, T.C. Gangadhar, P. Hersey, R. Dronca, R.W. Joseph, H. Zarour, B. Chmielowski, D.P. Lawrence, A. Algazi, N.A. Rizvi, B. Hoffner, C. Mateus, K. Gergich, J.A. Lindia, M. Giannotti, X.N. Li, S. Ebbinghaus, S.P. Kang, C. Robert, Association of pembrolizumab with tumor response and survival among patients with advanced melanoma, JAMA - J. Am. Med. Assoc. 315 (2016) 1600–1609. https://doi.org/10.1001/jama.2016.4059.

[49] E.B. Garon, N.A. Rizvi, R. Hui, N. Leighl, A.S. Balmanoukian, J.P. Eder, A. Patnaik, C. Aggarwal, M. Gubens, L. Horn, E. Carcereny, M.-J. Ahn, E. Felip, J.S. Lee, M.D. Hellmann, O. Hamid, J.W. Goldman, J.-C. Soria, M. Dolled-Filhart, R.Z. Rutledge, J. Zhang, J.K. Lunceford, R. Rangwala, G.M. Lubiniecki, C. Roach, K. Emancipator, L. Gandhi, Pembrolizumab for the Treatment of Non–Small-Cell Lung Cancer, N. Engl. J. Med. 372 (2015) 2018–2028. https://doi.org/10.1056/nejmoa1501824.

[50] M. Tahara, K. Muro, Y. Hasegawa, H.C. Chung, C.C. Lin, B. Keam, K. Takahashi, J.D. Cheng, Y.J. Bang, Pembrolizumab in Asia-Pacific patients with advanced head and neck squamous cell carcinoma: Analyses from KEYNOTE-012, Cancer Sci. 109 (2018) 771–776. https://doi.org/10.1111/cas.13480.

[51] M.R. Migden, D. Rischin, C.D. Schmults, A. Guminski, A. Hauschild, K.D. Lewis, C.H. Chung, L. Hernandez-Aya, A.M. Lim, A.L.S. Chang, G. Rabinowits, A.A. Thai, L.A. Dunn, B.G.M. Hughes, N.I. Khushalani, B. Modi, D. Schadendorf, B. Gao, F. Seebach, S. Li, J. Li, M. Mathias, J. Booth, K. Mohan, E. Stankevich, H.M. Babiker, I. Brana, M. Gil-Martin, J. Homsi, M.L. Johnson, V. Moreno, J. Niu, T.K. Owonikoko,

K.P. Papadopoulos, G.D. Yancopoulos, I. Lowy, M.G. Fury, PD-1 Blockade with Cemiplimab in Advanced Cutaneous Squamous-Cell Carcinoma, N. Engl. J. Med. (2018) 341–351. https://doi.org/10.1056/nejmoa1805131.

[52] Y. Yang, Z. Wang, J. Fang, Q. Yu, B. Han, S. Cang, G. Chen, X. Mei, Z. Yang, R. Ma, M. Bi, X. Ren, J. Zhou, B. Li, Y. Song, J. Feng, J. Li, Z. He, R. Zhou, W. Li, Y. Lu, Y. Wang, L. Wang, N. Yang, Y. Zhang, Z. Yu, Y. Zhao, C. Xie, Y. Cheng, H. Zhou, S. Wang, D. Zhu, W. Zhang, L. Zhang, Efficacy and Safety of Sintilimab Plus Pemetrexed and Platinum as First-Line Treatment for Locally Advanced or Metastatic Nonsquamous NSCLC: a Randomized, Double-Blind, Phase 3 Study (Oncology pRogram by InnovENT anti-PD-1-11), J. Thorac. Oncol. 15 (2020) 1636–1646. https://doi.org/10.1016/j.jtho.2020.07.014.

[53] A. Oaknin, A.V. Tinker, L. Gilbert, V. Samouëlian, C. Mathews, J. Brown, M.P. Barretina-Ginesta, V. Moreno, A. Gravina, C. Abdeddaim, S. Banerjee, W. Guo, H. Danaee, E. Im, R. Sabatier, Clinical Activity and Safety of the Anti-Programmed Death 1 Monoclonal Antibody Dostarlimab for Patients with Recurrent or Advanced Mismatch Repair-Deficient Endometrial Cancer: A Nonrandomized Phase 1 Clinical Trial, JAMA Oncol. 6 (2020) 1766–1772. https://doi.org/10.1001/jamaoncol.2020.4515.

[54] X. Ni, Y. Xing, X. Sun, J. Suo, The safety and efficacy of anti-PD-1/anti-PD-L1 antibody therapy in the treatment of previously treated, advanced gastric or gastro-oesophageal junction cancer: A meta-analysis of prospective clinical trials, Clin. Res. Hepatol. Gastroenterol. 44 (2020) 211–222. https://doi.org/10.1016/j.clinre.2019.05.007.

[55] M. Okada, T. Kijima, K. Aoe, T. Kato, N. Fujimoto, K. Nakagawa, Y. Takeda, T. Hida, K. Kanai, F. Imamura, S. Oizumi, T. Takahashi, M. Takenoyama, H. Tanaka, J. Hirano, Y. Namba, Y. Ohe, Clinical efficacy and safety of nivolumab: Results of a

multicenter, open-label, single-arm, Japanese phase II study in malignant pleural mesothelioma (MERIT), Clin. Cancer Res. 25 (2019) 5485–5492. https://doi.org/10.1158/1078-0432.CCR-19-0103.

[56] J. Larkin, V. Chiarion-Sileni, R. Gonzalez, J.J. Grob, P. Rutkowski, C.D. Lao, C.L. Cowey, D. Schadendorf, J. Wagstaff, R. Dummer, P.F. Ferrucci, M. Smylie, D. Hogg, A. Hill, I. Márquez-Rodas, J. Haanen, M. Guidoboni, M. Maio, P. Schöffski, M.S. Carlino, C. Lebbé, G. McArthur, P.A. Ascierto, G.A. Daniels, G. V. Long, L. Bastholt, J.I. Rizzo, A. Balogh, A. Moshyk, F.S. Hodi, J.D. Wolchok, Five-Year Survival with Combined Nivolumab and Ipilimumab in Advanced Melanoma, N. Engl. J. Med. 381 (2019) 1535–1546. https://doi.org/10.1056/nejmoa1910836.

[57] S.J. Antonia, H. Borghaei, S.S. Ramalingam, L. Horn, J. De Castro, A. Pluzanski, M.A. Burgio, M. Garassino, L.Q.M. Chow, L. Crinò, D. Planchard, C. Butts, A. Drilon, J. Wojcik-, G.A. Otterson, S. Agrawal, A. Li, J.R. Penrod, J. Brahmer, Four-year survival with nivolumab in patients with previously treated advanced non-small-cell lung cancer: a pooled analysis, Lancet Oncol. 20 (2019) 1395–1408. https://doi.org/10.1016/S1470-2045(19)30407-3.Four-year.

[58] C.S. Fuchs, T. Doi, R.W. Jang, K. Muro, T. Satoh, M. Machado, W. Sun, S.I. Jalal, M.A. Shah, J.P. Metges, M. Garrido, T. Golan, M. Mandala, Z.A. Wainberg, D. V. Catenacci, A. Ohtsu, K. Shitara, R. Geva, J. Bleeker, A.H. Ko, G. Ku, P. Philip, P.C. Enzinger, Y.J. Bang, D. Levitan, J. Wang, M. Rosales, R.P. Dalal, H.H. Yoon, Safety and efficacy of pembrolizumab monotherapy in patients with previously treated advanced gastric and gastroesophageal junction cancer: Phase 2 clinical KEYNOTE-059 trial, JAMA Oncol. 4 (2018) 1–8. https://doi.org/10.1001/jamaoncol.2018.0013.

[59] Y.C. Chuang, J.C. Tseng, L.R. Huang, C.M. Huang, C.Y.F. Huang, T.H. Chuang, Adjuvant Effect of Toll-Like Receptor 9 Activation on Cancer Immunotherapy Using

Checkpoint Blockade, Front. Immunol. 11 (2020) 1–14. https://doi.org/10.3389/fimmu.2020.01075.

[60] S.M. Mangsbo, L.C. Sandin, K. Anger, A.J. Korman, A. Loskog, T.H. Tötterman, Enhanced tumor eradication by combining CTLA-4 or PD-1 blockade with CpG therapy, J. Immunother. 33 (2010) 225–235. https://doi.org/10.1097/CJI.0b013e3181c01fcb.

[61] K. Kapp, B. Volz, D. Oswald, B. Wittig, M. Baumann, M. Schmidt, Beneficial modulation of the tumor microenvironment and generation of anti-tumor responses by TLR9 agonist lefitolimod alone and in combination with checkpoint inhibitors, Oncoimmunology. 8 (2019). https://doi.org/10.1080/2162402X.2019.1659096.

[62] F. Sato-Kaneko, S. Yao, A. Ahmadi, S.S. Zhang, T. Hosoya, M.M. Kaneda, J.A. Varner, M. Pu, K.S. Messer, C. Guiducci, R.L. Coffman, K. Kitaura, T. Matsutani, R. Suzuki, D.A. Carson, T. Hayashi, E.E.W. Cohen, Combination immunotherapy with TLR agonists and checkpoint inhibitors suppresses head and neck cancer, JCI Insight. 2 (2017) 1–18. https://doi.org/10.1172/jci.insight.93397.

[63] S. Wang, J. Campos, M. Gallotta, M. Gong, C. Crain, E. Naik, R.L. Coffman, C. Guiducci, Intratumoral injection of a CpG oligonucleotide reverts resistance to PD-1 blockade by expanding multifunctional CD8+ T cells, Proc. Natl. Acad. Sci. U. S. A. 113 (2016) E7240–E7249. https://doi.org/10.1073/pnas.1608555113.

[64] A. Ribas, T. Medina, S. Kummar, A. Amin, A. Kalbasi, J.J. Drabick, M. Barve, G.A. Daniels, D.J. Wong, E. V. Schmidt, A.F. Candia, R.L. Coffman, A.C.F. Leung, R.S. Janssen, Sd-101 in combination with pembrolizumab in advanced melanoma: Results of a phase ib, multicenter study, Cancer Discov. 8 (2018). https://doi.org/10.1158/2159-8290.CD-18-0280.

[65] M.M. Milhem, G.V. Long, C.J. Hoimes, A. Amin, C.D. Lao, R.M. Conry, J. Hunt, G.A. Daniels, M. Almubarak, M.F. Shaheen, T.M. Medina, M.A. Barve, S.K. Bishnoi,

E.A. Abdi, M.J. Chisamore, B. Xing, A. Candia, E. Gamelin, R. Janssen, A. Ribas, Phase 1b/2, open label, multicenter, study of the combination of SD-101 and pembrolizumab in patients with advanced melanoma who are naïve to anti-PD-1 therapy, J. Clin. Oncol. 337 (2019) 9534-.

[66] C.A. Janeway, R. Medzhitov, Innate immune recognition, Annu. Rev. Immunol. 20 (2002) 197–216. https://doi.org/10.1146/annurev.immunol.20.083001.084359.

[67] G.Y. Chen, G. Nuñez, Sterile inflammation: Sensing and reacting to damage, Nat. Rev. Immunol. 10 (2010) 826–837. https://doi.org/10.1038/nri2873.

[68] B. Kelly, L.A.J. O'Neill, Metabolic reprogramming in macrophages and dendritic cells in innate immunity, Cell Res. 25 (2015) 771–784. https://doi.org/10.1038/cr.2015.68.

[69] P. Fang, X. Li, J. Dai, L. Cole, J.A. Camacho, Y. Zhang, Y. Ji, J. Wang, X.F. Yang, H. Wang, Immune cell subset differentiation and tissue inflammation, J. Hematol. Oncol. 11 (2018) 1–22. https://doi.org/10.1186/s13045-018-0637-x.

[70] T. Krausgruber, K. Blazek, T. Smallie, S. Alzabin, H. Lockstone, N. Sahgal, T. Hussell, M. Feldmann, I.A. Udalova, IRF5 promotes inflammatory macrophage polarization and TH1-TH17 responses, Nat. Imm. 12 (2011) 231–238.

[71] G. Lo Russo, M. Moro, M. Sommariva, V. Cancila, M. Boeri, G. Centonze, S. Ferro, M. Ganzinelli, P. Gasparini, V. Huber, M. Milione, L. Porcu, C. Proto, G. Pruneri, D. Signorelli, S. Sangaletti, L. Sfondrini, C. Storti, E. Tassi, A. Bardelli, S. Marsoni, V. Torri, C. Tripodo, M.P. Colombo, A. Anichini, L. Rivoltini, A. Balsari, G. Sozzi, M.C. Garassino, Antibody-Fc/FcR Interaction on Macrophages as a Mechanism for Hyperprogressive Disease in Non-small Cell Lung Cancer Subsequent to PD-1/PD-L1 Blockade, Clin. Cancer Res. 25 (2019) 989–999.

[72] E.K. Colvin, Tumor-associated macrophages contribute to tumor progression in ovarian cancer, Front. Oncol. 4 JUN (2014) 1–6. https://doi.org/10.3389/fonc.2014.00137.

[73] D.A. Chistiakov, Y.V. Bobryshev, N.G. Nikiforov, N.V. Elizova, I.A. Sobenin, A.N. Orekhov, Macrophage phenotypic plasticity in atherosclerosis: The associated features and the peculiarities of the expression of inflammatory genes, Int. J. Cardiol. 184 (2015) 436–445. https://doi.org/10.1016/j.ijcard.2015.03.055.

[74] N. Wang, H. Liang, K. Zen, Molecular mechanisms that influence the macrophage M1-M2 polarization balance, Front. Immunol. 5 (2014) 1–9. https://doi.org/10.3389/fimmu.2014.00614.

[75] X. Liao, N. Sharma, F. Kapadia, G. Zhou, Y. Lu, H. Hong, K. Paruchuri, G.H. Mahabeleshwar, E. Dalmas, N. Venteclef, C.A. Flask, J. Kim, B.W. Doreian, K.Q. Lu, K.H. Kaestner, A. Hamik, K. Clément, M.K. Jain, Krüppel-like factor 4 regulates macrophage polarization, J. Clin. Invest. 121 (2011) 2736–2749.

[76] M.A. Bouhlel, B. Derudas, E. Rigamonti, R. Dièvart, J. Brozek, S. Haulon, C. Zawadzki, B. Jude, G. Torpier, N. Marx, B. Staels, G. Chinetti-Gbaguidi, PPARγ Activation Primes Human Monocytes into Alternative M2 Macrophages with Anti-inflammatory Properties, Cell Metab. 6 (2007) 137–143. https://doi.org/10.1016/j.cmet.2007.06.010.

[77] S. Gordon, Alternative activation of macrophages, Nat. Rev. Immunol. 3 (2003) 23–35. https://doi.org/10.1038/nri978.

[78] F.O. Martinez, S. Gordon, The M1 and M2 paradigm of macrophage activation: Time for reassessment, F1000Prime Rep. 6 (2014) 1–13. https://doi.org/10.12703/P6-13.

[79] A. Sica, V. Bronte, Altered macrophage differentiation and immune dysfunction in tumor development, J. Clin. Invest. 117 (2007) 1155–1166. https://doi.org/10.1172/JCI31422.

[80] R. Ocaña-Guzman, L. Vázquez-Bolaños, I. Sada-Ovalle, Receptors that inhibit macrophage activation: Mechanisms and signals of regulation and tolerance, J. Immunol. Res. 2018 (2018). https://doi.org/10.1155/2018/8695157.

[81] P. Workman, E.O. Aboagye, F. Balkwill, A. Balmain, G. Bruder, D.J. Chaplin, J.A. Double, J. Everitt, D.A.H. Farningham, M.J. Glennie, L.R. Kelland, V. Robinson, I.J. Stratford, G.M. Tozer, S. Watson, S.R. Wedge, S.A. Eccles, V. Navaratnam, S. Ryder, Guidelines for the welfare and use of animals in cancer research, Br. J. Cancer. 102 (2010) 1555–1577. https://doi.org/10.1038/sj.bjc.6605642.

[82] E. Nardini, D. Morelli, P. Aiello, D. Besusso, C. Calcaterra, L. Mariani, M. Palazzo, A. Vecchi, S. Paltrinieri, S. Menard, A. Balsari, CpG-oligodeoxynucleotides induce mobilization of hematopoietic progenitor cells into peripheral blood in association with mouse KC (IL-8) production, J. Cell. Physiol. 204 (2005) 889–895. https://doi.org/10.1002/jcp.20360.

[83] M. De Cesare, C. Calcaterra, G. Pratesi, L. Gatti, F. Zunino, S. Mènard, A. Balsari, Eradication of ovarian tumor xenografts by locoregional administration of targeted immunotherapy, Clin. Cancer Res. 14 (2008) 5512–5518. https://doi.org/10.1158/1078-0432.CCR-08-0445.

[84] M. De Cesare, L. Sfondrini, M. Campiglio, M. Sommariva, F. Bianchi, P. Perego, N. Van Rooijen, R. Supino, C. Rumio, F. Zunino, G. Pratesi, E. Tagliabue, A. Balsari, Ascites regression and survival increase in mice bearing advanced-stage human ovarian carcinomas and repeatedly treated intraperitoneally with CpG-ODN, J. Immunother. 33 (2010) 8–15. https://doi.org/10.1097/CJI.0b013e3181affaa7.

[85] A. Ray, B.N. Dittel, Isolation of mouse peritoneal cavity cells, J. Vis. Exp. (2010) 9–11. https://doi.org/10.3791/1488.

[86] S. Camelliti, V. Le Noci, F. Bianchi, C. Storti, F. Arnaboldi, A. Cataldo, S. Indino, E. Jachetti, M. Figini, M.P. Colombo, A. Balsari, N. Gagliano, E. Tagliabue, L. Sfondrini, M. Sommariva, Macrophages impair tlr9 agonist antitumor activity through interacting with the anti-pd-1 antibody fc domain, Cancers (Basel). 13 (2021) 1–21. https://doi.org/10.3390/cancers13164081.

[87] V. Girish, A. Vijayalakshmi, Affordable image analysis using NIH Image/ImageJ, Indian J. Cancer. 41 (2004) 47.

[88] K.J. Livak, T.D. Schmittgen, Analysis of relative gene expression data using real-time quantitative PCR and the $2^{-\Delta\Delta CT}$ method, Methods. 25 (2001) 402–408. https://doi.org/10.1006/meth.2001.1262.

[89] T. Metsalu, J. Vilo, ClustVis: A web tool for visualizing clustering of multivariate data using Principal Component Analysis and heatmap, Nucleic Acids Res. 43 (2015) W566–W570. https://doi.org/10.1093/nar/gkv468.

[90] E.A. Said, F.P. Dupuy, L. Trautmann, Y. Zhang, Y. Shi, M. El-Far, B.J. Hill, A. Noto, P. Ancuta, Y. Peretz, S.G. Fonseca, J. Van Grevenynghe, M.R. Boulassel, J. Bruneau, N.H. Shoukry, J.P. Routy, D.C. Douek, E.K. Haddad, R.P. Sekaly, Programmed death-1-induced interleukin-10 production by monocytes impairs $CD4^+$ T cell activation during HIV infection, Nat. Med. 16 (2010) 452–459. https://doi.org/10.1038/nm.2106.

[91] X. Xiao, X.M. Lao, M.M. Chen, R.X. Liu, Y. Wei, F.Z. Ouyang, D.P. Chen, X.Y. Zhao, Q. Zhao, X.F. Li, C.L. Liu, L. Zheng, D.M. Kuang, PD-1hi Identifies a Novel Regulatory B-cell Population in Human Hepatoma That Promotes Disease Progression, Cancer Discov. 6 (2016) 546–559.

[92] M. Sommariva, M. de Cesare, A. Meini, A. Cataldo, N. Zaffaroni, E. Tagliabue, A. Balsari, High efficacy of CpG-ODN, Cetuximab and Cisplatin combination for very advanced ovarian xenograft tumors, J. Transl. Med. 11 (2013) 1. https://doi.org/10.1186/1479-5876-11-25.

[93] M. Sommariva, L. De Cecco, M. De Cesare, L. Sfondrini, S. Meńard, C. Melani, D. Delia, N. Zaffaroni, G. Pratesi, V. Uva, E. Tagliabue, A. Balsari, TLR9 agonists oppositely modulate DNA repair genes in tumor versus immune cells and enhance chemotherapy effects, Cancer Res. 71 (2011) 6382–6390.

https://doi.org/10.1158/0008-5472.CAN-11-1285.

[94] B.B. Batchu, O.V. Gruzdyn, B.K. Kolli, R. Dachepalli, P.S. Umar, S.K. Rai, N. Singh, P.S. Tavva, D.W. Weaver, S.A. Gruber, IL-10 Signaling in the Tumor Microenvironment of Ovarian Cancer, Adv. Exp. Med. Biol. 1290 (2021) 51–65.

[95] C. Ceci, M.G. Atzori, P.M. Lacal, G. Graziani, Targeting tumor-associated macrophages to increase the efficacy of immune checkpoint inhibitors: A glimpse into novel therapeutic approaches for metastatic melanoma, Cancers (Basel). 12 (2020) 1–32. https://doi.org/10.3390/cancers12113401.

[96] N. Liu, B. Zhang, Y. Sun, W. Song, S. Guo, Macrophage origin, phenotypic diversity, and modulatory signaling pathways in the atherosclerotic plaque microenvironment, Vessel Plus. 5 (2021). https://doi.org/10.20517/2574-1209.2021.25.

[97] E.R. Unanue, D.I. Beller, J. Calderon, J.M. Kiely, M.J. Stadecker, Regulation of immunity and inflammation by mediators from macrophages, Am. J. Pathol. 85 (1976) 465–478.

[98] M.I. Stunault, G. Bories, R.R. Guinamard, S. Ivanov, Metabolism plays a key role during macrophage activation, Mediators Inflamm. 2018 (2018). https://doi.org/10.1155/2018/2426138.

[99] M.N. Hasan, O. Capuk, S.M. Patel, D. Sun, The Role of Metabolic Plasticity of Tumor-Associated Macrophages in Shaping the Tumor Microenvironment Immunity, Cancers (Basel). 14 (2022). https://doi.org/10.3390/cancers14143331.

[100] M. Sommariva, V. Le Noci, C. Storti, F. Bianchi, E. Tagliabue, A. Balsari, L. Sfondrini, Activation of NK cell cytotoxicity by aerosolized CpG-ODN/poly(I:C) against lung melanoma metastases is mediated by alveolar macrophages, Cell. Immunol. 313 (2017) 52–58. https://doi.org/10.1016/j.cellimm.2017.01.004.

[101] I. Mattiola, M. Pesant, P.F. Tentorio, M. Molgora, E. Marcenaro, E. Lugli, M. Locati, D. Mavilio, Priming of Human Resting NK Cells by Autologous M1 Macrophages via

the Engagement of IL-1β, IFN-β, and IL-15 Pathways, J. Immunol. 195 (2015) 2818–2828. https://doi.org/10.4049/jimmunol.1500325.

[102] R. Dahan, E. Sega, J. Engelhardt, M. Selby, A.J. Korman, J. V. Ravetch, FcγRs Modulate the Anti-tumor Activity of Antibodies Targeting the PD-1/PD-L1 Axis, Cancer Cell. 28 (2015) 285–295. https://doi.org/10.1016/j.ccell.2015.09.011.

[103] R.H. Vonderheide, M.J. Glennie, Agonistic CD40 antibodies and cancer therapy, Clin. Cancer Res. 19 (2013) 1035–1043. https://doi.org/10.1158/1078-0432.CCR-12-2064.

[104] D.A. Rhodes, D.A. Isenberg, TRIM21 and the Function of Antibodies inside Cells, Trends Immunol. 38 (2017) 916–926. https://doi.org/10.1016/j.it.2017.07.005.

[105] A.F. Carpentier, L. Chen, F. Maltonti, J.Y. Delattre, Oligodeoxynucleotides containing CpG motifs can induce rejection of a neuroblastoma in mice, Cancer Res. 59 (1999) 5429–5432.

[106] B.K. Link, Z.K. Ballas, D. Weisdorf, J.E. Wooldridge, A.D. Bossler, M. Shannon, W.L. Rasmussen, A.M. Krieg, G.J. Weiner, Oligodeoxynucleotide CpG 7909 delivered as intravenous infusion demonstrates immunologic modulation in patients with previously treated non-Hodgkin lymphoma, J. Immunother. 29 (2006) 558–568. https://doi.org/10.1097/01.cji.0000211304.60126.8f.

[107] A.M. Krieg, Toll-like receptor 9 (TLR9) agonists in the treatment of cancer, Oncogene. 27 (2008) 161–167.

[108] J.P. Leonard, B.K. Link, C. Emmanouilides, S.A. Gregory, D. Weisdorf, J. Andrey, J. Hainsworth, J.A. Sparano, D.E. Tsai, S. Horning, A.M. Krieg, G.J. Weiner, Phase I trial of toll-like receptor 9 agonist PF-3512676 with and following rituximab in patients with recurrent indolent and aggressive non-Hodgkin’s lymphoma, Clin. Cancer Res. 13 (2007) 6168–6174. https://doi.org/10.1158/1078-0432.CCR-07-0815.

[109] M. Terme, E. Ullrich, L. Aymeric, K. Meinhardt, J.D. Coudert, M. Desbois, F. Ghiringhelli, S. Viaud, B. Ryffel, H. Yagita, L. Chen, S. Mécheri, G. Kaplanski, A. Prévost-Blondel, M. Kato, J.L. Schultze, E. Tartour, G. Kroemer, M. Degli-Esposti, N. Chaput, L. Zitvogel, Cancer-induced immunosuppression: IL-18-elicited immunoablative NK cells, Cancer Res. 72 (2012) 2757–2767. https://doi.org/10.1158/0008-5472.CAN-11-3379.

[110] M.L. Drakes, S. Mehrotra, M. Aldulescu, R.K. Potkul, Y. Liu, A. Grisoli, C. Joyce, T.E. O'Brien, M.S. Stack, P.J. Stiff, Stratification of ovarian tumor pathology by expression of programmed cell death-1 (PD-1) and PD-ligand- 1 (PD-L1) in ovarian cancer, J. Ovarian Res. 11 (2018) 1–11. https://doi.org/10.1186/s13048-018-0414-z.

[111] O. Marinelli, D. Annibali, C. Aguzzi, S. Tuyaerts, F. Amant, M.B. Morelli, G. Santoni, C. Amantini, F. Maggi, M. Nabissi, The Controversial Role of PD-1 and Its Ligands in Gynecological Malignancies, Front. Oncol. 9 (2019) 1–11. https://doi.org/10.3389/fonc.2019.01073.

[112] M. Jung, Y. Ma, R.P. Iyer, K.Y. DeLeon-Pennell, A. Yabluchanskiy, M.R. Garrett, M.L. Lindsey, IL-10 improves cardiac remodeling after myocardial infarction by stimulating M2 macrophage polarization and fibroblast activation, Basic Res. Cardiol. 112 (2017) 33.

[113] H. Roca, Z.S. Varcos, S. Sud, M.J. Craig, K.J. Pienta, CCL2 and interleukin-6 promote survival of human CD11b+ peripheral blood mononuclear cells and induce M2-type macrophage polarization, J. Biol. Chem. 284 (2009) 34342–34354. https://doi.org/10.1074/jbc.M109.042671.

[114] K.C.S. Pe, R. Saetung, V. Yodsurang, C. Chaotham, K. Suppipat, P. Chanvorachote, S. Tawinwung, Triple-negative breast cancer influences a mixed M1/M2 macrophage phenotype associated with tumor aggressiveness, PLoS One. 17 (2022) 1–18. https://doi.org/10.1371/journal.pone.0273044.

[115] S. Reinartz, T. Schumann, F. Finkernagel, A. Wortmann, J.M. Jansen, W. Meissner, M. Krause, A.M. Schwörer, U. Wagner, S. Müller-Brüsselbach, R. Müller, Mixed-polarization phenotype of ascites-associated macrophages in human ovarian carcinoma: Correlation of CD163 expression, cytokine levels and early relapse, Int. J. Cancer. 134 (2014) 32–42. https://doi.org/10.1002/ijc.28335.

[116] C. Boibessot, O. Molina, G. Lachance, C. Tav, A. Champagne, B. Neveu, J.F. Pelletier, F. Pouliot, V. Fradet, S. Bilodeau, Y. Fradet, A. Bergeron, P. Toren, Subversion of infiltrating prostate macrophages to a mixed immunosuppressive tumor-associated macrophage phenotype, Clin. Transl. Med. 12 (2022). https://doi.org/10.1002/ctm2.581.

[117] G.T. Bardi, M.A. Smith, J.L. Hood Melanoma exosomes promote mixed M1 and M2 macrophage polarization, Cytokine. 105 (2018) 63–72.

[118] P.J. Murray, Macrophage Polarization, Annu. Rev. Physiol. 79 (2017) 541–566. https://doi.org/10.1146/annurev-physiol-022516-034339.

[119] H.L. Lu, X.Y. Huang, Y.F. Luo, W.P. Tan, P.F. Chen, Y.B. Guo, Activation of M1 macrophages plays a critical role in the initiation of acute lung injury, Biosci. Rep. 38 (2018) 1–13. https://doi.org/10.1042/BSR20171555.

[120] L.X. Wang, S.X. Zhang, H.J. Wu, X.L. Rong, J. Guo, M2b macrophage polarization and its roles in diseases, J. Leukoc. Biol. 106 (2019) 345–358. https://doi.org/10.1002/JLB.3RU1018-378RR.

[121] L. Luckett-Chastain, K. Calhoun, T. Schartz, R. Gallucci, IL-6 influences the balance between M1 and M2 macrophages in a mouse model of irritant contact dermatitis, J. Immunol. 196 (2016).

[122] M. De la Fuente López, G. Landskron, D. Parada, K. Dubois-Camacho, D. Simian, M. Martinez, D. Romero, J.C. Roa, I. Chahuán, R. Gutiérrez, F. Lopez-K, K. Alvarez, U. Kronberg, S. López, A. Sanguinetti, N. Moreno, M. Abedrapo, M.J. González, R.

Quera, M.A. Hermoso-R, The relationship between chemokines CCL2, CCL3, and CCL4 with the tumor microenvironment and tumor-associated macrophage markers in colorectal cancer, Tumor Biol. 40 (2018) 1–12. https://doi.org/10.1177/1010428318810059.

[123] D.A. Chistiakov, V.A. Myasoedova, V. V. Revin, A.N. Orekhov, Y. V. Bobryshev, The impact of interferon-regulatory factors to macrophage differentiation and polarization into M1 and M2, Immunobiology. 223 (2018) 101–111. https://doi.org/10.1016/j.imbio.2017.10.005.

[124] A. Schneider, M. Weier, J. Herderschee, M. Perreau, T. Calandra, T. Roger, E. Giannoni, IRF5 Is a key regulator of macrophage response to lipopolysaccharide in newborns, Front. Immunol. 9 (2018) 1–13. https://doi.org/10.3389/fimmu.2018.01597.

[125] X. Wang, Z. Gray, J. Willette-Brown, F. Zhu, G. Shi, Q. Jiang, N.Y. Song, L. Dong, Y. Hu, Macrophage inducible nitric oxide synthase circulates inflammation and promotes lung carcinogenesis, Cell Death Discov. 4 (2018). https://doi.org/10.1038/s41420-018-0046-5.

[126] P.M. Ueland, Choline and betaine in health and disease, J. Inherit. Metab. Dis. 34 (2011) 3–15. https://doi.org/10.1007/s10545-010-9088-4.

[127] S. Slow, J. Elmslie, M. Lever, Dietary betaine and inflammation, Am. J. Clin. Nutr. 88 (2008) 247–248. https://doi.org/10.1093/ajcn/88.1.247.

[128] D.H. Kim, B. Sung, Y.J. Kang, J.Y. Jang, S.Y. Hwang, Y. Lee, M. Kim, E. Im, J.H. Yoon, C.M. Kim, H.Y. Chung, N.D. Kim, Anti-inflammatory effects of betaine on AOM/DSS-induced colon tumorigenesis in ICR male mice, Int. J. Oncol. 45 (2014) 1250–1256. https://doi.org/10.3892/ijo.2014.2515.

[129] S. Sun, X. Li, A. Ren, M. Du, H. Du, Y. Shu, L. Zhu, W. Wang, Choline and betaine consumption lowers cancer risk: A meta-analysis of epidemiologic studies, Sci. Rep.

6 (2016) 1–11. https://doi.org/10.1038/srep35547.

[130] A.E. Pegg, Mammalian polyamine metabolism and function, IUBMB Life. 61 (2009) 880–894.

[131] J.I. Odegaard, A. Chawla, Mechanisms of macrophages activation in obesity-induced insulin resistance, Nat. Clin. Pract. Endocrinol. Metab. (2008).

[132] Q. Yang, C. Zheng, J. Cao, G. Cao, P. Shou, L. Lin, T. Velletri, M. Jiang, Q. Chen, Y. Han, F. Li, Y. Wang, W. Cao, Y. Shi, Spermidine alleviates experimental autoimmune encephalomyelitis through inducing inhibitory macrophages, Cell Death Differ. 23 (2016) 1850–1861. https://doi.org/10.1038/cdd.2016.71.

[133] Y.L. Latour, A.P. Gobert, K.T. Wilson, The role of polyamines in the regulation of macrophage polarization and function, Amino Acids. 52 (2020) 151–160.

[134] N.B. Hao, M.H. Lü, Y.H. Fan, Y.L. Cao, Z.R. Zhang, S.M. Yang, Macrophages in tumor microenvironments and the progression of tumors, Clin. Dev. Immunol. 2012 (2012). https://doi.org/10.1155/2012/948098.

[135] D.R. Burton, Immunoglobulin G: Functional sites, Mol. Immunol. 22 (1985) 161–206.

[136] S.P. Arlauckas, C.S. Garris, R.H. Kohler, M. Kitaoka, M.F. Cuccarese, K.S. Yang, M.A. Miller, J.C. Carlson, J. Freeman, R.M. Anthony, R. Weissleder, M.J. Pittet, In vivo imaging reveals a tumor-associated macrophage mediated resistance pathway in anti-PD-1 therapy, Sci. Transl. Med. 9 (2017) 1–20. https://doi.org/10.1126/scitranslmed.aal3604.In.

[137] D.L. Mallery, W.A. McEwan, S.R. Bidgood, G.J. Towers, C.M. Johnson, L.C. James, Antibodies mediate intracellular immunity through tripartite motif-containing 21 (TRIM21), Proc. Natl. Acad. Sci. USA. 107 (2010) 19985–19990. https://doi.org/10.1073/pnas.1014074107.

[138] L.C. James, Intracellular antibody immunity and the cytosolic Fc receptor TRIM21, Curr. Top. Microbiol. Immunol. 382 (2014) 51–66.

[139] L.C. James, A.H. Keeble, Z. Khan, D.A. Rhodes, J. Trowsdale, Structural basis for PRYSPRY-mediated tripartite motif (TRIM) protein function, Proc. Natl. Acad. Sci. USA. 104 (2007) 6200–6205. https://doi.org/10.1073/pnas.0609174104.

[140] W.A. Mcewan, J.C.H. Tam, R.E. Watkinson, S.R. Bidgood, D.L. Mallery, L.C. James, Intracellular antibody-bound pathogens stimulate immune signaling via Fc-receptor TRIM21, 14 (2013) 327–336. https://doi.org/10.1038/ni.2548.Intracellular.

[141] N. Qureshi, S.N. Vogel, C. Van Way, C.J. Papasian, A.A. Qureshi, D.C. Morrison, The Proteasome: a central regulator of inflammation and macrophage function, 31 (2005) 243–260.

[142] J.J. Gao JJ, J. Shen, C. Kolbert, S. Raghavakaimal, C.J. Papasian, A.A. Qureshi, S.N. Vogel, D.C. Morrison, N. Qureshi, The proteasome regulates bacterial CpG DNA-induced signaling pathways in murine macrophages, Shock. 34 (2010) 390–401.

[143] N. Qureshi, D.C. Morrison, J. Reis, Proteasome protease mediated regulation of cytokine induction and inflammation, Biochim. Biophys. Acta - Mol. Cell Res. 1823 (2012) 2087–2093. https://doi.org/10.1016/j.bbamcr.2012.06.016.

[144] I. Larionova, G. Tuguzbaeva, A. Ponomaryova, M. Stakheyeva, N. Cherdyntseva, V. Pavlov, E. Choinzonov, J. Kzhyshkowska, Tumor-Associated Macrophages in Human Breast, Colorectal, Lung, Ovarian and Prostate Cancers, Front. Oncol. 10 (2020) 1–34. https://doi.org/10.3389/fonc.2020.566511.

[145] C. Wang, C. Ma, L. Gong, Y. Guo, K. Fu, Y. Zhang, H. Zhou, Y. Li, Macrophage Polarization and Its Role in Liver Disease, Front. Immunol. 12 (2021) 1–25. https://doi.org/10.3389/fimmu.2021.803037.